A Numerical Evaluation of Thermotropic Materials for Polymer Solar Thermal Collectors

A DISSERTATION
SUBMITTED TO THE FACULTY OF
UNIVERSITY OF MINNESOTA
BY

Adam Curtis Gladen

IN PARTIAL FULFILLMENT OF THE REQUIREMENTS
FOR THE DEGREE OF
DOCTOR OF PHILOSOPHY

Prof. Susan C. Mantell and Prof. Jane H. Davidson

July 2014

Acknowledgements

There are numerous people who deserve recognition for this dissertation becoming a reality. First, to the person who has endured the brunt of my long hours and late nights, my wife Rissa. She has been patient, supportive, and loving through this long process of graduate school, and, when necessary, she has helped to remind me that there is a life outside of my research.

I would like to thank my advisers, Prof. Susan Mantell and Prof. Jane Davidson, for their much needed guidance, insight, and wisdom throughout my years of research. I am indebted to them for all that I have learned about being a scientist and an engineer.

My family has been immensely supportive of my education and has been an essential source of encouragement. To my parents, Dennis and Ruth, for introducing me to engineering and for pushing me to do my very best, to my sister Kelsey for weathering the first few years of graduate school with me, and to my sister Kathryn for her wonderful encouragement, I say thank you.

I would like to thank my lab mates and my colleagues in the Solar Energy Laboratory for their discussions with me, words of advice, and insights. I would also like to thank John, the Gradfather, Gardner for helping me navigate the bureaucracy of grad school.

Ephesians 3:20-21

Abstract

Thermotropic materials offer the potential to provide a low cost, passive overheat protection mechanism for glazed, polymer collectors. A series of numerical studies of thermotropic materials are conducted to develop a theoretical basis for the selection and design of phase change thermotropic materials for polymer collectors.

The optical requirements for a thermotropic material to provide overheat protection are identified by modeling a polymer, flat plate collector with a thermotropic material. In the clear state, high solar-weighted transmittance (≥80%, preferably ≥85%) is necessary to maintain high optical efficiency for the collector. In the translucent state, high solar-weighted reflectance is necessary to limit the stagnation temperature of the collector to less than the material temperature limit of commodity polymers. To protect an absorber of polypropylene, material temperature limit of 115 °C, the solar-weighted reflectance of the thermotropic material must be ≥50%. Other commodity polymers require higher levels of reflectance in the translucent state.

To determine how to achieve these optical requirements, the radiative transfer within thermotropic materials is modeled with a Monte Carlo ray tracing algorithm. A parametric study of the radiative transfer in thermotropic materials is conducted. The results are presented as dimensionless plots of transmittance and reflectance as a function of the overall optical thickness τ_L, the scattering albedo ω, and the particle size parameter x. The study demonstrates that to achieve ≥85% transmittance in the clear state, the optical thickness must be low. To achieve ≥50% reflectance in the translucent state necessitates a significant increase in optical thickness with temperature. Additionally, the

material must have small particles ($x \leq 2.5$) and be weakly absorbing ($\omega \geq 0.990$). For example, for a size parameter of 2, the optical thickness in the clear state must be ≤0.35. The optical thickness in the translucent state must be ≥10 for a scattering albedo of 0.995.

The data contained in these dimensionless plots can be used to identify and optimize thermotropic materials. A method for indentifying potential thermotropic material combinations is presented. Some potential thermotropic materials identified are poly(ethylene-co-vinyl acetate) in a matrix of poly(methyl methacrylate), n-hexatriacontane in a matrix of polycarbonate, hydroxystearic acid in poly(methyl methacrylate), and low molecular weight polyethylene in a matrix of poly(methyl methacrylate). To demonstrate optimizing a thermotropic material, low molecular mass polyethylene in poly(methyl methacrylate) is further investigated through a case study. The solar-weighted transmittance and reflectance for this combination are predicted as a function of thickness and volume fraction of particles. To achieve a solar-weighted transmittance of ~85% in the clear state and a solar-weighted reflectance in the translucent state of ~50%, with 200 nm radius particles, the slab thickness should be 1 mm and the volume fraction should be 15%.

Using encapsulated particles in a thermotropic material is also investigated. The transmittance and reflectance of hydroxystearic acid in poly(methyl methacrylate) are predicted as a function of shell refractive index, shell thickness, and particle volume fraction. The study demonstrates that a thermotropic material with encapsulated particles can achieve the optical requirements for use in a solar collector. Additionally, the study reveals that a wide range of shell relative refractive indices, from 0.95 to 1.0, and thicknesses, up to 35 nm, provide acceptable optical performance.

Table of Contents

List of Tables

List of Figures

1 Introduction

1.1 Polymer Solar Collectors

The National Renewable Energy Laboratory projects that with current technology, solar thermal systems could provide more than 85% of the energy required for hot water in the United States [1]. Despite this potential, nearly 100% of the energy for hot water and space heating is met with fossil fuel sources [1]. A switch from water heated by fossil fuels to water heated by solar energy would result in a significant decrease in greenhouse emissions. It has been estimated that if solar hot water systems were utilized on half of American homes and two-thirds of American commercial buildings, the end-use fuel savings would exceed 147 TWhr, saving $8.4 billion per year and reducing the CO_2 emissions in the building sector by 2-3% [1].

The main limiting factor for the adoption of solar thermal systems is the high initial cost [2, 3]. Over the past decade there has been an international effort to reduce the cost of solar thermal collectors for domestic hot water and space heating through the development of polymeric absorbers and glazings [2, 4-14]. The most probable design for a glazed polymer collector is a fat plate construction [15]. Commodity polymers are low cost, light weight, and are amendable to high-volume, low cost manufacturing processes [13] and thus offer the potential to reduce the initial cost of the collector – by as much as 50% [14, 16, 17]. However, in a solar thermal collector, the material temperature limit of these polymers can be exceeded in the summer months or during dormant periods [18-20]. During these periods, the temperature of the absorber can exceed 150 °C [21]. The material temperature limit of most commodity polymers is between 80 and 120 °C [22]. Consequently, a low cost and passive overheat protection mechanism is needed. One means for providing overheat protection is with thermotropic materials which are the focus of this dissertation. In particular, phase change thermotropic materials are investigated for this application.

1.2 Phase Change Thermotropic Materials

The defining characteristic of thermotropic materials is optical properties (transmittance, reflectance, and absorptance) that are a function of temperature [23, 24] (Figure 1-1). Overheat protection is provided for the underlying polymer absorber when the thermotropic layer changes from highly transparent (referred to as the clear state) to highly reflective (the translucent state) when the absorber temperature approaches its material temperature limit. This change in optical properties is achieved through volumetric radiation scattering. Phase change thermotropic materials have small particles, collectively referred to as the scattering domain, embedded in an optically matched matrix material. In the clear state, the particles are in the solid phase and refractive indices of the two materials match. Consequently, radiation is not scattered. In the translucent state, the particles are in the liquid phase. The change in phase causes a change in their refractive

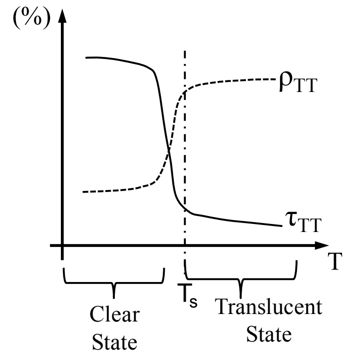

Figure 1-1 Temperature dependency of the optical properties of thermotropic materials.

index. Consequently, the refractive indices of the particles and matrix materials do not match, radiation is scattered, and the reflectance is increased.

Prior material development of these materials has relied on a time intensive empirical approach and has meet with only limited success [23-34]. This limited success is due, in part, to a lack of guidance from theoretical studies on the effects of material choice, particle size, volume fraction, and material thickness on the optical behavior of the thermotropic material in the clear and translucent state. Prior theoretical studies of radiative transfer in thermotropic materials [35, 36] are limited to modeling specific materials and do not provide much guidance for designing thermotropic materials. The most notable contribution from these studies is the recommendation of Nitz et al. that the particle radius should be 100 to 300 nm [35].

1.3 Objective and Scope of the Dissertation

The objective of the present study is to develop a theoretical basis for the design of phase change thermotropic materials for polymer collectors. This dissertation consists of a series of papers (published or submitted for publication) detailing the studies undertaken to accomplish this objective. Thus, each chapter has its own introduction, conclusions, and reference list. A common bibliography is provided at the end of the dissertation.

Chapter 2 specifies the optical properties a thermotropic material must have to provide overheat protection for a polymer collector. To identify these optical requirements, a glazed flat plate, polymer collector with a thermotropic material on absorber is modeled. The model is used to determine the effect of the solar-weighted transmittance of a thermotropic material in the clear state has on the optical efficiency of the collector, and the effect of the solar-weighted reflectance of a thermotropic material in the translucent state has on stagnation temperature of the collector. From this analysis, the required solar-weighted reflectance in the translucent state to provide overheat protection for various polymer absorber materials is identified. These optical requirements provide the context in which the remaining parts of the study are interpreted.

Chapters 3-5 develop the theoretic knowledge base necessary to identify and design a phase change thermotropic material capable of achieving the requirements outlined in Chapter 2. The radiative transfer within a thermotropic material is model via a Monte Carlo ray tracing algorithm. The model is used to investigate the effects of constituent material properties (refractive index and absorptive index) and fabrication parameters (particle size, volume fraction, and thickness) on the optical properties of thermotropic materials.

Chapter 3 is focused on identifying potential thermotropic material combinations (matrix and scattering domain). The optical properties are predicted at a wavelength of

589 nm because there is a plethora of polymer refractive index data at that wavelength, and because it is near the peak intensity of the solar spectrum. A method for identifying thermotropic materials from relative refractive index data is presented. A number of potential thermotropic material combinations are identified.

Chapter 4 expands the study of Chapter 3 to model thermotropic materials across the solar spectrum. A parametric study of radiative transfer in thermotropic materials is conducted and the results are presented in dimensionless form. Thus, thermotropic materials can be identified using the process outlined in Chapter 3 and optimized using the results of Chapter 4 as is illustrated through a case study.

Chapter 5 details the first numerical evaluation of radiative transfer in a thermotropic material with encapsulated particles. Encapsulation of the phase change material prior to combining with the matrix is one means to control the particle size. The optical properties in the clear and translucent state are predicted as a function of shell thickness, shell refractive index, and volume fraction of particles. The study demonstrates that a thermotropic material with encapsulated particles can achieve the optical requirements for use in a solar collector and outlines, for the potential thermotropic material investigated, the acceptable combinations of shell thickness and refractive index.

Chapter 6 summarizes the findings of Chapters 2-5, provides concluding remarks on the dissertation, and considerations for future work. Lastly, the appendix presents the results of preliminary material development initiated from the studies of Chapters 2-5. The data contained in the appendix includes the refractive index as a function of temperature for various polymers, fabrication processing parameters, and transmittance and reflectance data as a function of temperature.

1.4 References

[1] Denholm, P., 2007, "The Technical Potential of Solar Water Heating to Reduce Fossil Fuel use and Greenhouse Gas Emissions in the United States." National Renewable Energy Laboratory (NREL). Technical Report. NREL/TP-640-41157.

[2] Hudon, K., Merrigan, T., Burch, J., 2012, "Low-Cost Solar Water Heating Research and Development Roadmap," National Renewable Energy Laboratory (NREL). Technical Report. NREL/TP-550054793.

[3] Merrigan, T., 2007, "Solar Heating & Lighting: Solar Water Heating R&D - DOE Solar Energy Technologies Program," Denver, CO,

[4] IEA Task 39, 2014, "Polymeric Materials for Solar Thermal Applications, Solar Heating & Cooling Program, International Energy Agency (IEA). Http://task39.Iea-Shc.Org/," **2014**(02/24).

[5] Kohl, M., Meir, M.G., Papillon, P., 2012, "Polymeric Materials for Solar Thermal Applications," Wiley-VCH Verlag & Co., Weinheim, German, pp. 393.

[6] Burch, J. D., 2006, "Polymer-based solar thermal systems: past, present and potential products," Proceedings of the 64th Annual Technical Conference & Exhibition, Society of Plastic Engineers, Charlotte, North Carolina, pp. 7-11.

[7] Martinopoulos, G., Missirlis, D., Tsilingiridis, G., 2010, "CFD Modeling of a Polymer Solar Collector," Renewable Energy, **35**(7) pp. 1499-1508.

[8] Tsilingiris, P., 2002, "Back Absorbing Parallel Plate Polymer Absorbers in Solar Collector Design," Energy Conversion and Management, **43**(1) pp. 135-150.

[9] Mintsa Do Ango, A., Medale, M., and Abid, C., 2013, "Optimization of the Design of a Polymer Flat Plate Solar Collector," Solar Energy, **87** pp. 64-75.

[10] Cristofari, C., Notton, G., Poggi, P., 2002, "Modelling and Performance of a Copolymer Solar Water Heating Collector," Solar Energy, **72**(2) pp. 99-112.

[11] Siqueira, D. A., Vieira, L. G. M., and Damasceno, J. J. R., 2011, "Analysis and Performance of a Low-Cost Solar Heater," Renewable Energy, **36**(9) pp. 2538-2546.

[12] Meir, M., and Rekstad, J., 2003, "Der Solarnor Kunststoffkollektor–The development of a polymer collector with glazing," Proceedings 1. Leobner Symposium Polymeric Solar Materials, November 6-7, pp. II-1-II-8.

[13] Resch, K., and Wallner, G.M., 2012, "Polymeric Materials for Solar Thermal Applications,"Wiley-VCH Verlag & Co., Weinheim, German, pp. 129-134, Chap. 7.

[14] Rhodes, R. O., 2010, "Polymer Thin-Film Design Reduces Installed Cost of Solar Water Heater," Proceedings of the 39th ASES national Solar Conference, Phoenix, AZ, pp. 1588.

[15] Brunold, S., Papillon, P., Plaschkes, M., 2012, "Polymeric Materials for Solar Thermal Applications,"Wiley-VCH Verlag & Co., Weinheim, German, pp. 301-348, Chap. 15.

[16] Burch, J., Merrigan, T., Jorgensen, G., 2006, "Low-Cost Residential Solar Thermal Systems," http://www1.eere.energy.gov/solar/review_meeting/pdfs/p_68_burch_nrel.pdf. accessed 07/21/2014.

[17] Fischer, S., Druck, H., Bachmann, S., 2012, "Polymeric Materials for Solar Thermal Applications,"Wiley-VCH Verlag & Co., Weinheim, German, pp. 73-106, Chap. 4.

[18] Wallner, G. M., Resch, K., and Hausner, R., 2008, "Property and Performance Requirements for Thermotropic Layers to Prevent Overheating in an all Polymeric Flat-Plate Collector," Solar Energy Materials and Solar Cells, **92**(6) pp. 614-620.

[19] Gladen, A. C., Davidson, J. H., and Mantell, S. C., Under Review, "The Effect of a Thermotropic Material on the Optical Efficiency and Stagnation Temperature of a Polymer Flat Plate Solar Collector," Journal of Solar Energy Engineering.

[20] Gladen, A. C., Mantell, S. C., and Davidson, J. H., 2014, "A Parametric Numerical Study of Optical Behavior of Thermotropic Materials for Solar Thermal Collectors," Journal of Heat Transfer, doi: 10.1115/1.4027153.

[21] Reiter, C., Trinkl, C., and Zorner, W., 2012, "Thermal Loads on Solar Collectors and Options for their Reduction,"Wiley-VCH Verlag & Co., Weinheim, German, pp. 107-117, Chap. 5.

[22] Mantell, S.C., and Davidson, J.H., 2012, "Polymeric Materials for Solar Thermal Applications," Wiley-VCH Verlag & Co., Weinheim, German, pp. 187-210, Chap. 10.

[23] Nitz, P., and Hartwig, H., 2005, "Solar Control with Thermotropic Layers," Solar Energy, **79**(6) pp. 573-582.

[24] Seeboth, A., Ruhmann, R., and Muehling, O., 2010, "Thermotropic and Thermochromic Polymer Based Materials for Adaptive Solar Control," Materials, **3**(12) pp. 5143-5168.

[25] Weber, A., and Resch, K., 2014, "Thermotropic Glazings for Overheating Protection. I. Material Preselection, Formulation, and light-shielding Efficiency," Journal of Applied Polymer Science, **131**(4) pp. doi: 10.1002/app.39950.

[26] Weber, A., Schmid, A., and Resch, K., 2014, "Thermotropic Glazings for Overheating Protection. II. Morphology and structure–property Relationships," Journal of Applied Polymer Science, **131**(4) pp. doi: 10.1002/app.39910.

[27] Weber, A., and Resch, K., 2014, "Thermotropic Systems with Fixed Domains Exhibiting Enhanced Overheating Protection Performance," Journal of Applied Polymer Science, **131**(12) pp. n/a-n/a.

[28] Weber, A., Schlögl, S., and Resch, K., 2013, "Effect of Formulation and Processing Conditions on Light Shielding Efficiency of Thermotropic Systems with Fixed Domains Based on UV Curing Acrylate Resins," Journal of Applied Polymer Science, **130**(5) pp. 3299-3310.

[29] Weber, A., and Resch, K., 2012, "Thermotropic Glazings for Overheating Protection," Energy Procedia, **30**pp. 471-477.

[30] Resch, K., and Wallner, G. M., 2009, "Thermotropic Layers for Flat-Plate collectors—A Review of various Concepts for Overheating Protection with Polymeric Materials," Solar Energy Materials and Solar Cells, **93**(1) pp. 119-128.

[31] Resch, K., Wallner, G. M., and Hausner, R., 2009, "Phase Separated Thermotropic Layers Based on UV Cured Acrylate Resins – Effect of Material Formulation on Overheating Protection Properties and Application in a Solar Collector," Solar Energy, **83**(9) pp. 1689-1697.

[32] Muehling, O., Seeboth, A., Haeusler, T., 2009, "Variable Solar Control using Thermotropic core/shell Particles," Solar Energy Materials and Solar Cells, **93**(9) pp. 1510-1517.

[33] Raicu, A., Wilson, H. R., Nitz, P., 2002, "Facade Systems with Variable Solar Control using Thermotropic Polymer Blends," Solar Energy, **72**(1) pp. 31-42.

[34] Georg, A., Graf, W., Schweiger, D., 1998, "Switchable Glazing with a Large Dynamic Range in Total Solar Energy Transmittance (TSET)," Solar Energy, **62**(3) pp. 215-228.

[35] Nitz, P., Ferber, J., Stangl, R., 1998, "Simulation of Multiply Scattering Media," Solar Energy Materials and Solar Cells, **54**(1-4) pp. 297-307.

[36] Wilson, H., and Eck, W., 1992, "Transmission Variation using scattering/transparent Switching Layers," Proceedings of SPIE, **1728**(1) pp. 261-11.

2 The Effect of a Thermotropic Material on the Optical Efficiency and Stagnation Temperature of a Polymer Flat Plate Solar Collector

Published in the ASME Journal of Solar Energy Engineering

2.1 Summary

Solar hot water and space heating systems constructed of commodity polymers have the potential to reduce the initial cost of solar thermal systems. However, a polymer absorber must be prevented from exceeding its maximum service temperature during stagnation. Here the addition of a thermotropic material to the surface of the absorber is considered. The thermotropic layer provides passive overheat protection by switching from high transmittance during normal operation to high reflectance if the temperature of the absorber becomes too high. A one dimensional model of a glazed, flat-plate collector with a polymer absorber and thermotropic material is used to determine the effects of the optical properties of the thermotropic material on the optical efficiency and the stagnation temperature of a collector. A key result is identification of the reflectance in the translucent state required to provide overheat protection for potential polymer absorber materials. For example, the reflectance of a thermotropic material in the translucent state should be greater than or equal to 52% for a polypropylene absorber which has a maximum service temperature of 115 °C.

2.2 Introduction

The global market penetration of solar thermal hot water and space heating systems remains far below its potential in part because of the high initial cost relative to conventional gas and electric systems [1, 2]. To lower initial and installation costs, there is an international effort to develop flat plate collectors with polymer absorbers [1, 3-14]. One of the challenges in this development effort is prevention of the polymer absorber from exceeding its material temperature limit, especially for glazed collectors during stagnation. Operating for extended periods of time at temperatures greater than the material service temperature leads to a degradation in the mechanical properties of the absorber and ultimately to structural failure. Numerous approaches for overheat protection have been proposed [15-29], including the addition of a thermotropic material to the surface of the absorber [25-37]. The optical properties (transmittance and reflectance) of thermotropic materials change with temperature [36, 37]. Passive overheat protection is provided when the thermotropic material switches from a state of high transmittance (referred to as the clear state) at temperatures less than the material limit of the absorber, to a state of high reflectance (referred to as the translucent state) at temperatures near the material's limit, as illustrated in Figure 2-1. Ideally, the switch (or transition) from the clear to the translucent state (which occurs at the switching temperature) would be a step function at the material temperature limit of the absorber. The shape of the transition curve in Figure 2-1 is for illustration only and occurs over a narrow temperature range. If a thermotropic material has non-ideal switching behavior,

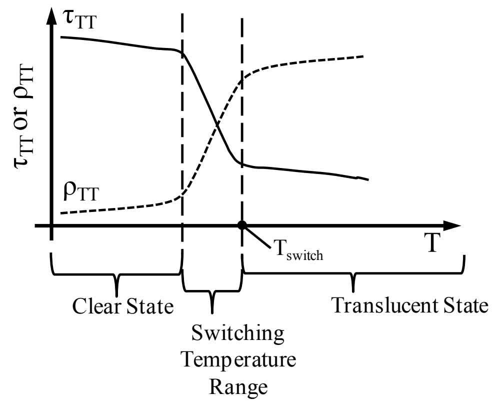

Figure 2-1 Temperature dependency of the optical properties of thermotropic materials

i.e. it switches at too low a temperature or over a large temperature range, the collector will be less efficient during operation.

The focus of efforts to develop thermotropic materials for solar collectors is phase change thermotropic materials [26-36]. These materials can be applied in a thin layer on top of the absorber. They have discrete particles, collectively referred to as the scattering domain, embedded in a matrix material. In the clear state, the refractive indices of the particles and matrix are equal and radiation propagates through the material without being scattered. In the translucent state, the particles change phase which causes a change in their refractive index and creates a mismatch between the refractive index indices of the matrix and the particles. The particles scatter the radiation, and the material reflects a portion of the incident solar radiation, thereby reducing the radiation at the absorber. To date, the best performing, in terms of change in transmittance with temperature, phase change thermotropic materials consist of an alkane mixture [26] or paraffin wax [38] scattering domain embedded in an acrylate based UV resin matrix. For the alkane mixture scattering domain, the solar weighted transmittance changed from 75% and 69% at 20°C

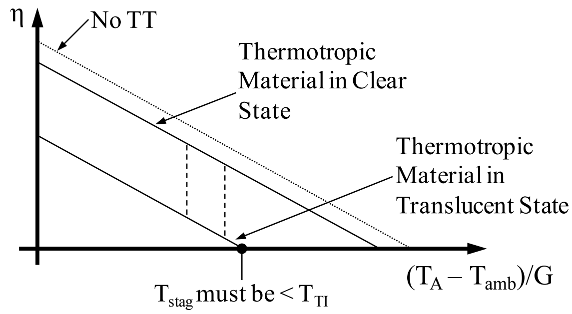

Figure 2-2 Representative efficiency curves for a collector with- and without a thermotropic material. Dashed vertical lines represent a step change from clear to translucent state. Abscissa location of change depends on ambient conditions and T_{switch}.

to 54% and 41%, respectively, above 45°C [26]. For the paraffin scattering domain, the solar-weighted transmittance changed from 73 at 20°C to 49% at 70°C [38].

To illustrate the effect of adding a thermotropic layer to the absorber of a non concentrating solar thermal collector, we show a hypothetical efficiency curve for two collectors, one with- and one without a thermotropic material, in Figure 2-2. The collector with a thermotropic layer has two distinct regimes depending on the state of the thermotropic material. Ideally, when the thermotropic material is in the clear state, the efficiency of the collector is identical to the efficiency of the same collector without a thermotropic material. When the thermotropic material is in the translucent state, the efficiency of the collector is lower, but the absorber is protected from overheating.

Two questions arise in designing thermotropic materials for application to polymer collectors. What is the detrimental impact on optical efficiency during normal operation (i.e., in the clear state)? What are the required optical properties in the translucent state to prevent overheating? Wallner, et al. [25] calculated the useful energy gain of a glazed, polymer collector as a function of absorber temperature for the boundary conditions of 1200 $W \cdot m^{-2}$ direct, normal insolation, no wind, and an ambient temperature of 30°C at a working fluid flow rate of 50 kg m^{-2} h^{-1}. Transmittances from 85 to 90% in the clear state and from 10 to 60% in the translucent state were considered. From this analysis, it was recommended that the transmittance in the clear state be ≥85ºC and that the transmittance in the translucent state be ≤60ºC. Achieving both of these recommendations has proven difficult for phase change thermotropic materials developed to date [26, 30, 33, 38]. The recommended maximum transmittance in the translucent state was determined by identifying the transmittance at which the efficiency was zero at an absorber temperature of ~130ºC. However, in their analysis, the absorber temperature was prescribed a priori and was thus incorrectly decoupled from the boundary conditions. Therefore, further consideration of the question is warranted.

In the present study, we develop a one-dimensional model of a glazed, flat plate collector with a polymer absorber coated with a thin layer of thermotropic material. The model is applied to illustrate the impact of the optical properties of a thermotropic material on the collector optical efficiency in the clear state and stagnation temperature in the translucent state. The transition between states is not considered. From this analysis, we recommend the normal-hemispherical, solar-weighted reflectance of a thermotropic material in its translucent state required to provide overheat protection for solar absorbers fabricated from various polymeric materials.

2.3 Analysis

The representative, glazed, polymer collector modeled is shown in Figure 2-3. Table 2-1 lists the assumed material properties and geometric parameters of the collector.

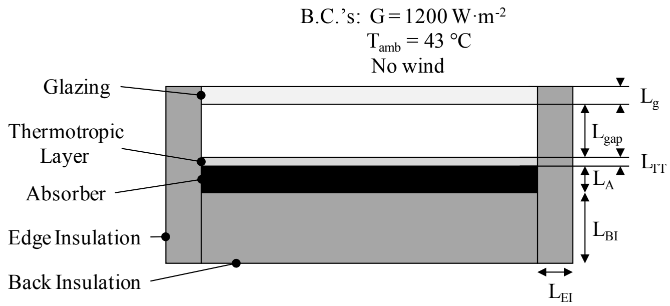

Figure 2-3 Schematic cross-sectional view of the modeled collector

Table 2-1 Material properties and geometric parameters of the collector

Component	τ_{solar}	τ_{IR}	ε_{IR}	**L (mm)**	**k ($W \cdot m^{-1} \cdot K^{-1}$)**
Glazing	82	0	90	4	0.2
TT Layer	Variable	0	90	1	0.2
Absorber	0	0	90	10	0.2
Back Insulation	N/A	N/A	N/A	50	0.038
Edge Insulation	N/A	N/A	N/A	30	0.038
Tilt Angle	30°				
L_{gap}	10 mm				
Aperture Area	2 m^2				

The material properties are representative of commercial materials. The glazing has a solar weighted transmittance of 82%, typical of polycarbonate or poly(methyl methacrylate) glazing materials [39, 40]. The diffuse reflectance of the glazing $\rho_{g,d}$ is assumed to be 15% [41]. The polymer absorber is non-selective with a normal incidence, solar-weighted absorptivity of 90%; representative of polymer absorbers based on data from unglazed polymer collectors [42, 43]. A thermal conductivity of 0.2 $W \cdot m^{-1} \cdot K^{-1}$ is assumed for the polymer components; this value represents unfilled polymers [40]. A thermal conductivity of 0.038 $W \cdot m^{-1} \cdot K^{-1}$ is assumed for the insulation; typical of collector insulating materials [40, 44]. The thermotropic layer is assumed to be 1 mm thick and placed directly on top surface of the absorber. The collector is positioned at a tilt angle of 30°; a value representative of residential roofs.

The boundary conditions for an energy balance on the collector represent a worst case scenario for overheating, i.e. they induce higher stagnation temperatures, and thus give more stringent requirements for the thermotropic material. The incident solar radiation is assumed to be direct, normal at 1200 $W \cdot m^{-2}$. The ambient and sky temperatures are 43°C. There is no wind.

It is assumed that the thermotropic material does not absorb radiation in the solar spectrum. Additionally, it is assumed that the thermotropic material and the glazing are opaque to the infrared radiation emitted by the absorber. These assumptions lead to a conservative estimate of the required reflectance to protect the absorber.

The stagnation temperature is determined based on a one-dimensional energy balance on the collector assuming normal incidence,

$$q_u = G(\tau\alpha)_n - U_L(T_A - T_{amb}). \tag{2.1}$$

Where q_u is the useful energy output of a collector per unit area, and $(\tau\alpha)_n$ is the optical efficiency at normal incidence. The loss term is expressed as the product of the temperature dependent overall loss coefficient U_L and the difference in absorber and ambient temperatures.

When there is no flow through the collector or when the thermal losses are equal to the solar gain, the useful energy q_u is zero and the stagnation temperature of the absorber is determined from an iterative solution [45] of

$$T_{stag} = \frac{G(\tau\alpha)_n}{U_L} + T_{amb}. \tag{2.2}$$

By considering the impact of optical properties on the stagnation temperature, we interpret the results to determine the reflectance in the translucent state required to limit the stagnation temperature to less than the service temperature of the absorber. This approach, as differentiated from the analysis in [25], provides guidance on selection of material properties.

The overall heat transfer coefficient U_L is calculated using the resistance network shown in Figure 2-4. The convective resistance between the glazing and absorber is based on the Nusselt-Rayleigh number correlation for natural convection between inclined flat plates developed by Hollands et al. [46]. Heat loss from the glazing to the ambient environment is treated as the natural convection from a vertical plate [47] plus radiation to the sky [48]. This estimate yields high stagnation temperatures because convective cooling due to wind is neglected. Radiative transfer between the top surface of the thermotropic layer and the bottom surface of the glazing is calculated using the radiative heat transfer coefficient for radiative exchange between parallel plates with a view factor of one [48]. A semi-gray approximation is used for the radiative properties of the component surfaces with the radiative properties assumed constant in the solar spectrum ($250 \leq \lambda \leq 3000$nm) and infrared spectrum ($\lambda \geq 3000$nm). The radiative properties in the solar spectrum and infrared spectrum are listed in Table 2-1 for the relevant components. Conduction through the thermotropic material, absorber, glazing, back insulation, and edge insulation is determined based on the thermal conductivity and thickness for each component listed in Table 2-1. For the stated assumptions, the overall heat transfer

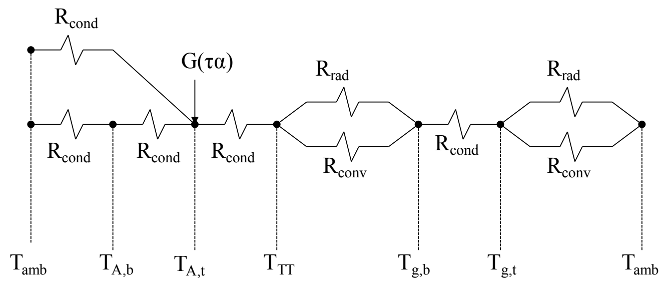

Figure 2-4 Resistance network used to calculate the overall heat transfer coefficient

coefficient is calculated to be 7 $W \cdot m^{-2} \cdot K^{-1}$ at stagnation for a collector with a thermotropic material which has a reflectance in the translucent state of zero.

The transmittance-absorptance product $(\tau\alpha)_n$ for a collector with a thermotropic material on the top surface of the absorber is

$$(\tau\alpha)_n = \frac{(1-\rho')\tau_g}{1-\rho_{g,d}\rho'} . \tag{2.3}$$

Where the overall reflectance of the thermotropic material-absorber laminate ρ' is

$$\rho' = \rho_{TT} + \frac{\tau_{TT}^2 (1-\alpha_A)}{1-\rho_{TT}(1-\alpha_A)} . \tag{2.4}$$

Equations (3) and (4) were derived using a radiostiy analysis. The derivation is provided in the Appendix. If $\rho_{TT} = 0$ and $\tau_{TT} = 1$, i.e. there is no thermotropic layer, eq. (2.4) reduces to $\rho' = (1-\alpha_A)$ and eq. (2.3) reduces to conventional expression for the transmittance-absorptance product of a glazed flat plate collector [45]. With the exception of the absorber absorptivity α_A, the optical properties in eqs. (2.3) and (2.4) are the overall (surface and volumetric) optical properties of the component. Equation (2.4) can be used for any collector with a plane-parallel thermotropic layer (absorbing or non-absorbing) on a plane-parallel absorber. Equations (2.3) and (2.4) are also used to determine the effect of the transmittance of a thermotropic material in the clear state on the optical efficiency of the collector.

2.4 Results

Figure 2-5 shows the optical efficiency of the collector (the normal, transmittance-absorptance product) as a function of the solar-weighted [49], normal-hemispherical transmittance of a thermotropic material in the clear state. If there is no thermotropic material (i.e. $\tau_{TT,CS} = 1$), the optical efficiency is 0.75. The addition of a thermotropic material with a solar-weighted transmittance of 80% to the absorber is predicted to decrease the optical efficiency to 0.62. To have an optical efficiency equivalent to the average (0.692) of the similar (glazed without a selective surface absorber and with a heat transfer coefficient between 6 and 8 $W \cdot m^{-2} \cdot K^{-1}$) collectors certified by the SRCC [43], the required transmittance in the clear state is 90%. Although a reduction in the collector optical efficiency is not desirable, without overheat protection most polymer absorbers will reach a temperature that exceeds the material temperature limit.

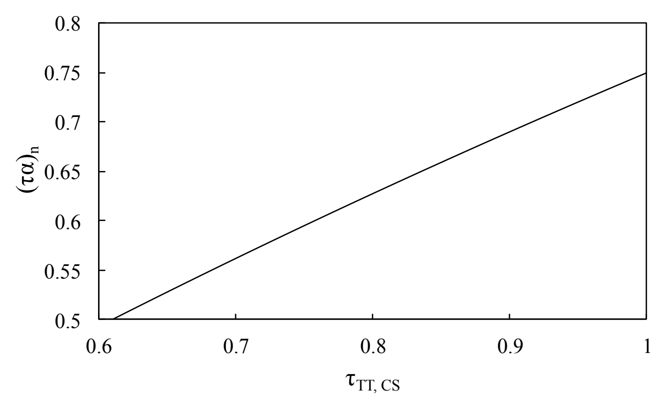

Figure 2-5 Collector optical efficiency versus the transmittance of a thermotropic material in its clear state

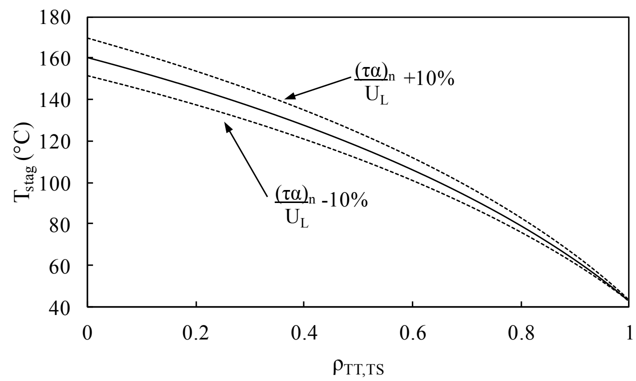

Figure 2-6 Predicted stagnation temperature as a function of the reflectance of the thermotropic material in its translucent state. Solid line represents nominal collector parameters

Figure 2-6 shows the stagnation temperature of the absorber as a function of the solar-weighted, normal-hemispherical reflectance of a thermotropic material in the translucent state. This figure can be used to determine the reflectance required to limit the stagnation temperature to less than the material temperature limit. As stated previously, these recommendations are based on extreme ambient conditions, including high solar irradiance, high ambient temperature and no wind. Thus the recommended reflectance is higher than would be required if the stagnation temperature were lower due to convective cooling by wind or for cooler, less sunny conditions. For the current case, if the absorber material temperature limit is 100°C, Figure 2-6 shows that the reflectance of the thermotropic material in the translucent state must be ≥65% to protect the absorber. Without any overheat protection, the stagnation temperature is 160°C.

Table 2-2 lists potential absorber polymers [50], the material temperature limit (represented by relative thermal index or heat distortion temperature), and the required

Table 2-2 Reflectance for a thermotropic material in its translucent state to provide overheat protection for potential absorber materials

Polymer	$\mathbf{T_{TI}}$	$\mathbf{T_{HDT}}$	$\boldsymbol{\rho_{TT,TS}}$	**Type**
ABS	60 - 65	<98	92 - 89%	C
PE	65	80	89%	C
AC	90	120	72%	C
PEX	100	-	65%	C
CPVC	-	100	65%	C
PPO	105	145	61%	E
PP	115	143	52%	C
PVDF	150	118	49%	P
PC	130	132	37%	E
PSU	150	180	14%	P
PPS	200	260	NR	P
PEEK	250	315	NR	P

C: Commodity polymer; E: Engineering polymer; P: Performance polymer; NR: overheat protection Not Required

reflectance in the translucent state for a thermotropic material to provide adequate overheat protection for the assumed boundary conditions. The relative thermal index and the heat distortion temperature have both been suggested as the temperature limit for polymer absorbers [27, 51]. The relative thermal index is the temperature at which there is 50% reduction in mechanical properties (impact resistance, strength, or stiffness) after 100,000 hours of conditioning at that temperature [52]. The heat distortion temperature is the temperature at which a test specimen deflects a specified distance under a specified bending load [53]. Because the relative thermal index includes the long term effects of high temperature on the mechanical properties of a polymer, we recommended it be used as the material temperature limit. The heat distortion temperature should be used only if it is less than the relative thermal index or if the relative thermal index data are unavailable.

The polymers in Table 2-2 are classified as performance, engineering, or commodity polymers. The classification of a polymer depends on the material temperature limit and the material cost [12]. A performance polymer refers to thermoplastics with a temperature limit generally greater than 150°C and which cost $5.50 to 14+ per kg (€4-10+). Engineering polymers have temperature limits between 100 and 150°C and cost between $2.75 and 5.50 per kg (€2-4). Commodity polymers generally have maximum operation temperatures around 100°C and cost less than $2.75 per kg (≤€2) [12].

As shown in Table 2-2, absorbers made of performance polymers such as PSU and PPS require little ($\rho_{TT,TS} \geq 14\%$ for PSU) to no (for PPS) overheat protection. However, to maximize the reduction in the cost of the collector created by switching to polymer components, commodity polymers must be utilized. For a polypropylene absorber, the commodity polymer with the highest relative thermal index (115°C), the reflectance of a thermotropic layer in the translucent state should be ≥52% in order for a thermotropic material to provide adequate overheat protection. Other commodity polymers such as CPVC and PEX require even higher reflectance (≥65%) from a thermotropic material in its translucent state.

The sensitivity of the recommended reflectance of a thermotropic material to modifications in collector design is indicated in Figure 2-6 by the dashed lines which represent a ±10% change to the ratio of the transmittance-absorptance product to the overall heat transfer coefficient. The recommended reflectance for a thermotropic material is sensitive to a change in this ratio when the absorber has a high temperature limit. For example, if the transmittance-absorptance product is increased by 10% (e.g. by having a glazing with a transmittance of 90.2% rather than 82%), the required reflectance for a thermotropic material in the translucent state increases from 14 to 24% for a PSU absorber. For absorber polymers with a lower temperature limit ($T \leq 80°C$), the recommended reflectance is insensitive to a ±10% change in this ratio. For example, for a 10% increase in the ratio, the required reflectance for a thermotropic material in the translucent state increases from 89 to 90% to protect a PE absorber, which has a material temperature limit of 65°C.

2.5 Conclusion

The present study applies a one dimensional model of a flat plate, polymer, solar collector with a thermotropic material to quantify the effect of the optical properties of the thermotropic material on the optical efficiency and stagnation temperature of the collector. The results show that for ambient conditions that stress the collector (hot and sunny with no wind), the requirements for a thermotropic material to successfully provide overheat protection are stringent. In agreement with the prior recommendations [25], the thermotropic material must be highly transparent in the clear state to maintain high overall optical efficiency of the collector during normal operation. The optical requirement for a thermotropic material in its translucent state is much more stringent that previously recommended, particularly for commodity polymer absorbers. High solar-weighted reflectance in the translucent state is necessary for a thermotropic material to adequately provide overheat protection for a commodity polymer absorber. The recommended reflectance is on the order of 50% if the absorber is polypropylene. For absorbers fabricated from other commodity polymers, all of which have lower material temperature limits, the recommended reflectance of a thermotropic material is higher. The dual requirements of high transmittance in the clear state and high reflectance in the translucent state pose stringent requirements on the development of thermotropic materials for this application.

2.6 Funding

This research is funded by the University of Minnesota Initiative for Renewable Energy and the Environment (IREE) and by the National Renewable Energy Laboratory (NREL).

2.7 Nomenclature

G	insolation	$W \cdot m^{-2}$
k	thermal conductivity	$W \cdot m^{-1} \cdot K^{-1}$
L	thickness	m
q_u	useful energy	$W \cdot m^{-2}$
R	thermal resistance	$K \cdot m^{2} \cdot W^{-1}$
T	temperature	K
U_L	overall heat transfer coefficient	$W \cdot m^{-2} \cdot K^{-1}$
Greek Symbols		
α	surface absorptivity	%
ε	surface emissivity	%
η	efficiency	%
λ	wavelength	nm
ρ	volumetric reflectance	%
ρ'	overall reflectance of thermotropic layer-absorber laminate	%
τ	volumetric transmittance	%

$(\tau\alpha)_n$	normal irradiance transmittance-absorptance product	%

Subscripts

A	absorber
amb	ambient
b	bottom surface
BI	back insulation
CS	clear state
cond	conduction
conv	convection
d	diffuse
EI	edge insulation
g	glazing
gap	air gap between glazing and thermotropic layer
HDT	heat distortion temperature
IR	infrared spectrum
rad	radiation
solar	solar-weighted
switch	switching
t	top surface
TI	relative thermal index
TS	translucent state
TT	Thermotropic

Abbreviations

ABS	Acrylonitrile-butadiene-styrene
AC	Acetal copolymer
CPVC	Chlorinated poly(vinyl chloride)
PC	Polycarbonate
PE	Polyethylene
PEEK	Poly(ether ether ketone)

PEX	Crosslinked Polyethylene
PP	Polypropylene
PPO	Poly(phenylene oxide)
PPS	Poly(phenylene sulfide)
PSU	Polysulfone
PVDF	Poly(vinylidene fluoride)

2.8 Appendix

This appendix presents the derivation of the transmittance-absorptance product for a collector with a thermotropic material on the absorber. In this analysis, the normal-hemispherical optical properties of the thermotropic material are assumed equal to the diffuse-hemispherical optical properties. The key difference between the transmittance-absorptance product of a collector with- and without a thermotropic material is the overall reflectance and absorptance of the thermotropic material-absorber laminate.

Figure 2-7 shows the irradiances and radiosities of the laminate system. The irradiances and radiosities are drawn at an angle for clarity. The irradiance on the top surface of the absorber H_{TT} is taken to be unity. The radiosity leaving the top surface of the thermotropic material J_{TT} is the overall reflectance of the laminate system ρ' and is equal to fraction of H_{TT} reflected by the thermotropic material plus the fraction of the radiosity leaving the absorber surface J_A that is transmitted through the thermotropic material,

$$J_{TT} = \rho_{TT} H_{TT} + \tau_{TT} J_A = \rho_{TT} + \tau_{TT} J_A . \tag{2.6}$$

The irradiance on the surface of the absorber H_A is equal to the fraction of H_{TT} transmitted through the thermotropic material plus the fraction of J_A reflected back to the absorber,

$$H_A = \tau_{TT} H_{TT} + \rho_{TT} J_A = \tau_{TT} + \rho_{TT} J_A . \tag{2.7}$$

The radiosity leaving the surface of the absorber J_A is equal to the irradiance incident on the absorber times the reflectivity (equal to one minus the absorptivity) of the absorber,

$$J_A = (1 - \alpha_A) H_A . \tag{2.8}$$

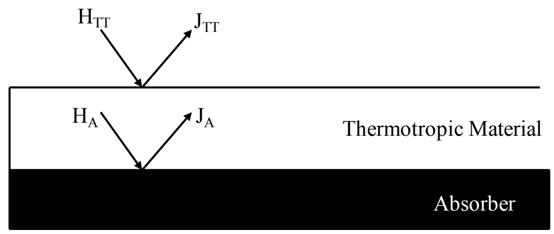

Figure 2-7 Schematic drawing of radiosities and irradiances used to determine the overall reflectance of the thermotropic material-absorber laminate

Thus there are three equations and three unknowns. Substituting Eq. 2.7 into Eq. 2.8 and solving for J_A yields,

$$J_A = \frac{\rho_A \tau_{TT}}{\left(1-\rho_{TT}\left(1-\alpha_A\right)\right)}. \tag{2.9}$$

Substituting the express for J_A into Eq. 2.6 yields the equation for the overall reflectance of laminate system,

$$J_{TT} = \rho' = \rho_{TT} + \frac{\tau_{TT}^2\left(1-\alpha_A\right)}{1-\rho_{TT}\left(1-\alpha_A\right)}. \tag{2.10}$$

The overall absorptance of the thermotropic material-absorber laminate is one minus the overall reflectance. To determine the transmittance-absorptance product for the collector, the overall reflectance and absorptance of the laminate are used in the place of the reflectivity and absorptivity of the absorber in the equation for the transmittance-absorptance product of a glazed, flat plate collector [41].

2.9 References

[1] Hudon, K., Merrigan, T., Burch, J., 2012, "Low-Cost Solar Water Heating Research and Development Roadmap," National Renewable Energy Laboratory (NREL). Technical Report. NREL/TP-550054793.

[2] Merrigan, T., 2007, "Solar Heating & Lighting: Solar Water Heating R&D - DOE Solar Energy Technologies Program," April 17-19, 2007, Denver, CO, .

[3] IEA Task 39, 2014, "Polymeric Materials for Solar Thermal Applications, Solar Heating & Cooling Program," International Energy Agency (IEA). http://task39.iea-shc.org/, 2014(02/24).

[4] Kohl, M., Meir, M.G., Papillon, P., Wallner, G.M., and Saile, S., 2012, "Polymeric Materials for Solar Thermal Applications," Wiley-VCH Verlag & Co., Weinheim, German, pp. 393.

[5] Burch, J. D., 2006, "Polymer-based solar thermal systems: past, present and potential products," Proceedings of the 64th Annual Technical Conference & Exhibition, Society of Plastic Engineers, May 7-11, 2006, Charlotte, North Carolina, pp. 7-11.

[6] Martinopoulos, G., Missirlis, D., Tsilingiridis, G., Yakinthos, K., and Kyriakis, N., 2010, "CFD Modeling of a Polymer Solar Collector," Renewable Energy, **35**(7) pp. 1499-1508.

[7] Tsilingiris, P., 2002, "Back Absorbing Parallel Plate Polymer Absorbers in Solar Collector Design," Energy Conversion and Management, **43**(1) pp. 135-150.

[8] Mintsa Do Ango, A., Medale, M., and Abid, C., 2013, "Optimization of the Design of a Polymer Flat Plate Solar Collector," Solar Energy, **87**pp. 64-75.

[9] Cristofari, C., Notton, G., Poggi, P., and Louche, A., 2002, "Modelling and Performance of a Copolymer Solar Water Heating Collector," Solar Energy, **72**(2) pp. 99-112.

[10] Siqueira, D. A., Vieira, L. G. M., and Damasceno, J. J. R., 2011, "Analysis and Performance of a Low-Cost Solar Heater," Renewable Energy, **36**(9) pp. 2538-2546.

[11] Meir, M., and Rekstad, J., 2003, "Der Solarnor Kunststoffkollektor–The development of a polymer collector with glazing," Proceedings 1. Leobner Symposium Polymeric Solar Materials, November 6-7, pp. II-1-II-8.

[12] Resch, K., and Wallner, G.M., 2012, "Polymeric Materials for Solar Thermal Applications," *Polymeric Materials for Solar Thermal Applications*, Kohl, M., Meir, M.G., Papillon, P., Wallner, G.M., and Saile, S., eds., Wiley-VCH Verlag & Co., Weinheim, German, pp. 129-134, Chap. 7.

[13] Rhodes, R. O., 2010, "Polymer Thin-Film Design Reduces Installed Cost of Solar Water Heater," *Proceedings of the 39th ASES national Solar Conference;*, May 17-22, 2010, Phoenix, AZ, pp. 1588.

[14] Russell, L., and Guven, H., 1982, "Modeling and Analysis of an all-Plastic Flat-Plate Solar Collector," J.Sol.Energy Eng., **104**(4) pp. 333-339.

[15] Baer, S. C., 1985, "Thermal Control System for Solar Collector," US Patent (4,528,976) .

[16] Harrison, S., and Cruickshank, C. A., 2012, "A Review of Strategies for the Control of High Temperature Stagnation in Solar Collectors and Systems," Energy Procedia, **30** pp. 793-804.

[17] Thür, A. V., Hintringer, C., Richtfeld, A., 2013, "Status Quo Der Entwicklungen Eines Überhitzungsgeschützten Kunststoffkollektors," Erneuerbare Energie, http://www.aee.at/aee/index.php?option=com_content&view=article&id=749&Itemid=113, 2014(6/12).

[18] Buckley, B. S., and Guldman, T. A., 1983, "Method and Apparatus for Overtemperature Control of Solar Water Heating System," US Patent (4,399,807) .

[19] Kusyy, O., and Vajen, K., 2011, "Theoretical Investigation on a Control-based Approach to Avoid Stagnation of Solar Heating Systems," Proceeding of ISES Solar World Congress, Kassel, August 28 – September 2,Germany, Kassel, Germany, pp. 3323-3330.

[20] Kearney, M., Davidson, J., and Mantell, S., 2005, "Polymeric Absorbers for Flat-Plate Collectors: Can Venting Provide Adequate Overheat Protection?" Journal of Solar Energy Engineering, **12**7(3) pp. 421-424.

[21] Mahdjuri, F., 1999, "Solar Collector with Temperature Limitation using Shape Memory Metal," Renewable Energy, **1**6(1) pp. 611-617.

[22] Roberts, J., Brandemuehl, M., Burch, J., 2000, "Overheat Protection for Solar Water Heating Systems Using Natural Convection Loops," Proceedings of the Solar Conference, Anonymous American Solar Energy Society; American Institute of Architects, pp. 273-278.

[23] Rich, A. C., 1995, "Solar Collector Venting System," US Patent (5,404,867) .

[24] Slaman, M., and Griessen, R., 2009, "Solar Collector Overheating Protection," Solar Energy, **8**3(7) pp. 982-987.

[25] Wallner, G. M., Resch, K., and Hausner, R., 2008, "Property and Performance Requirements for Thermotropic Layers to Prevent Overheating in an all Polymeric Flat-Plate Collector," Solar Energy Materials and Solar Cells, **9**2(6) pp. 614-620.

[26] Muehling, O., Seeboth, A., Haeusler, T., 2009, "Variable Solar Control using Thermotropic core/shell Particles," Solar Energy Materials and Solar Cells, **93**(9) pp. 1510-1517.

[27] Gladen, A. C., Davidson, J. H., and Mantell, S. C., 2013, "Selection of Thermotropic Materials for Overheat Protection of Polymer Absorbers," Solar Energy, **104**, pp. 42-51. doi: 10.1016/j.solener.2013.10.026.

[28] Gladen, A. C., Mantell, S. C., and Davidson, J. H., 2013, "A Parametric Numerical Study of Radiative Transfer in Thermotropic Materials," ASME 2013 Heat Transfer Summer Conference collocated with the ASME 2013 7th International Conference on Energy Sustainability and the ASME 2013 11th International Conference on Fuel Cell Science, Engineering and Technology, American Society of Mechanical Engineers, Minneapolis, MN, pp. V001T01A002-V001T01A002.

[29] Resch, K., Hausner, R., and Wallner, G. M., 2009, "All Polymeric Flat-Plate Collector — Potential of Thermotropic Layers to Prevent Overheating," Proceedings of ISES World Congress 2007 (Vol. I – Vol. V), D. Y. Goswami and Y. Zhao, eds. Springer Berlin Heidelberg, pp. 561-565.

[30] Weber, A., and Resch, K., 2014, "Thermotropic Glazings for Overheating Protection. I. Material Preselection, Formulation, and light-shielding Efficiency," Journal of Applied Polymer Science, **131**(4) pp. doi: 10.1002/app.39950.

[31] Weber, A., Schmid, A., and Resch, K., 2014, "Thermotropic Glazings for Overheating Protection. II. Morphology and structure–property Relationships," Journal of Applied Polymer Science, **131**(4) pp. doi: 10.1002/app.39910.

[32] Weber, A., Schlögl, S., and Resch, K., 2013, "Effect of Formulation and Processing Conditions on Light Shielding Efficiency of Thermotropic Systems with Fixed Domains Based on UV Curing Acrylate Resins," Journal of Applied Polymer Science, **130**(5) pp. 3299-3310.

[33] Weber, A., and Resch, K., 2012, "Thermotropic Glazings for Overheating Protection," Energy Procedia, **30** pp. 471-477.

[34] Resch, K., and Wallner, G. M., 2009, "Thermotropic Layers for Flat-Plate collectors—A Review of various Concepts for Overheating Protection with Polymeric Materials," Solar Energy Materials and Solar Cells, **93**(1) pp. 119-128.

[35] Gladen, A. C., Mantell, S. C., and Davidson, J. H., 2014, "A Parametric Numerical Study of Optical Behavior of Thermotropic Materials for Solar Thermal Collectors," Journal of Heat Transfer, **136**(7) pp. 072703-1 – 072703-12. doi: 10.1115/1.4027153.

[36] Seeboth, A., Ruhmann, R., and Muehling, O., 2010, "Thermotropic and Thermochromic Polymer Based Materials for Adaptive Solar Control," Materials, **3**(12) pp. 5143-5168.

[37] Nitz, P., and Hartwig, H., 2005, "Solar Control with Thermotropic Layers," Solar Energy, **79**(6) pp. 573-582.

[38] Weber, A., and Resch, K., 2014, "Thermotropic Systems with Fixed Domains Exhibiting Enhanced Overheating Protection Performance," Journal of Applied Polymer Science, **131**(12), doi: 10.1002/app.40417.

[39] Brunold, S., Ruesch, F., Kunic, R., 2012, "Polymeric Materials for Solar Thermal Applications," *Polymeric Materials for Solar Thermal Applications*, Kohl, M., Meir, M.G., Papillon, P., Wallner, G.M., and Saile, S., eds., Wiley-VCH Verlag & Co., Weinheim, German, pp. 319-349, Chap. 16.

[40] Lenel, U. R., and Mudd, P. R., 1984, "A Review of Materials for Solar Heating Systems for Domestic Hot Water," Solar Energy, **32**(1) pp. 109-120.

[41] Duffie, J., and Beckman, W., 2006, "Solar Engineering of Thermal Processes Third Edition," Wiley-Interscience, Hoboken, NJ, pp. 204-237, Chap. 5.

[42] Papillon, P., and Wilhelms, C., 2012, "Polymeric Materials for Solar Thermal Applications," *Polymeric Materials for Solar Thermal Applications*, Kohl, M., Meir, M.G., Papillon, P., Wallner, G.M., and Saile, S., eds., Wiley-VCH Verlag & Co., Weinheim, German, pp. 29-70, Chap. 3.

[43] Solar Ratings & Certification Corporation (SRCC), OG-100 certification, http://www.solar-rating.org/ratings/index.html, 2014(06/17).

[44] Fischer, S., Druck, H., Bachmann, S., Streicher, E., Ullmann, J., and Traub, B., 2012, "Conventional Collectors, Heat Stores, and Coatings," *Polymeric Materials for Solar Thermal Applications*, Kohl, M., Meir, M.G., Papillon, P., Wallner, G.M., and Saile, S., eds., Wiley-VCH Verlag & Co., Weinheim, German, pp. 73-106, Chap. 4.

[45] Duffie, J., and Beckman, W., 2006, "Solar Engineering of Thermal Processes Third Edition," Wiley-Interscience, Hoboken, NJ, pp. 908.

[46] Hollands, K., Unny, T., Raithby, G., 1976, "Free Convective Heat Transfer Across Inclined Air Layers," Journal of Heat Transfer, **98**(2) pp. 189-193.

[47] McAdams, W.H., 1954, "Heat transmission," McGraw-Hill, New York.

[48] Duffie, J., and Beckman, W., 2006, "Solar Engineering of Thermal Processes Third Edition," Wiley-Interscience, Hoboken, NJ, pp. 139-173, Chap. 3.

[49] ASTM Standard G173, 2012, "Standard Tables for Reference Solar Spectral Irradiances: Direct Normal and Hemispherical on 37^{o} Tilted Surface," Annual Book of ASTM Standards, **14.04**.

[50] Mantell, S.C., and Davidson, J.H., 2012, "Polymer Durability for Solar Thermal Applications," *Polymeric Materials for Solar Thermal Applications*, Kohl, M., Meir, M.G., Papillon, P., Wallner, G.M., and Saile, S., eds., Wiley-VCH Verlag & Co., Weinheim, German, pp. 187-210, Chap. 10.

[51] Raman, R., Mantell, S., Davidson, J., 2000, "A Review of Polymer Materials for Solar Water Heating Systems," Transactions-American Society of Mechanical Engineers Journal of Solar Energy Engineering, **122**(2) pp. 92-100.

[52] UL746B, 1998, "Polymeric Materials - Long Term Property Evaluations. Underwriters Laboratories, Inc., Northbrook, IL." .

[53] ASTM Standard D648, 2007, "Test Method for Deflection Temperature of Plastics Under Flexural Load." Annual Book of ASTM Standards, **08.01**.

3 Selection of Thermotropic Materials for Overheat Protection of Polymer Absorbers

Published in the Journal of Solar Energy

3.1 Summary

Thermotropic materials offer the potential to provide passive overheat protection for polymer solar absorbers. These materials are comprised of a matrix in which a second material, referred to as the scattering domain, is dispersed as small particles. Overheat protection is provided by a change in transmittance and reflectance at elevated temperature. The magnitude of this change depends on the change in the relative refractive index between the matrix and the scattering domain, the volume fraction and size of the dispersed particles, and the thickness of the material. To predict the effect of these parameters on the normal-hemispherical transmittance and reflectance, thermotropic materials are modeled as a non-absorbing slab comprised of discrete, anisotropic scattering, spherical particles embedded in a matrix material. A Monte Carlo ray tracing algorithm predicts the transmittance and reflectance of the slab. The model predictions are compared with: the analytical solution for a slab of non-absorbing, non-scattering media, and the measured transmittance of 0.3 mm thick polymer samples containing 400 nm particles. A parametric study of the effects of the design parameters on the transmittance is presented to identify potential material combinations which will produce a thermotropic composite capable of providing overheat protection for flat plate solar collectors. Relatively short chain alkanes or low molecular mass polyethylene in a matrix of polycarbonate are identified as promising materials.

3.2 Introduction

Residential buildings account for approximately 27% and 22% of total energy consumption in the EU [1] and the U.S. [2], respectively, and are a major contributor to global emissions of CO_2 due to the reliance on fossil fuels for electricity and heating [1, 2]. Solar thermal systems have tremendous potential to displace the use of fossil fuels as an energy source in residential buildings because a large fraction of energy consumption is for space heating and hot water. In northern and central European countries, such as Denmark, Germany, and Austria, 86 to 92% of household energy consumption is for space heating and hot water [3]. In the U.S., 57% of the energy consumed in residential buildings is for space heating and hot water [4].

Despite the potential of using solar thermal systems to meet space heating and hot water loads, currently <1% of the energy consumed in EU [3]and U.S. [5] buildings is provided by solar. One impediment to greater market penetration is the high cost of systems [5, 6], particularly for moderate and cold climate regions. In the U.S., the cost to install a residential solar water heater capable of producing 190 to 380 liters of hot water per day is reported to range from $6,000 to $10,000 [5]. The National Renewable Energy Laboratory (NREL) predicts that if the cost could be lowered to $1,000-$3,000, without compromising durability or performance, solar water heaters would be at break-even cost with natural gas, and the market for solar thermal would be transformed [5]. The need to develop low-cost solar collectors is more acute for space heating, which requires larger collector areas.

One pathway to achieve significant cost savings is development of polymeric collectors suitable for all climate zones [5, 7-9]. Currently, most of the solar thermal collectors intended for space heating and domestic hot water use copper absorbers with wavelength selective coatings and a low-iron glass cover. Polymeric collectors offer the potential to significantly reduce the installed cost (at least 50%) by reducing the material and manufacturing costs and by reducing the weight of the collector which in turn reduces the cost of installation [5, 10]. Polymer collectors are the norm for pool heating, but unglazed and un-insulated pool collectors are not suitable for building applications in cool climates. One of the most relevant impediments to the development of glazed, polymer collectors is overheating of the absorber in the summer or during long dormant periods (e.g., when the homeowners are on vacation) [5, 11, 12]. The relative thermal index [13] has been suggested as a recommended maximum service temperature for polymer absorbers [14]. However, with relative thermal indices between 80 and 120 °C [15], the maximum service temperature of polymer absorbers can easily be exceeded under the conditions discussed. A low cost, passive overheat protection mechanism is needed to successfully launch glazed polymer collectors to the market.

Numerous approaches to overheat protection have been suggested for flat plate collectors. They can be divided into two broad categories: 1) those that increase thermal losses from the collector, and 2) those that decrease incident radiation at the absorber. Methods for increasing the thermal losses include various approaches to circulate cooling fluid through the collector [16-23], venting [18, 24-30], and evaporative cooling [24]. These methods often require additional hardware, active control, and increase parasitic energy. Venting is ineffective unless it can be implemented above and below the absorber plate [24]. However venting below the collector necessitates the removal of insulation which decreases collector performance during times when overheat protection is not needed. Venting may also introduce atmospheric contaminants and moisture into the collector thus degrading performance and potentially promoting material degradation [18]. Evaporative cooling is effective when combined with venting [24], but requires active pumping to maintain a saturated evaporation surface.

Methods for decreasing the incident radiation at the absorber include shading systems [18], prismatic glazing [31], and the addition of thermotropic material to either the glazing or absorber [11, 12, 32, 33]. Shading systems and prismatic glazing both require active control.

Thermotropic materials hold out the promise of low cost, passive overheat protection [11, 12, 33, 34]. By definition, the transmittance and reflectance of these materials depend on temperature [35, 36]. Overheat protection is provided when the material switches from highly transparent below the switching temperature to reflective above this temperature (Figure 3-1). In normal operation of a collector, the transmission of incident solar radiation through the thermotropic material is high and the collector operates at high efficiency. When overheat protection is needed, a significant portion of the incident radiation is reflected by the thermotropic material, thus preventing the absorber from exceeding its maximum service temperature. The high transmittance state is referred to as the clear state while the high reflectance state is referred to as the translucent state. The thermotropic material can be added to the glazing or the absorber but is most effective if it is in direct contact with the absorber [37].

For a thermotropic material to be used for overheat protection it must withstand temperatures below freezing (for cool climates) to temperatures near the relative thermal index of the absorber material. The switching temperature of the thermotropic material should be slightly less than the relative thermal index of the absorber material. The switch should occur over a small

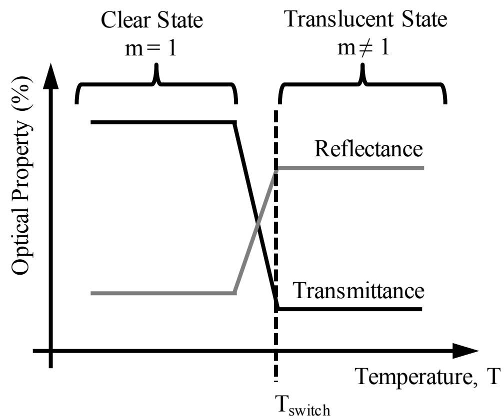

Figure 3-1 Desired change in optical properties with temperature for thermotropic materials used for overheat protection in polymer solar collectors.

temperature range, and it must be reliable over many repetitions. It has been suggested that to provide adequate overheat protection while minimizing any detrimental effect of the thermotropic material on the collector efficiency during normal operation, a thermotropic material should have a solar-weighted transmittance ≥85% in the clear state and ≤60% in the translucent state [37].

The focus of efforts to develop thermotropic materials for solar collectors is phase change thermotropic materials [32, 33, 38]. These materials have discrete particles, collectively referred to as the scattering domain, embedded in a matrix material. As illustrated by Figure 3-2, ideally, below the switching temperature, the refractive indices of the particles and matrix are equal and the relative index of refraction, *m,*

$$m \equiv \frac{n_{particle}}{n_{matrix}}, \tag{3.1}$$

equals unity. In this situation, radiation propagates through the material unattenuated (assuming absorption is negligible). Above the switching temperature, the particles change phase and the refractive indices are unequal ($m \neq 1$); radiation is scattered by the particles and the material reflects a portion of the incident solar radiation. The most significant change in relative refractive index occurs when the scattering domain melts because it is across the phase change that the most

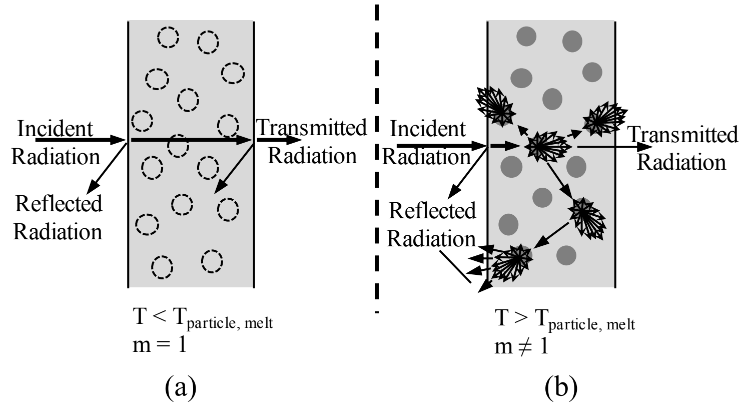

Figure 3-2 Schematic of radiation scattering by phase change thermotropic materials in the (a) clear state (Ideally, m = 1) and the (b) translucent state (m ≠ 1). Note: radiation reflected at the interface is shown at an angle for clarity.

significant change in density, ρ, and thus refractive index of the scattering domain, $n_{particle}$, occurs. The matrix material, however, should remain in the solid phase and thus undergo very little change in refractive index, n_{matrix}.

In addition to relative refractive index, the size of the particles is an important parameter. The particle size is expressed in dimensionless form as the particle size parameter x:

$$x = \frac{2\pi a}{\lambda}. \tag{3.2}$$

In eq. (3.2), a is the particle radius and λ is the wavelength of the incident radiation. The larger the value of x, the more effectively radiation will be scattered by the particles, but the angle between the incident and scattered directions will be smaller [39]. Conversely, the smaller the value of x, the less effectively radiation will be scattered, but the angle between the incident and scattered directions will be larger [39]. Thermotropic materials rely on multiple scattering events to effect significant change in the optical properties; therefore, the volume fraction of particles, f_v, and the thickness, L, of the material influence the transmittance and reflectance. In phase change thermotropic materials, only the relative refractive index, m, is a function of temperature. Volume fraction, thickness, and particle size are independent of temperature.

Prior theoretical studies of radiative transfer in thermotropic materials have examined the effects of particle size [40, 41], and material thickness [41] but have been restricted to specific materials. Nitz, et al. [40] suggest a particle radius of 150 to 350 nm to achieve maximum reflectance in the translucent state. Wilson and Eck [41] predict that the solar-weighted, normal-hemispherical transmittance of a non-absorbing material with m = 1.06, a particle radius of 500 nm, and a volume fraction of 40% will decrease from 83.7% at L = 1 μm to 40.3% at L = 1600 μm. However, this prediction must be used carefully as the assumption of independent scattering is likely invalid at the high volume fraction considered. The identification of potential thermotropic material combinations based on the relative refractive index of the two materials in the clear and translucent state has not been considered in prior work and is one focus of the present work.

This paper provides a theoretical basis for the identification of thermotropic material combinations. To achieve this objective, a parametric study of radiative transfer in thermotropic materials is conducted, and the results of the study are presented in dimensionless form. The thermotropic materials are modeled as a thin, non-absorbing slab containing spherical particles. The transmittance and reflectance of the slab are determined by a Monte Carlo ray tracing algorithm. The process of using the dimensionless results to identify potential thermotropic material combinations is discussed and utilized to identify promising combinations.

3.3 Model

The thermotropic material is modeled as a slab of uniform thickness, L, irradiated on the z = 0 interface at normal incidence with monochromatic radiation of wavelength, λ (Figure 3-3). The slab comprises a matrix material with index of refraction, n_{matrix}, and monodispersed, randomly distributed, spherical particles with radius, a, and index of refraction, $n_{particle}$, at a

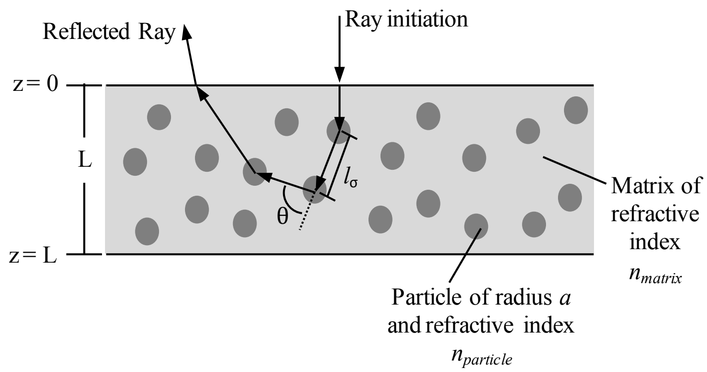

Figure 3-3 The computational domain. Arrows indicate the 2D tracking process of the Monte Carlo ray tracing algorithm. Actual simulation is in 3D.

volume fraction, f_v. Independent scattering by the particles is assumed and volumetric absorption is neglected. The assumption of independent scattering is valid when the average distance between particles divided by λ is greater than 0.5 [42]. For the range of particle sizes considered ($0.5 \leq x \leq 7$), this ratio is greater than 0.5 for $f_v \leq 10\%$ [42]. The material is modeled as non-absorbing because it is undesirable for a thermotropic material to absorb a significant portion of the incident radiation. To neglect absorption, the scattering albedo, ω

$$\omega = \frac{\sigma_s}{\beta}, \tag{3.3}$$

of the material must be near unity. For $\omega \approx 1$, the extinction coefficient, β, must approximate the scattering coefficient, σ_s; this requirement implies that the dominate means of radiation attenuation is scattering. For thin polymer thermotropic materials, attenuation is expected to be dominated by scattering for much of the visible and near infrared spectrum because polymers which have high transmittance in the solar spectrum, and thus are suitable candidates for the matrix material, are weak absorbers at those wavelengths. For example, Khashan and Nassif (2001) [43] report a spectral absorptance of less than 2% for a 2.4 mm thick sample of poly(methyl methacrylate) for $400 \leq \lambda \leq 1000$ nm. The wavelengths at which suitable polymers are stronger absorbers are generally less than 400 nm (due to electron excitation) or greater than 1000 nm (due to vibration of atoms or chemical bonds).

At the interface of the slab and the surrounding media (air), radiation can be reflected or transmitted, due to a difference in refractive index of the air and the slab. To calculate the reflectivity of the interface, a refractive index of 1.5, which is representative of the data reported for polymers [44], is used in the model (the only exception is for experimental validation of the model as described in section 3). Inside the slab, the radiation propagates until incident upon an embedded particle. The particle scatters the radiation. The process of scattering and internal reflections is repeated, as shown in Figure 3-3, until the radiation is either transmitted through the slab (the radiation exits at z = L) or reflected out of the slab (radiation exits at z = 0). Specular reflection is assumed at the interface.

Volumetric scattering and reflection are governed by the radiative transfer equation (RTE). The RTE is an integral-differential equation which describes the change in radiative intensity, *I*, along the direction of propagation, $\hat{\boldsymbol{s}}$. For a non-absorbing, non-emitting medium irradiated with monochromatic radiation, the RTE is

$$\frac{dI}{ds} = -\sigma_s I + \frac{\sigma_s}{4\pi}\int_{\Omega_i}^{4\pi} I(\hat{s}_i)\ \Phi(\hat{s}_i, \hat{s}) d\Omega_i \,. \tag{3.4}$$

The first term on the right hand side of eq. (3.4), the product of the scattering coefficient, σ_s, and radiative intensity, *I*, represents the radiative intensity scattered out of $\hat{\boldsymbol{s}}$. Physically σ_s is the inverse of the mean free path length travelled by a ray of radiation before being scattered. The second term is the radiative intensity scattered into $\hat{\boldsymbol{s}}$ from all other directions, $\hat{\boldsymbol{s}}_i$. The integrand of the second term includes the scattering phase function, Φ, which describes the probability that radiation from $\hat{\boldsymbol{s}}_i$ will be scattered into $\hat{\boldsymbol{s}}$.

The RTE is often expressed in terms of the dimensionless optical thickness. The overall optical thickness, τ_L, of a non-absorbing material of thickness, L, with randomly distributed particles of constant radius, a, is:

$$\tau_L = \sigma_s L = \frac{3}{4}\frac{f_v Q_s}{a} L\,, \tag{3.5}$$

where Q_s is the scattering efficiency factor of a single particle. Q_s and Φ are determined by Mie theory. Mie theory is a solution to Maxwell's equations for an electromagnetic wave that is incident upon a single spherical particle embedded in non-absorbing medium [45]. Q_s and Φ are functions of m and x.

A collision Monte Carlo ray tracing technique [46, 47] is used to solve the RTE. Monte Carlo ray tracing techniques track individual photon packages of radiation, referred to as rays, as each photon package propagates through and interacts with the material. The paths of many individual rays ($10^5 - 10^7$) must be tracked to obtain statistically relevant results.

The algorithm begins by launching a ray at normal incidence at the interface of $z = 0$ (Figure 3-3). The reflectivity of the interface and the probability of the ray being reflected are calculated by applying the Fresnel equations for normal incidence. If the ray is reflected, the reflectance count, N_r, is incremented and a new ray is launched. If the ray is transmitted through the $z = 0$ interface, the path length l_σ travelled by the ray is determined by the random number R_σ between zero and unity.

$$l_\sigma = \frac{1}{\sigma_s}\ln\left(\frac{1}{R_\sigma}\right). \tag{3.6}$$

If $l_\sigma < L$, the ray is scattered and the scattering angle, θ, is found by inverting eq. (3.7):

$$R_\theta = \frac{1}{2}\int_{\theta'=0}^{\theta} \Phi(\theta')\sin\theta'\, d\theta'\,. \tag{3.7}$$

The inversion of eq. (3.7) is obtained through numerical integration at intervals of 0.026 radians (~1.5°). Scattered angles within the integration interval are determined by linear interpolation. The scattering phase function, Φ, is calculated by the Mie scattering program BHMIE [45]. The azimuth angle, ψ, of scattered radiation is determined by the random number R_ψ:

$$\psi = 2\pi R_\psi \, . \tag{3.8}$$

Together θ and ψ describe the direction of the ray after scattering. A new l_σ is calculated, and the position vector is updated. The scattering algorithm of eqs. (3.6) – (3.8) is repeated until the ray intersects an interface (either the z =0 or z=L interface). When a ray intersects an interface, the transmissivity of the interface, as a function of the incidence angle is calculated, and another random number is generated. If the generated random number is less than the transmissivity of the interface for the incident angle, the ray is transmitted through the interface. The transmittance count, N_t, is incremented when a ray is transmitted through the z = L interface. Similarly, the reflectance count, N_r, is incremented when a ray is transmitted through the z = 0 interface. If the generated random number is greater than the transmissivity of the interface, the ray is reflected and the scattering algorithm is continued. After N rays, monochromatic, normal-hemispherical reflectance, $\bar{\rho}$, $\bar{\rho}$and transmittance, $\bar{\tau}$, of the slab are determined by,

$$\bar{\rho} = \frac{N_r}{N} \, ; \quad \bar{\tau} = \frac{N_t}{N} \, . \tag{3.9}$$

Subsequently, the spectral, normal-hemispherical transmittance and reflectance are referred to as transmittance and reflectance unless otherwise noted.

3.4 Model Validation

For validation, the model predictions are compared with the analytical solution for a slab of non-absorbing, non-scattering medium, and the measured transmittance of thin polymer samples containing particles. To represent a thermotropic material in the translucent state, the samples were prepared with different scattering domain materials. These materials have different refractive indices and thus different values of *m* are obtained. Because in phase change thermotropic materials, *m* is a function of temperature, evaluating the model at different values of *m* is equivalent to modeling a thermotropic material at various temperatures.

3.4.1 Comparison to Analytical Solution

The analytical solution for the reflectance and transmittance of a slab of non-absorbing, non-scattering (m = 1 or f_v = 0) medium is given in standard reference texts, e.g. [48]. This medium represents the ideal clear state. For n = 1.50, the analytical solutions for transmittance and reflectance are 92.31% and 7.69%, respectively. The model predicts $\bar{\tau}$ = 92.30% and $\bar{\rho}$ = 7.70%. Figure 3-4 shows the agreement of the Monte Carlo predictions to the analytical solution. At 10^4 rays, The Monte Carlo prediction agrees to within 0.1% of the analytical solution. To validate the number of rays used in subsequent simulations, Figure 3-4 also shows the convergence of a highly scattering scenario (m = 0.96, x = 2.5, L = 0.5 mm, and f_v = 10%). The simulation converges at $4x10^4$ rays to <0.1% of the value at 10^7 rays. For all reported simulations, $5x10^5$ rays are tracked.

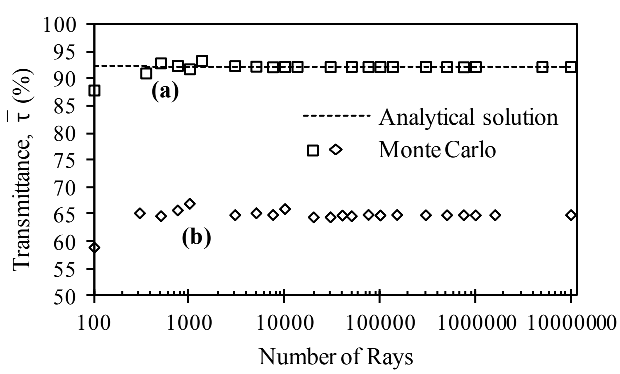

Figure 3-4 Predicted transmittance versus number of rays. (a) Agreement of predicted transmittance to analytical solution for a non-scattering, non-absorbing material with nmatrix = 1.50. (b) Convergence of transmittance for a highly scattering scenario of m = 0.9

3.4.2 Sample Fabrication and Experimental Procedure

For the experimental validation, 0.3 mm thick samples with a matrix of polyvinyl acetate (PVA) (n_{matrix} = 1.47 at 23 °C [44]) and 200 nm radius particles were prepared. Relative indices of refraction, *m*, of 0.973, 1.014, and 1.083 were obtained by using scattering domains of silica (n = 1.43, manufacture provided: bangslabs.com), poly (methyl methacrylate) (PMMA) (n = 1.491, [49]), and polystyrene (PS) (n = 1.592, [49]), respectively. All refractive index values are for a wavelength of 589 nm. For each value of *m*, samples were prepared at a volume fraction of f_v = 9.6 %. Samples with *m* = 1.083 (PS particles in PVA) were also fabricated at volume fractions of 5 and 13.5%. Since $m \neq 1$, the samples represent a thermotropic material that has changed to the translucent state. The scattering albedos of the samples were calculated to between 0.973 and 0.999 and thus radiation attenuation is expected to be dominated by scattering. One sample was prepared without scattering domains (100% matrix material) to represent *m* = 1. All samples were prepared by an aqueous emulsion of PVA and the scattering domain material. The mixture was allowed to equilibrate for one hour before one gram of the mixture was spread onto a 3.8 cm diameter form. The samples were dried on the form at ambient temperature in a fume hood for 20 hours.

For each combination of *m* and f_v, three samples were prepared. The normal-hemispherical, spectral transmittance of each sample was measured using a Lambda 1050 spectrophotometer equipped with a 150 mm integrating sphere. Based on the manufacturer's specifications, the instrument has a photometric accuracy of ±0.003A in the visible spectrum and a wavelength accuracy of ±0.08 nm in the UV/VIS. All measurements were made at 24 °C and repeated twice. The data reported in Figure 3-5 and Figure 3-6 represent the average for that combination m and f_v. The 95% confidence integral about the mean is indicated by the uncertainty bars.

3.4.3 Comparison to Experimental Data

Figure 3-5 compares predicted and measured transmittance at f_v = 9.6% as a function of m. The model predictions are within 8% of the measured data. There is a greater discrepancy between the predicted and the measured value as m approaches unity. Because the model prediction at m = 1 is in excellent agreement with the analytical solution for a non-scattering (m = 1 or f_v = 0%) and non-absorbing material, the increased discrepancy near m = 1 is attributed to defects in the samples. The samples of $m \neq 1$ also have defects but the radiation scattering caused by the defects is minor compared to the scattering due to the embedded particles and, therefore, the model more accurately predicts the transmittance of these samples. For m = 1.014, the prediction is within 5 percentage points of the measured value and for m = 1.083 the model predications are within 1 percentage point. The measured and predicted monochromatic transmittance have a maximum of 85% and 92%, respectively, at m = 1. As the mismatch in refractive indices increases (m < 1 or m > 1), the transmittance decreases. At m = 1.083, the measured transmittance is 52% and the predicted transmittance is 51%.

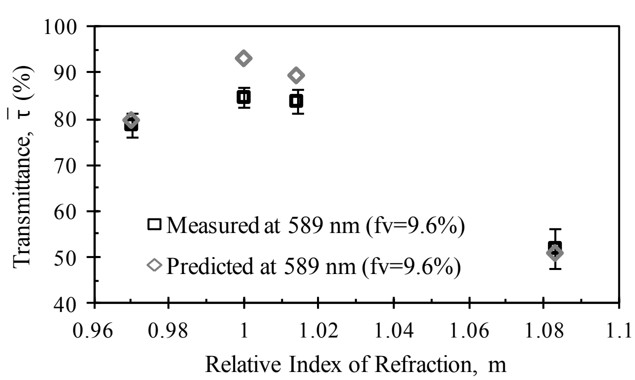

Figure 3-5 Model predictions compared to measured transmittance for fv = 9.6%, a = 200 nm, and L = 0.3mm. The uncertainty bars represent 95% confidence interval.

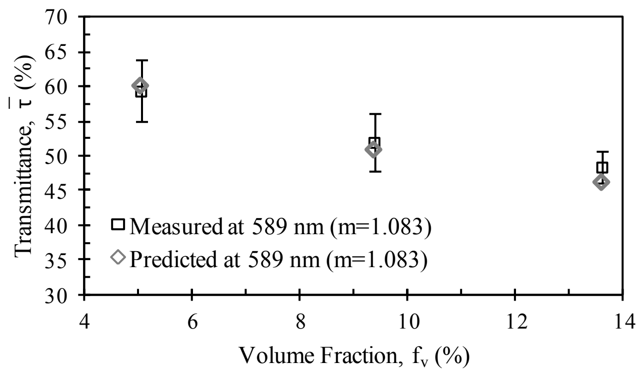

Figure 3-6 Model predictions compared to measured transmittance for m = 1.083, a = 200 nm, and L = 0.3mm. . The uncertainty bars represent 95% confidence interval.

Figure 3-6 shows the predicted and measured monochromatic transmittances as a function of volume fraction, f_v, for m = 1.083. The transmittance decreases with increasing f_v from a measured value of 59% (60% predicted) at f_v = 5% to 48% (46% predicted) at f_v = 13.5%. The difference between the model prediction and the measured values is within two percentage points.

3.5 Results and Discussion

To examine the effects of geometry and material properties on the predicted spectral, volumetric transmittance of thermotropic materials, we constructed the dimensionless plot shown in Figure 3-7of transmittance versus optical thickness for various particle size parameters. The value of Figure 3-7 is that it can be used either to select the two materials that comprise a thermotropic composite based on desired performance criteria (e.g., high transmittance in the clear state and low transmittance in the translucent state), or to predict the transmittance of a specific combination of materials in the clear and translucent states. The transmittance of the composite material is a function of optical thickness, τ_L, and particle size parameter, x. For phase change thermotropic materials, τ_L is a function of temperature while x is a function of particle size

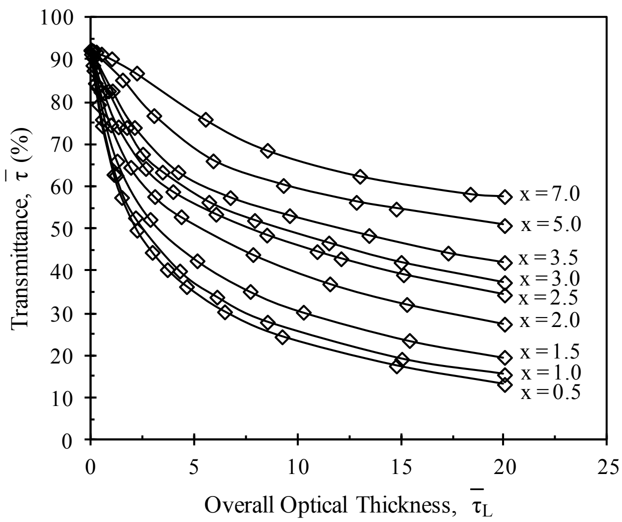

Figure 3-7 Predicted monochromatic transmittance plotted with respect to τ_L and x.

and incident wavelength. The optical thickness is determined using eq. (3.5). The value of scattering efficiency factor, Q_s, required for this calculation is provided, for the convenience of the reader, in Figure 3-8 as a function of the relative index of refraction, m, [45]. The temperature dependency of τ_L is through the temperature dependent value of m. To help identify potential scattering domain and matrix material combinations, the refractive index (at a wavelength of 589nm) as a function of temperature is shown in Figure 3-9 for potential scattering domain materials and in Figure 3-10 for potential matrix materials. The refractive indices are calculated by using the Lorentz and Lorenz equation (shown here solved for the refractive index), and

$$n = \left(\frac{1 + 2\dfrac{\sum_i R_i}{M/\rho}}{1 - \dfrac{\sum_i R_i}{M/\rho}} \right)^{1/2} . \tag{3.10}$$

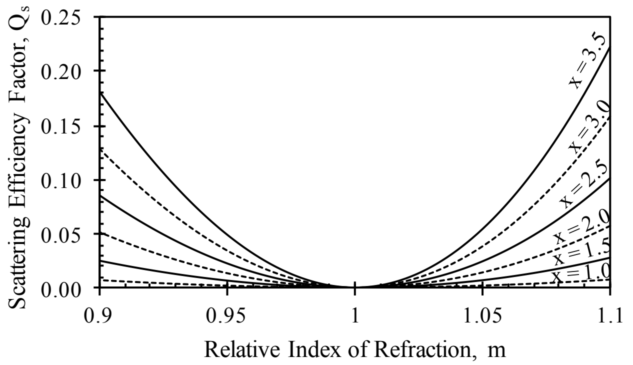

Figure 3-8 Scattering efficiency factor plotted with respect to m. The results are from Mie theory for a single particle (Bohren and Huffman, 1998).

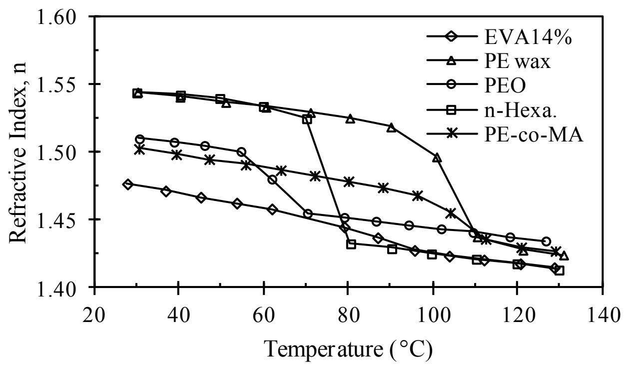

Figure 3-9 Predicted refractive index versus temperature for potential scattering domain polymers. EVA 14% – poly(ethylene-co-vinyl acetate), 14% wt vinyl acetate; PE wax – low molecular weight (M = 1 kg/mol) polyethylene; PEO – polyethylene oxide; n-Hexa. – n-Hexatriacontane; PE-co-MA – poly(ethylene-co-methacrylic acid), 4% wt methacrylic acid

the temperature dependent density, ρ, data from Walsh and Zoller (1995) [50]. The molar refractivity, R, is calculated by summing the contributions of the functional groups present in the molecule [51-53].

First consider the selection of materials to meet desired criteria, for example the criteria suggested by Wallner, et al. (2008) [37]: the solar-weighted transmittance should be ≥85% in the clear state and ≤60% in the translucent state. Using a particle size of $x = 2.5$, Figure 3-7 shows τ_L should be ≤ 0.47 to achieve spectral transmittance ≥ 85% in the clear state, and τ_L should be ≥ 3.68 to achieve spectral transmittance ≤60% in the translucent state. Potential thermotropic

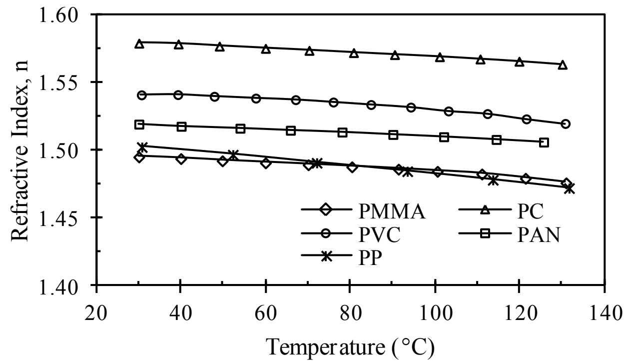

Figure 3-10 Predicted refractive index versus temperature for potential matrix polymers. PMMA – poly(methyl methacrylate); PC – polycarbonate; PVC – poly(vinyl chloride); PAN – polyacrylonitrile; PP – polypropylene.

material combinations can then be identified by using Figure 3-9 and Figure 3-10 and eq. (3.1) to determine the relative refractive index as a function of temperature. Then Figure 3-8 and eq. (3.5) are used to calculate the optical thickness as a function of temperature. Using this approach, one potential material combination is poly(ethylene-co-vinyl acetate) (EVA) in a matrix of poly(methyl methacrylate) (PMMA). For this material combination, the relative refractive is calculated to be $m_{30°C}$ = 0.989 in the clear state and $m_{110°C}$ = 0.958 in the translucent state. To achieve the desired optical thickness in each state for this material combination, one option is to use a volume fraction of f_v = 10% and a thickness of L = 0.75 mm. In this case, the optical thickness increases from 0.3 at 30 °C to 4.2 at 110 °C which corresponds to a decrease in transmittance, as shown in Figure 3-11, from 87% to 58%. Another potential thermotropic combination is n-hexatriacontane ($C_{36}H_{74}$) in a matrix of polycarbonate ($m_{30°C}$ = 0.9777; $m_{110°C}$ = 0.907). For f_v = 5% and L = 0.5 mm, the optical thickness increases from 0.4 at 30 °C to 6.6 at 110 °C (Figure 3-11). Correspondingly, the transmittance decreases from 86% at 30 °C to 52% at 110 °C. Additionally, this combination of materials is expected to have a sharp change in transmittance with temperature because n-hexatriacontane has a distinct melting temperature for a polymer (Figure 3-9).

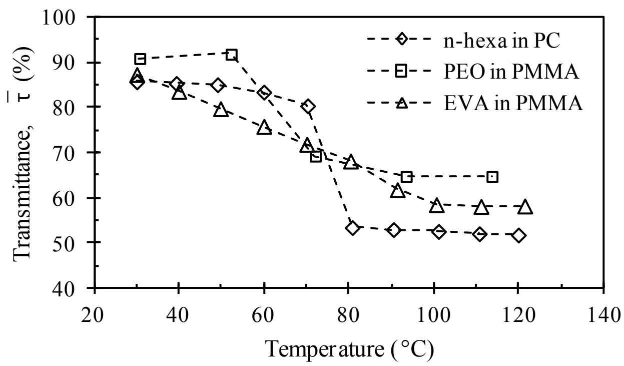

Figure 3-11 Predicted transmittance (at λ = 589 nm) vs. temperature for n-hexatriacontane in a matrix of PC (x = 2.5, fv = 5%, L = 0.5mm); EVA in a matrix of PMMA (x = 2.5, fv = 10%, L = 0.75mm); and PEO in a matrix of iPP (x = 2.5, fv = 10%, L = 1.0mm).

Now consider the use of Figure 3-7 to predict the transmittance of a specific combination of scattering domain and matrix materials. For example, consider the selection of poly(ethylene oxide) as the scattering domain and polypropylene as the matrix material. This selection is reasonable because the refractive indices match at 30 °C (m = 1.005). Using Figure 3-9 and Figure 3-10, the relative refractive index is found to be 0.974 at 93 °C. For L = 1.0 mm, f_v = 10%, and x = 2.5, the overall optical thickness is 0.08 at 30 °C and 2.55 at 93 °C. Using Figure 3-7, the predicted

transmittance is 91.1% at 30 °C and 65% at 93 °C as shown by Figure 3-11. Repeating the process, Figure 3-7 can be used to predict the transmittance as a function of temperature for other thickness, volume fraction, and particle size combinations.

To further illustrate how the selection of the matrix and scattering domain materials affects the transmittance of the thermotropic composite, Figure 3-12 is presented. This figure shows the transmittance as a function of relative refractive index, m, for three volume fractions, f_v = {2.5%, 5%, 10%}. For this figure, a particle radius of 187 nm is selected in accordance with the recommendation of Nitz, et al. (1998) [35]. At an incident wavelength of 589 nm, this particle radius corresponds to a particle size parameter of 2. The thickness of L = 1mm is representative

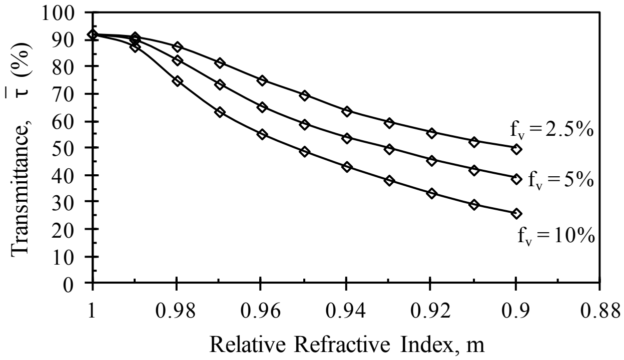

Figure 3-12 Predicted transmittance as a function of relative refractive index for a = 187 nm, λ = 589 nm, and L = 1 mm.

of published phase change thermotropic materials [33, 54]. Figure 3-12 shows that transmittance is more sensitive to a change in relative refractive index than to volume fraction. For example, at m = 0.97, doubling the volume fraction (from f_v = 5% to 10%) corresponds to a 14% decrease in transmittance. However decreasing the relative refractive index by only 5% (from m = 0.97 to 0.92) results in a 38% decrease in transmittance, at f_v = 5%. Therefore, Figure 3-12 demonstrates how crucial the selection of both materials is on the effectiveness of a thermotropic material. A potential scattering domain material cannot be vetted based solely on its change in refractive index with temperature, but consideration must also be given to the matrix material with which it will be combined.

3.6 Conclusion

Thermotropic materials have the potential to provide a means for passive overheat protection of polymer solar absorbers because their optical properties depend on temperature. The present work presents a parametric study of radiative transfer in thermotropic materials. This study provides a theoretical basis for the selection of scattering domain and matrix material combinations based on a model of radiative transfer in a matrix containing a dispersed phase of particles.

The model results show the importance of the relative refractive index of the two materials in assuring a change in transmittance with temperature. Based on optical properties, potential thermotropic material combinations are identified for use as overheat protection: poly(ethylene-co-vinyl acetate) as the scattering domain material in a matrix of poly(methyl methacrylate), and relatively short chain alkanes such as n-hexatriacontane in a matrix of polycarbonate. Other potential thermotropic material combinations can be identified using the process outlined in the text. Additional considerations for selecting materials include crystallinity and manufacturing compatibility of the constituents.

3.7 Acknowledgements

Sample fabrication was carried out by Jihua Zhang of Prof. Marc Hillmyer's research group in the Department of Chemistry at the University of Minnesota. This research is funded by the University of Minnesota Initiative for Renewable Energy and the Environment (IREE) and by the National Renewable Energy Laboratory (NREL).

3.8 Nomenclature

Latin Symbols

a	radius of scattering domain (nm)
f_v	volume fraction of scattering domains (%)
I	radiative intensity ($W \cdot m^{-2} \cdot sr^{-1}$)
L	material thickness (mm)
l_σ	path length travelled by ray (mm)
m	relative index of refraction
M	molar mass ($kg \cdot mol^{-1}$)
$n_{particle}$	refractive index of scattering domains material
n_{matrix}	refractive index of matrix material
N	total number of rays used in Monte Carlo simulation
N_r	number of rays reflected

N_t	number of rays transmitted
Q_s	scattering efficiency factor
R	molar refractivity ($cm^3 \cdot mol^{-1}$)
R_σ	random number used to determine the path length
R_θ	random number used to determine the scattering angle
R_ψ	random number used to determine the azimuth
$\hat{\mathbf{s}}$	unit vector describing direction of ray
$\hat{\mathbf{s}}_\mathbf{i}$	unit vector describing direction of radiation before being scattered into $\hat{\mathbf{s}}$
x	particle size parameter
z	direction of material thickness

Greek Symbols

β	extinction coefficient (mm^{-1})
θ	scattering angle (radians)
λ	wavelength of incident radiation (nm)
ρ	density ($kg \cdot m^{-3}$)
$\bar{\rho}$	slab reflectance (%)
σ_s	scattering coefficient (mm^{-1})
τ_L	overall optical thickness
$\bar{\tau}$	slab transmittance (%)
$\bar{\tau}_{solar}$	solar-weighted transmittance (%)
Φ	scattering phase function
ψ	azimuth angle (radians)
Ω	Solid angle (sr)
ω	scattering albedo

3.9 References

[1] European Commission, "Energy Markets in the European Union in 2011," 2011, http://ec.europa.eu/energy/observatory/annual_reports/annual_reports_en.html **2013**(08/08).

[2] U.S. Energy Information Agency, 2011, "2011 Annual Energy Review 2011," http://www.eia.gov/totalenergy/data/annual/index.cfm#consumption, **2013**(08/08) .

[3] Weiss, W., and Biermayr, P., 2006, "Potential of Solar Thermal in Europe," European Solar Thermal Industry Federation, http://www.estif.org/, **2013**(08/08) .

[4] U.S. Energy Information Agency, 2009, "2009 Residential Energy Consumption Survey - Consumption and Expenditure Tables (by End use)," http://www.eia.gov/consumption/residential/data/2009/index.cfm?view=consumption#end-use, **2013**(01/30) .

[5] Hudon, K., Merrigan, T., Burch, J., 2012, "Low-Cost Solar Water Heating Research and Development Roadmap," National Renewable Energy Laboratory (NREL). Technical Report. NREL/TP-550054793.

[6] Merrigan, T., 2007, "Solar Heating & Lighting: Solar Water Heating R&D - DOE Solar Energy Technologies Program," DOE Solar Energy Technologies Program Peer Review meeting. April 17-19, 2007, Denver, CO, .

[7] Fischer, S., Druck, H., Bachmann, S., 2012, "Polymeric Materials for Solar Thermal Applications,"Wiley-VCH Verlag & Co., Weinheim, German, pp. 73-106, Chap. 4.

[8] Rhodes, R. O., 2010, "Polymer Thin-Film Design Reduces Installed Cost of Solar Water Heater," Proceedings of the 39th ASES national Solar Conference;, May 17-20, 2010. Phoenix, AZ, pp. 1588.

[9] Tsilingiris, P. T., 1999, "Towards Making Solar Water Heating Technology feasible—the Polymer Solar Collector Approach," Energy Conversion and Management, **40**(12) pp. 1237-1250.

[10] Burch, J., Merrigan, T., Jorgensen, G., 2006, "Low-Cost Residential Solar Thermal Systems," DOE Solar Energy Technologies Program Peer Review meeting. April 17-19, 2007. Denver, CO USA.

[11] Resch, K., Hausner, R., and Wallner, G. M., 2009, "All Polymeric Flat-Plate Collector — Potential of Thermotropic Layers to Prevent Overheating," Proceedings of ISES World Congress 2007 (Vol. I – Vol. V), D. Y. Goswami and Y. Zhao, eds. Springer Berlin Heidelberg, pp. 561-565.

[12] Resch, K., and Wallner, G. M., 2009, "Thermotropic Layers for Flat-Plate collectors—A Review of various Concepts for Overheating Protection with Polymeric Materials," Solar Energy Materials and Solar Cells, **93**(1) pp. 119-128.

[13] UL746B, 1998, "Polymeric Materials - Long Term Property Evaluations. " Underwriters Laboratories, Inc., Northbrook, IL.

[14] Raman, R., Mantell, S., Davidson, J., 2000, "A Review of Polymer Materials for Solar Water Heating Systems," Transactions-ASME Journal of Solar Energy Engineering, **122**(2) pp. 92-100.

[15] Mantell, S.C., and Davidson, J.H., 2012, "Polymeric Materials for Solar Thermal Applications,"Wiley-VCH Verlag & Co., Weinheim, German, pp. 187-210, Chap. 10.

[16] Baer, S. C., 1985, "Thermal Control System for Solar Collector," US Patent (4,528,976).

[17] Buckley, B. S., and Guldman, T. A., 1983, "Method and Apparatus for Overtemperature Control of Solar Water Heating System," US Patent (4,399,807).

[18] Harrison, S., and Cruickshank, C. A., 2012, "A Review of Strategies for the Control of High Temperature Stagnation in Solar Collectors and Systems," Energy Procedia, **30** pp. 793-804.

[19] Harrison, H. C., 1979, "Protective Cooling System for Solar Heat Collector," US Patent (4,153,040).

[20] Kusyy, O., and Vajen, K., 2011, "Theoretical Investigation on a Control-based Approach to Avoid Stagnation of Solar Heating Systems," Proceeding of ISES Solar World Congress, Kassel, Germany, Kassel, Germany, pp. 3323-3330.

[21] Laing, K., 1985, "Intermittent through-Flow Collector," US Patent (4,519,380).

[22] Wylie, R., 1993, "Passive Three-Phase Heat Tube for the Protection of Apparatus from Exceeding Maximum Or Minimum Safe Working Temperatures," US Patent (5,135,575) .

[23] Palmatier, E. P., 1983, "Solar Heating System," US Patent (4,384,568) .

[24] Kearney, M., Davidson, J., and Mantell, S., 2005, "Polymeric Absorbers for Flat-Plate Collectors: Can Venting Provide Adequate Overheat Protection?" Journal of Solar Energy Engineering, **127**(3) pp. 421-424.

[25] Mahdjuri, F., 1999, "Solar Collector with Temperature Limitation using Shape Memory Metal," Renewable Energy, **16**(1) pp. 611-617.

[26] Rich, A. C., 1995, "Solar Collector Venting System," US Patent (5,404,867) .

[27] Roberts, J., Brandemuehl, M., Burch, J., 2000, "Overheat Protection for Solar Water Heating Systems Using Natural Convection Loops," Proceedings of the Solar Conference, American Solar Energy Society; American Institute of Architects, pp. 273-278.

[28] Russell, L., and Guven, H., 1982, "Modeling and Analysis of an all-Plastic Flat-Plate Solar Collector," J.Sol.Energy Eng., **104**(4) pp. 333-339.

[29] Scharfman, H., 1977, "Vented Solar Collector," US Patent (4,043,317) .

[30] Scott, P. B., 1977, "Solar Heater with Automatic Venting," US Patent (4,046,134) .

[31] Slaman, M., and Griessen, R., 2009, "Solar Collector Overheating Protection," Solar Energy, **83**(7) pp. 982-987.

[32] Resch, K., Wallner, G. M., and Hausner, R., 2009, "Phase Separated Thermotropic Layers Based on UV Cured Acrylate Resins – Effect of Material Formulation on Overheating Protection Properties and Application in a Solar Collector," Solar Energy, **83**(9) pp. 1689-1697.

[33] Weber, A., and Resch, K., 2012, "Thermotropic Glazings for Overheating Protection," Energy Procedia, **30** pp. 471-477.

[34] Ruhmann, R., Seeboth, A., Muehling, O., 2013, "Thermotropic Materials for Adaptive Solar Control," Advances in Science and Technology, **77** pp. 124-131.

[35] Nitz, P., and Hartwig, H., 2005, "Solar Control with Thermotropic Layers," Solar Energy, **79**(6) pp. 573-582.

[36] Seeboth, A., Ruhmann, R., and Muehling, O., 2010, "Thermotropic and Thermochromic Polymer Based Materials for Adaptive Solar Control," Materials, **3**(12) pp. 5143-5168.

[37] Wallner, G. M., Resch, K., and Hausner, R., 2008, "Property and Performance Requirements for Thermotropic Layers to Prevent Overheating in an All Polymeric Flat-Plate Collector," Solar Energy Materials and Solar Cells, **92**(6) pp. 614-620.

[38] Weber, A., Schlögl, S., and Resch, K., 2013, "Effect of Formulation and Processing Conditions on Light Shielding Efficiency of Thermotropic Systems with Fixed Domains Based on UV Curing Acrylate Resins," Journal of Applied Polymer Science, **130**(5) pp. 3299-3310.

[39] Modest, M., 2003, "Radiative Heat Transfer, Second Edition,"Academic Press, USA, Chap. 11.

[40] Nitz, P., Ferber, J., Stangl, R., 1998, "Simulation of Multiply Scattering Media," Solar Energy Materials and Solar Cells, **54**(1-4) pp. 297-307.

[41] Wilson, H., and Eck, W., 1992, "Transmission Variation using scattering/transparent Switching Layers," Proceedings of SPIE, **1728**(1) pp. 261-11.

[42] Tien, C. L., and Drolen, B., 1987, "Thermal radiation in particulate media with dependent and independent scattering," In: Annual review of numerical fluid mechanics and heat transfer.

Volume 1 (A88-18971 06-34). Washington, DC, Hemisphere Publishing Corp., 1987, p. 1-32. **1,** pp. 1-32.

[43] Khashan, M., and Nassif, A., 2001, "Dispersion of the Optical Constants of Quartz and Polymethyl Methacrylate Glasses in a Wide Spectral Range: 0.2–3 Mm," Optics Communications, **188**(1) pp. 129-139.

[44] Gooch, J.W., 2011, "Encyclopedic Dictionary of Polymers, 2nd ed." Springer Science & Business Media, New York, NY USA, pp. 520.

[45] Bohren, C.F., and Huffman, D.R., 1998, "Absorption and Scattering of Light by Small Particles," Wiley-Interscience, pp. 530.

[46] Farmer, J.T., and Howell, J.R., 1998, "Advances in Heat Transfer,"Elsevier, pp. 333-429.

[47] Modest, M., 2003, "Radiative Heat Transfer, Second Edition,"Academic Press, USA, pp. 644-679, Chap. 20.

[48] Modest, M., 2003, "Radiative Heat Transfer, Second Edition,"Academic Press, USA, pp. 31-60, Chap. 2.

[49] Kasarova, S. N., Sultanova, N. G., Ivanov, C. D., 2007, "Analysis of the Dispersion of Optical Plastic Materials," Optical Materials, **29**(11) pp. 1481-1490.

[50] Walsh, D., and Zoller, P., 1995, "Standard Pressure Volume Temperature Data for Polymers," Technomic Publishing Company, Inc. Lancaster, PA USA.

[51] Goedhart, D., 1969, "Communication Gel Permeation Chromatography International Seminar," Monaco, Oct 12-15.

[52] Krevelen, D.W.v., and Nijenhuis, K., 2009, "Properties of Polymers - Their Correlation with Chemical Structure; Their Numerical Estimation and Prediction from Additive Group Contributions (4th, Completely Revised Edition)," Elsevier, Chp. 10.

[53] Schael, G. W., 1964, "Determination of Polyolefin Film Properties from Refractive Index Measurements," Journal of Applied Polymer Science, **8**(6) pp. 2717-2722.

[54] Muehling, O., Seeboth, A., Haeusler, T., 2009, "Variable Solar Control using Thermotropic core/shell Particles," Solar Energy Materials and Solar Cells, **93**(9) pp. 1510-1517.

4 A Parametric Numerical Study of Optical Behavior of Thermotropic Materials for Solar Thermal Collectors

Published in the ASME Journal of Heat Transfer

4.1 Summary

A Monte Carlo model is applied to determinate the steady state, solar-weighted optical properties of potential thermotropic composite materials for overheat protection of polymer solar absorbers. The key results are dimensionless plots of normal-hemispherical transmittance, reflectance and absorptance as a function of particle size parameter, scattering albedo, and overall optical thickness. The optical behavior of thermotropic materials at different temperatures is represented by a change in the relative refractive index which affects the scattering albedo and optical thickness. At low temperatures where overheat protection is not required, referred to as the clear state, the overall optical thickness should be less than 0.3 to ensure high transmittance for the preferred particle size parameter of 2. At higher temperatures where overheat protection is required, referred to as the translucent state, the overall optical thickness should be greater than 10 and the scattering albedo should be greater than 0.995 to achieve 50% reflectance. A case study of low molecular weighted polyethylene in poly(methyl methacrylate) is presented to illustrate use of the results to guide the design of thermotropic materials.

Key Words
Thermotropic, Optical, Overheat Protection, Absorber

4.2 Introduction

Hot water accounts for 18% of energy consumption in residential buildings in the United States [1]. Depending on the aperture area, tank volume, hot water demand, and geographic location, domestic solar thermal hot water systems can provide 40 to over 95% of the hot water energy requirements [2]. Despite this potential, adoption of solar thermal collectors for domestic hot water has been limited by the payback period required to recoup the initial system cost [3, 4].

Glazed solar thermal collectors constructed of commodity polymers offer the potential to reduce the initial cost [3, 5-7], but overheat protection of the absorber is required to avoid exceeding the maximum allowable temperature of the polymer [8-10]. The relative thermal index, defined as the temperature at which there is 50% reduction in mechanical properties (impact resistance, strength, or stiffness) after conditioning 100,000 hours at that temperature [11], is recommended as the maximum allowable temperature for polymers for this application [12]. Commodity polymers such as polyethylene (PE) and polypropylene (PP) have a relative thermal index of 105 and 115°C, respectively [13]. Such temperatures could easily be exceeded during periods when there is no hot water demand, referred to as stagnation. Simulations of glazed polymer collectors in Phoenix, AZ and Minneapolis, MN indicate that stagnation temperatures could exceed 100°C for 2169 and 1012 hours per year, respectively [8].

One proposed approach to control the temperature of polymer absorbers is the addition of a thin layer of thermotropic material to the surface of the absorber [9, 14, 15]. Thermotropic materials are dispersed media with optical properties that change as a function of temperature [16, 17]. Ideally when the temperature of a solar absorber is lower than the relative thermal index, the thermotropic material is in a 'clear state' characterized by high transmittance. When the temperature of the absorber approaches the relative thermal index, the thermotropic material switches from the clear to a 'translucent state', characterized by low transmittance and high reflectance. It has been suggested that a thermotropic material should have a solar weighted transmittance ≥85% in the clear state and ≤60% in the translucent state [15]. However, the recommendation of 60% transmittance in the translucent state is for a maximum absorber temperature of 130 °C which exceeds the relative thermal index temperature of many commodity polymers. Using the relative thermal index of polypropylene, the solar-weighted reflectance in the translucent state should be ≥50% to prevent the stagnation temperature from exceeding 115 °C for the worst case conditions (1200 W/m^2 normal irradiation, ambient temperature of 30 °C, no wind) suggested by [15].

The focus of efforts to develop thermotropic materials for solar collectors is phase change thermotropic materials [14, 18-20]. As illustrated in Figure 4-1, these materials have discrete particles, collectively referred to as the scattering domain, embedded in an optically clear matrix material. Ideally, in the clear state, the refractive indices of the two materials are equivalent and the real part of the relative index of refraction, *m*, is equal to

$$m = \frac{n_{particle}}{n_{matrix}} \tag{4.1}$$

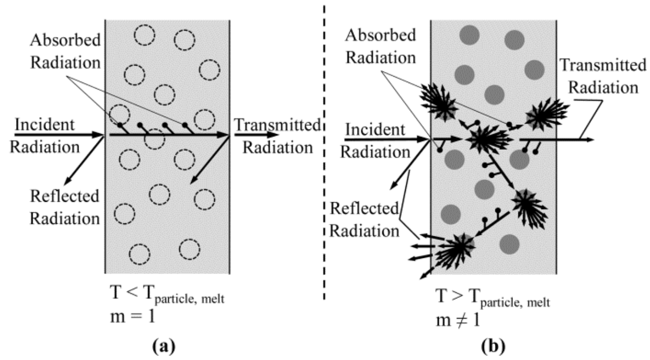

Figure 4-1 Schematic of radiation scattering by phase change thermotropic materials in the (a) clear state and (b) translucent state. Reflection is shown at an angle for clarity.

unity. In this situation, volumetric scattering by the particles is insignificant and transmission in the solar spectrum is excellent. At or near the thermal index temperature, the scattering domain undergoes a phase change which is accompanied by a significant change in density and thus refractive index. In this case, $m \neq 1$ and transmittance is reduced significantly due to the increase in volumetric reflection (Figure 4-1b). The change in refractive index with density is described by the Lorentz-Lorenz equation [21, 22]. In a single scattering event, most of the radiation is forward scattered, in accordance with the scattering phase function, at small angles relative to the direction of propagation of the incident radiation. However, at each scattering event, a fraction of the radiation incident on the particle is scattered toward the irradiated interface of the thermotropic material (Figure 4-1), and thus multiple scattering events yield a cumulative increase in reflectance.

To date, numerous phase change thermotropic materials have been evaluated [17-20, 23-30], but none meets the dual requirements of high transmittance in the clear state and high reflectance in the translucent state. Muehling, et al. [25] used a mixture of n-octadecane/n-eicosane/n-docosane/n-tetracosane as the scattering domain in an acrylate-based UV curable resin, at a 6% weight concentration of particles and a sample thickness of 1.7 mm. The two samples with the most significant change in solar-weighted transmittance changed from 75% and 69% in the clear state to 54% and 41%, respectively, in the translucent state [25]. The material has been commercialized as Solardim®-Eco (http://www.thermotropic-polymers.com/). Resch, et al. [18] utilized a wax for the scattering domain and a UV-cured resin for the matrix. The material was 0.8 mm thick and contained 5% weight concentration of particles. The best performing samples, based on a change in transmittance with temperature, had solar-weighted transmittances of 87% and 83% in the clear state, and 75 and 69%, respectively, in the translucent state [18]. In a study of 36 unspecified material combinations, the two combinations with the most significant change in solar-weighted transmittance changed from 80 and 77% in the clear state to 68% and 64%, respectively, in the translucent state [20]. In the study, all samples were prepared at a thickness of 0.9 mm and a weight fraction of 5% of scattering domain material [20]. A recent study by the same research group considered 24 scattering domain materials and 7 matrix materials. The matrix materials consisted of both thermoplastics and UV curable resins. From these two groups of materials, 43 combinations were evaluated. Samples 0.8 mm (UV curable resin matrix) or 0.9 mm (thermoplastic matrix) thick were fabricated at a theoretical weight faction of 5% of scattering domain material [29]. The resulting materials did not perform significantly better than previous thermotropic materials. The best performing samples, were glycerine monostearate in a matrix of polyester acrylate ($\bar{\tau}_{solar}$ = 76% to 67%) and fatty acids in a matrix of aromatic urethane acrylate ($\bar{\tau}_{solar}$ = 79% to 71%), epoxy acrylate ($\bar{\tau}_{solar}$ = 72% to 60%), or polyester acrylate ($\bar{\tau}_{solar}$ = 79% to 65%) [29]. The limited change in transmittance was attributed to the large particle diameter (1 to 100 μm) [19, 30-32] and sample defects [30, 32]. Nitz, et al. [33] suggest using a particle radius of 150 to 350 nm to achieve maximum reflectance in the translucent state.

Development of thermotropic materials based solely on an empirical approach employing extensive laboratory tests performed on numerous variants of existing materials has met with limited success. This limitation is due, in part, because of a poor understanding of the effects of material choice, particle size, volume fraction, and slab thickness on the optical behaviour in the clear state versus the translucent state. In prior work, the authors suggest potential thermotropic material combinations based on predictions of the normal-hemispherical transmittance in both states at 589 nm for non-absorbing slabs [14]. The present work expands the model to consider absorption and provides a parametric examination of the effects of the relative refractive index, *m*, the particle size parameter, *x*,

$$x = \frac{2\pi a}{\lambda} \tag{4.2}$$

the absorptive index, *k*, the thickness, *L*, and the volume fraction of the disperse phase, f_v, on the normal-hemispherical transmittance, reflectance, and absorptance (for the solar spectrum) in the clear and the translucent states. Results are presented in dimensionless form in terms of the particle size parameter, *x*, the scattering albedo, ω, and the overall optical thickness, τ_L. The model captures the steady state behavior in the two states. Interpretation of the results is illustrated through presentation of a case study of low molecular weight (<1k) polyethylene (PE) dispersed in a matrix of poly(methyl methacrylate) (PMMA). The spectral refractive indices of the two materials are obtained from the literature [34, 35]. The spectral absorptive index is determined experimentally as discussed in section 4.5.2.

4.3 Model Description

The thermotropic material is modeled, as shown in Figure 4-2, as a slab of uniform thickness, L, irradiated with collimated radiation of wavelength, λ, at normal incidence. The slab comprises a matrix material with complex index of refraction, N_{matrix},

$$N_{matrix} = n_{matrix} - ik_{matrix} \tag{4.3}$$

and monodispersed, randomly distributed, spherical particles with radius, a, and complex index of refraction, $N_{particle}$,

$$N_{particle} = n_{particle} - ik_{particle} \tag{4.4}$$

at a volume fraction, f_v.

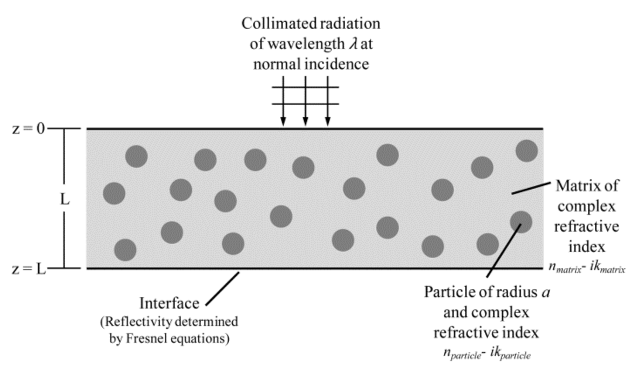

Figure 4-2 The modeling domain.

The major assumptions of the model are as follows.

1. The thermotropic material is isothermal and at steady state. The model represents a thermotropic material at different temperatures by a change in the relative refractive index. This change in relative refractive index causes a change in the scattering albedo and optical thickness. The scope of the study excludes the transient transition between the clear and translucent states. While understanding the transient heat transfer and phase change within the material is relevant as the material switches from the clear to the translucent state, it is not necessary to capture the transient process to identify materials that are most promising for future development.
2. Particles are monodisperse, randomly distributed and spherical. The assumption of spherical particles is supported by microscopic images of synthesized melt mix polymer blends [27, 36, 37]. At the low volume fractions of practical interest ($f_v < 20\%$), spheres are formed preferentially in the mixing process to minimize the free energy of the dispersed particles.
3. Particles scatter radiation independently. This assumption is valid when the distance between particles is greater than half the wavelength of incident radiation [38]. For example, if $f_v = 15\%$ then x should be ≥ 2 and if $f_v = 10\%$ then x should be ≥ 1.5 [38].
4. The thermotropic material is cold. At a maximum temperature of ~423 K, the temperature of the thermotropic material is an order of magnitude lower than the effective black body temperature of the sun (5777 K). Therefore emission

by the thermotropic material does not significantly contribute to the optical properties of the material in the solar spectrum.

5. A matrix refractive index of 1.50, representative of many polymers [39], is assumed.
6. The surrounding media is assumed to be air with a refractive index of one.
7. Specular reflection at the interface is assumed.

Volumetric scattering and absorption within the slab are governed by the equation of radiative transfer (RTE), which describes the change in radiative intensity, *I*, along the direction of propagation [40-42]. Neglecting reemission, the RTE is

$$\frac{dI_\lambda}{d\tau_\lambda} = -I_\lambda + \frac{\omega_\lambda}{4\pi}\int_{4\pi} I_\lambda(\hat{s}_i)\Phi_\lambda(\hat{s}_i,\hat{s})d\Omega \tag{4.5}$$

where the overall optical thickness, τ_L, is

$$\tau_{L,\lambda} = (\sigma_{s,\lambda} + \kappa_{eff,\lambda})L \tag{4.6}$$

and the scattering albedo, ω, is

$$\omega_\lambda = \frac{\sigma_{s,\lambda}}{(\sigma_{s,\lambda} + \kappa_{eff,\lambda})}. \tag{4.7}$$

The first term on the right hand side of eq. (4.5) is the attenuated radiative intensity of wavelength, λ. The second term describes the radiative intensity scattered into the direction of interest, $\hat{\boldsymbol{s}}$, from all other directions. The integrand of the second term includes the scattering phase function, Φ, which describes the probability that radiation from $\hat{\boldsymbol{s}}_i$ will be scattered into $\hat{\boldsymbol{s}}$. For disperse media with monodisperse particles, the scattering coefficient, σ_s, and effective absorption coefficient, κ_{eff}, reduce to the forms shown in eq. (4.8) and (4.9) [43, 44], respectively

$$\sigma_{s,\lambda} = \frac{0.75 f_v Q_s}{a} \tag{4.8}$$

$$\kappa_{eff,\lambda} = \frac{4\pi k_{matrix}}{\lambda} + \frac{0.75 f_v \left(Q_{ext} - Q_s\right)}{a}. \tag{4.9}$$

The Mie theory based code BHMIE [45] is used to calculate the scattering efficiency factor, Q_s, the extinction efficiency factor, Q_{ext}, and scattering phase function. Mie theory is a solution to Maxwell's equations for an electromagnetic wave incident upon a single spherical particle, and the results are valid for the ranges of k_{matrix} ($<10^{-4}$) and x (<15) investigated in the present work [46, 47]. The inputs to Mie theory are m, x, and $k_{particle}$.

A pathlength Monte Carlo ray tracing algorithm is used to solve the RTE and calculate the normal-hemispherical transmittance, reflectance, and absorptance of the slab. Monte Carlo ray tracing techniques are stochastic methods which track individual photon packages of radiation, referred to as rays, as each photon package propagates through and interacts with the medium. The paths of many individual rays must be tracked to obtain statistically relevant results. Detailed explanation of the various Monte Carlo techniques can be found in standard monographs such as [48] and [49]. In the present work, only the key points relevant to modeling a thermotropic material are discussed.

The term pathlength Monte Carlo technique is used as in [49] to refer to a technique which calculates the path length traveled by the ray using σ_s. The ray is scattered at the end of the path length. To determine the scattered angle, θ, corresponding to the generated random number, R_θ, the cumulative distribution equation,

$$R_\theta = \int_0^\theta \Phi(\theta')\sin\theta' d\theta' \Bigg/ \int_0^\pi \Phi(\theta')\sin\theta' d\theta', \tag{4.10}$$

is inverted through numerical integration. To determine scattering angles between the integration points, linear interpolation is used. A linear approximation within a 0.026 radian integration interval was found to provide a smooth curve. The linearity of the cumulative distribution function between the integration points was checked for accuracy by refining the interval of integration to 0.0014 radians. Absorption occurs along the entire path length. This method is referred to as energy partitioning in [48]. The process of volumetric scattering and absorption is truncated when the energy of the ray reaches 0.01% of its initial value. When a ray intersects an interface, the reflectivity of the interface is determined, as a function of the incidence angle, by the full Fresnel equations [50].

The predictions of the model are presented in terms of the relevant dimensionless parameters, x, τ_L, and ω. Although the scattering phase function is a function of m and x, for the range of m relevant for thermotropic materials ($0.9 \leq m \leq 1.1$), the scattering phase function is more strongly dependent on x than m. This dependency is exemplified by the dependency of the asymmetry factor, g,

$$g = \overline{\cos\theta} = \frac{1}{4\pi}\int_{4\pi} \Phi(\theta)\cos\theta d\Omega . \tag{4.11}$$

on the particle size parameter. For a constant m, g increases from 0.04 to 0.95 as x increases from 0.5 to 7, but for a constant x and $0.9 \leq m \leq 1.1$, g changes by $\leq$0.01. This change in g with respect to m has a little effect on the model predictions. Thus the results can be expressed as a function of x. The asymmetry factor and range for $0.9 \leq m \leq 1.1$ is reported for each particle size.

4.4 Model Validation

To validate the Monte Carlo code, the predictions of the model are compared to the solution for the transmittance and reflectance of a gray, isothermal, cold, scattering media irradiated with collimated [51] or diffuse radiation [52].

In Table 4-1, the model predictions are compared to the exact transmittance of a non-absorbing media (ω = 1) of overall optical thicknesses of 1, 2, 5, and 10 [51]. Isotropic and anisotropic scattering are considered. For anisotropic scattering, the linear anisotropic phase functions

$$\Phi_1 = 1 + 0.5\cos\theta; \quad \Phi_2 = 1 + \cos\theta p \backslash \tag{4.12}$$

are used. Model predictions are in excellent agreement with the analytical solution.

Table 4-1 Comparison of model predictions to exact solution for a scattering, non-absorbing medium

Φ	τ_L	ω	$\bar{\tau}_{exact}$ (%)	$\bar{\tau}_{MC}$ (%)
Isotropic	1	1	34.13	34.12
Isotropic	2	1	51.75	51.81
Isotropic	5	1	73.87	73.82
Isotropic	10	1	85.3	85.25
1 + 0.5cosθ	1	1	29.24	28.92
1 + 0.5cosθ	2	1	46.54	46.23
1 + 0.5cosθ	5	1	69.97	69.7
1 + 0.5cosθ	10	1	82.79	82.61
1 + cosθ	1	1	23.55	23
1 + cosθ	2	1	40.06	39.42
1 + cosθ	5	1	64.71	64.22
1 + cosθ	10	1	79.24	78.8

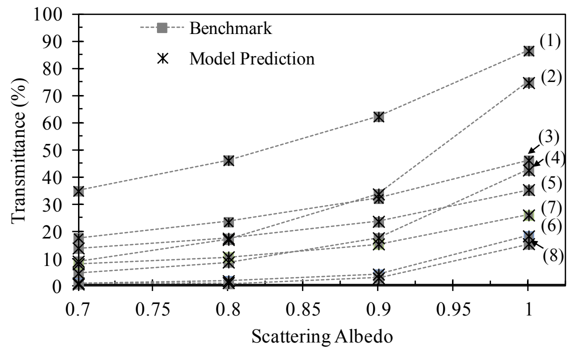

(a)

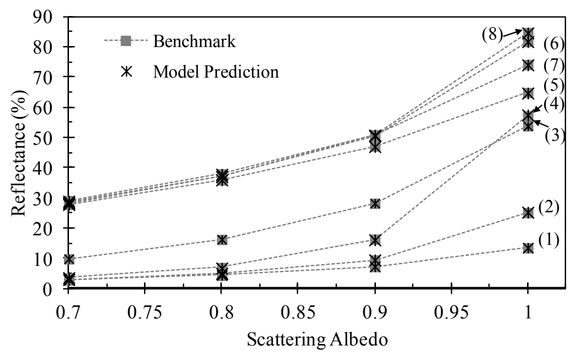

(b)

Figure 4-3 Comparison of model predictions to benchmark solution for (a) transmittance and (b) reflectance. (1) Φ=F; ρ=0.0; τL = 2; (2) Φ=F; ρ=0.0; τL = 5; (3) Φ=F; ρ=0.5; τL = 2; (4) Φ=F; ρ=0.5; τL = 5; (5) Φ=B; ρ=0.0; τL = 2; (6) Φ=B; ρ=0.0; τL = 5; (7) Φ=B; ρ=0

In Figure 4-3, the model predictions are compared to the transmittance and reflectance of an absorbing and anisotropic scattering medium [52] which has been used as a benchmark solution [53, 54]. A P-11 spherical harmonics approximation was used to solve the problem. At the $\tau = \tau_L$ boundary, the medium is bounded by either a transparent interface ($\rho = 0$) or a specular reflecting interface ($\rho = 0.5$). A strongly forward scattering (representative of $m = 1.2$, $x = 10$) and a strongly back scattering (representative of $m = \infty$, $x = 1$) phase function are considered. The phase functions are approximated using a 27 term and a 6 term Legendre polynomial for the forward and backward scattering functions, respectively [52, 53]. Overall optical thickness of 2 and 5, and scattering albedos between 0.7 and 1 are examined. Again, there is excellent agreement between the

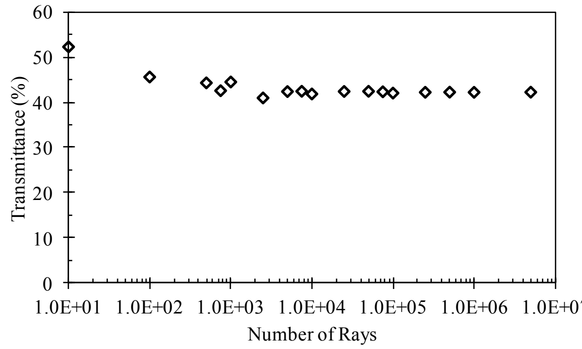

(a)

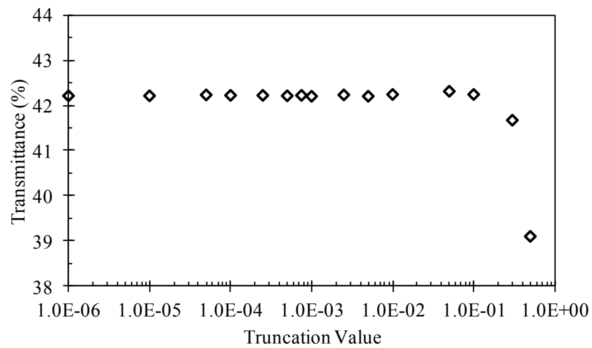

(b)

Figure 4-4 Transmittance for m = 0.98, x = 2.5, λ = 550 nm, L = 3.5 mm, k = 10-6 and fv = 10% versus: (a) number of rays for a truncation value of 0.0001; (b) truncation value for 5x105 rays.

model predictions and the benchmark solutions with less than 0.3 percentage point difference between the two.

The effect of the number of rays and the truncation value on the predicted transmittance materials was evaluated for m = 0.98, x = 2.5, λ = 550 nm, L = 3.5 mm, k = 10^{-6} and f_v = 10% as shown in Figure 4-4. At a truncation value of 0.01%, the simulation converges at $2.5\text{x}10^4$ rays to <0.4% of the transmittance at $5\text{x}10^6$ rays (Figure 4-4a). When using $5\text{x}10^5$ rays, the simulation converges at a truncation value of 1% to within 0.1% of the predicted value at a truncation value of 0.0001% (Figure 4-4b). All simulations used $5\text{x}10^5$ rays and a truncation value of 0.01%.

4.5 Results and Discussion

4.5.1 Parametric Study

The results are presented in dimensionless form for $0.5 \leq x \leq 15$, $0 \leq \tau_L \leq 30$, and $0.75 \leq \omega \leq 1$. The dimensionless results are interpreted to identify potential thermotropic material combinations and to optimize the volume fraction, thickness, and particle size for the best optical performance in the clear and translucent states. This process of selection and optimization is demonstrated through a case study.

A change in x is equivalent to examining a thermotropic material with fixed particle radius at different wavelengths or conversely, a thermotropic material at one wavelength but with different particle radii. An increase in τ_L corresponds to an increase in L, f_v, k, or $|1 - m|$. For a phase change thermotropic material with fixed L, f_v, and k, τ_L increases with temperature in response to an increase in $|1 - m|$. Thus an increase in τ_L is equivalent to examining a thermotropic material at higher temperature. Physically, an increase in ω corresponds to an increase in f_v or $|1 - m|$, or to a decrease in k. Since, for phase change materials, only $|1 - m|$ depends on temperature, ω increases from the clear to the translucent state.

The transmittance and reflectance, as a function of τ_L and ω, are given in Figure 4-5 and Figure 4-6 for $x = 2$ and $x = 7$, respectively. These particle sizes are highlighted because, at the peak wavelength of the solar spectrum (550nm), they represent a particle radius inside ($a = 175$ nm for $x = 2$) and outside ($a = 613$ nm for $x = 7$) the particle radius range suggested by [33]. The plots for other values of x are provided in the Appendix. As is expected from Bouguer's law, the transmittance decreases exponentially with

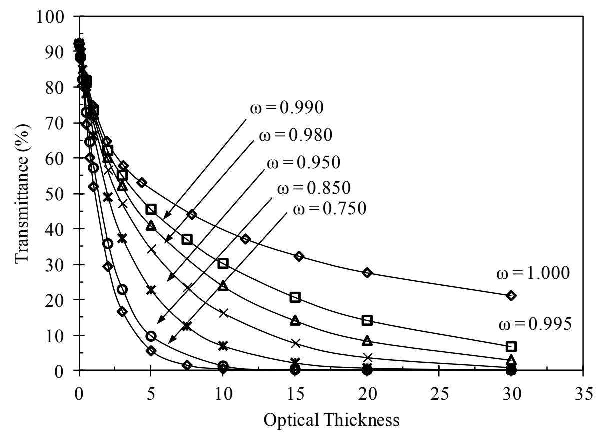

(a)

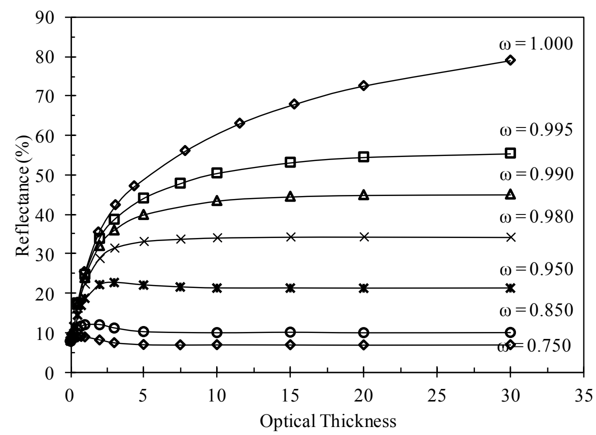

(b)

Figure 4-5 Normal-hemispherical (a) transmittance and (b) reflectance for x = 2 (g = 0.608±0.01).

increasing τ_L. For both $x = 2$ and $x = 7$, the further ω is from unity, the faster is the rate of decrease in transmittance with increasing τ_L. Comparing Figure 4-5 to Figure 4-6, it is seen that transmittance decreases, and reflectance increases, more rapidly with respect to τ_L for smaller values of x. At a single scattering event, smaller particles back scatter a larger fraction of the incident radiation than larger particles. Thus the larger the particle, the more scattering events (higher τ_L) are required to effect a reduction in transmittance. For $0 \leq \tau_L \leq 5$, the reflectance increases sharply with increasing τ_L. At higher values of τ_L, reflectance is independent of τ_L. The point at which reflectance becomes independent of

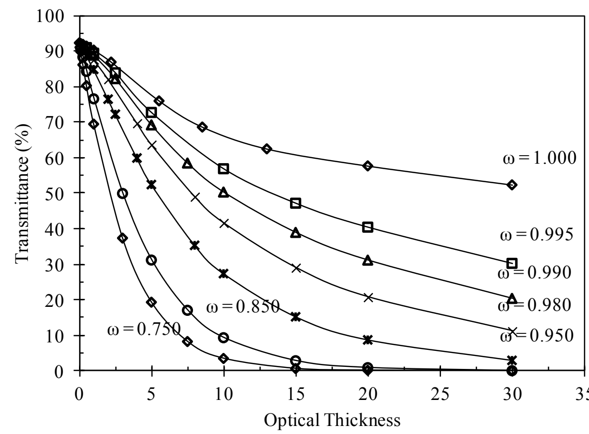

(a)

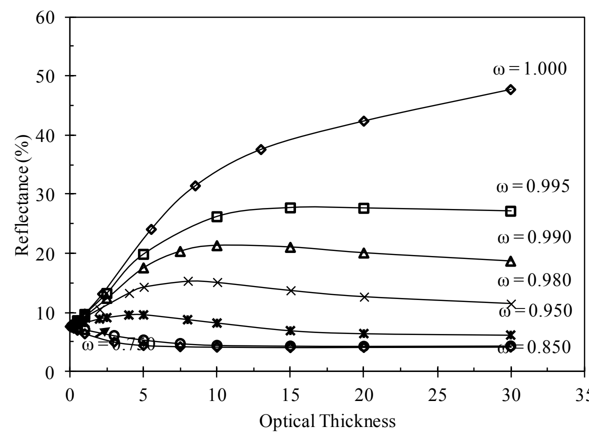

(b)

Figure 4-6 Normal-hemispherical (a) transmittance and (b) reflectance for x = 7 (g = 0.946±0.003).

τ_L depends on x. Figure 4-5 and Figure 4-6 show that for each value of ω, except for $\omega = 1$, the reflectance reaches an asymptote by $\tau_L = 10$ for $x = 2$ and by $\tau_L = 15$ for $x = 7$. Physically, reflectance becomes independent of τ_L because to increase τ_L without changing ω requires increasing L. The asymptote therefore indicates that there is a thickness at which back scattered radiation cannot escape the material before being absorbed.

How $|1 - m|$, and therefore τ_L and ω, change with temperature is material specific, but the values of τ_L and ω in the clear state and translucent state can be identified for the different values of x. The change in τ_L between the clear and translucent state should occur within a small temperature range. In the clear state, high transmittance is necessary to prevent a significant decrease in the optical efficiency of a solar collector. To achieve transmittance greater than 85% in the clear state, τ_L must be less than ~0.3 for $x = 2$. In the clear state for $x = 2$, the value of ω is less important than the value of τ_L because at low values of τ_L there is little difference between the ω curves. For x = 7, the value of τ_L to achieve >85% transmittance depends on ω. If $\omega = 0.75$, τ_L must be <0.25, but if $\omega = 1$, τ_L must be <2.2. To achieve ≥50% reflectance in the translucent state for $x = 2$ and $\omega = 0.995$, τ_L must be ≥10. For $x = 7$ and ω = 0.995, the reflectance asymptotes to 27% which corresponds to a stagnation temperature of 138°C for the collector and conditions of [15] (if the spectral reflectance at $x = 7$ is representative of the solar-weighted reflectance).

The reduction in transmittance from the clear to the translucent state must correspond to an increase in reflectance. If the thermotropic layer absorbs a significant portion of the incident radiation, it may overheat. For instance, although the transmittance for $x = 2$, $\tau_L = 5$, and $\omega = 0.75$ is 5% and therefore seems likely to provide adequate overheat protection, the absorption is 88%. Thus the thermotropic layer would behave like an absorber. Even at $\omega = 0.99$, the absorptance is 20%. Therefore to achieve high reflectance and to avoid significant absorption in the translucent state, ω should be ≥0.995 for much of the solar spectrum. Because absorption is driven by the matrix material for low f_v, to achieve $\omega \approx 1$ the absorptive index of the matrix material must be small. This requirement limits the selection of the matrix material to optical quality polymers [55] which have high transmittance in the visible and near infrared spectrum, such as poly(methyl methacrylate) and polycarbonate [55, 56].

4.5.2 Case Study

Having outlined the dimensionless material requirements, the results of the parametric study can be used to design thermotropic materials. To illustrate this design process, a case study thermotropic material is investigated. In addition to the assumptions outlined for the model, the following assumptions are assumed specifically for the case study:

1. The particle radius is 200 nm.
2. The predicted change in refractive index at 589 nm [14] for the two materials is applied at all wavelengths considered because data are not available for multiple wavelengths.
3. The asymptotic value of the available data (1.488) [35] is used for the refractive index of PE for wavelengths greater than 1500 nm.
4. The absorptive index for low molecular weight PE is assumed equivalent to PMMA because of a lack of data for the absorptive index of low molecular weight PE in the solar spectrum.
5. The absorptive index is not a function of temperature. Absorption in polymers depends primarily on the molecular structure. In the ultraviolet and visible spectra, absorption is caused by electron transitions, while at infrared wavelengths absorption is caused by vibrational transitions [55]. The

temperature range of interest for overheat protection (<120°C) is not sufficient to alter the molecular structure of PMMA.

The first step of the design process is to identify a potential scattering domain and matrix combination. Low molecular weight PE in a matrix of PMMA is selected for several reasons. At room temperature, the refractive indices of low molecular weight PE [35] and PMMA [34] are very similar and $|1 - m| \leq 0.01$. Thus the material combination is expected to perform well in the clear state. The refractive index of low molecular weight PE changes significantly with temperature whereas the refractive index of PMMA is stable [14]. Thus reflection is expected to increase in the translucent state.

Next, the absorptive index must be considered. Figure 4-7 shows the calculated spectral absorptive index of PMMA. The absorptive index is $<10^{-8}$ for $\lambda < 900$, and generally increases with wavelength for $\lambda >1000$ nm with local peaks at $\lambda =1190$, 1400, and 1700 nm. The absorptive index of PMMA was calculated by the standard method of determining absorptive index from the normal-hemispherical data of a homogeneous material [46, 57, 58]. The refractive index of PMMA for $400 \leq \lambda \leq 1100$ nm is taken from [34]. For $\lambda \geq 1100$ nm, the asymptotic value of data, 1.483, is used. The normal-hemispherical transmittance of five 100% PMMA samples was measured in repeated tests for $250 \leq \lambda \leq 2500$ nm using a PerkinElmer Lambda 1050 spectrophotometer equipped with a 150 mm integrating sphere. In the visible spectrum the spectrophotometer has a photometric accuracy of ±0.003A at 5A and ±0.002A at 0.5A. The wavelength accuracy is ±0.08 nm in the UV/VIS and ±0.30 nm in the NIR. The

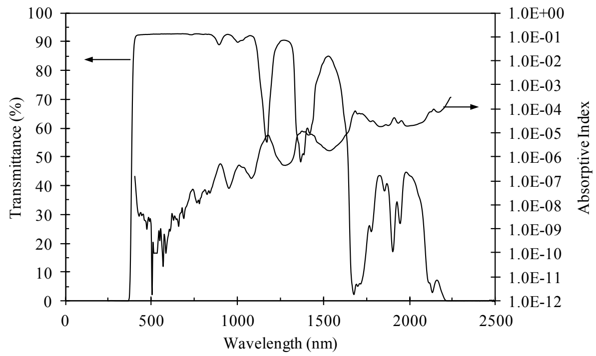

Figure 4-7 The calculated absorptive index for PMMA and the measured normal-hemispherical transmittance for a 5.9 mm thick sample.

thicknesses of the samples are 3.1, 3.3, 5.9, 9.3, and 9.6 mm. Figure 4-7 also shows the measured transmittance data for the 5.9 mm thick sample.

The thickness, L, and volume fraction, f_v, of the PE/PMMA composite are initially taken to be 1 mm and 5%, respectively, to be representative of values reported in the literature for phase change thermotropic materials [18, 20, 25]. In the clear state (30°C), because m is near unity and k is low, τ_L is ≤ 0.07 for $400 \leq \lambda \leq 1250$ nm. The predicted relative decrease in the refractive index of PE and PMMA from 30 to 110°C is 7 and 1%, respectively [14]. Therefore in the translucent state (110°C), τ_L is calculated to be ≥ 1 for $400 \leq \lambda \leq 1000$ nm and ≥ 3 for $400 \leq \lambda \leq 650$ nm. The scattering albedo is between 1 and 0.918 for $400 \leq \lambda \leq 1250$ nm. The dimensionless model results are used to predict the spectral, normal-hemispherical transmittance, reflectance, and absorptance of the PE/PMMA blend at eleven wavelengths between 400 and 2500 nm. To calculate the solar-weighted, normal-hemispherical optical properties for an air mass of 1.5, a stepwise approximation of the spectral transmittance and reflectance curves is used.

Figure 4-8 shows the predicted spectral, normal-hemispherical transmittance and reflectance of the PE/PMMA blend in the clear (30°C) and translucent (110°C) states for

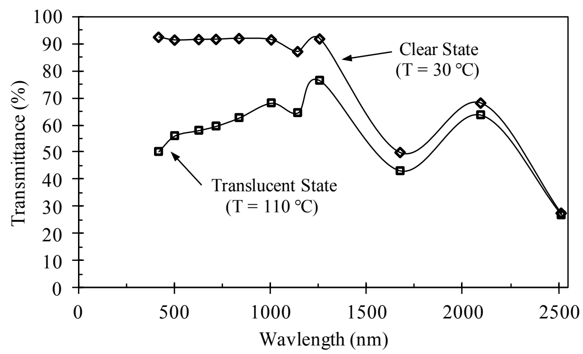

(a)

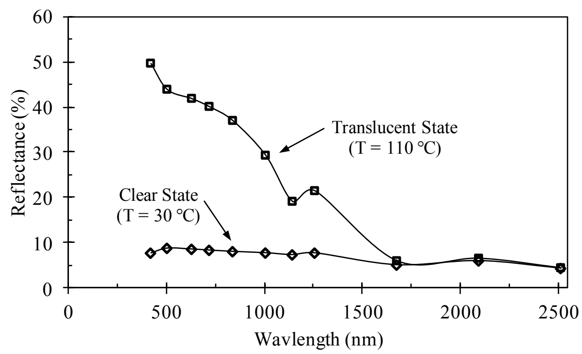

(b)

Figure 4-8 Spectral, normal-hemispherical (a) transmittance and (b) reflectance in the clear and translucent states for low molecular weight PE in PMMA. fv = 5%; L = 1 mm.

L = 1.0 mm and f_v = 5%. In the clear state, there is negligible reduction in transmittance from the measured value of 92% for pure PMMA for 400 ≤ λ ≤ 1200 nm. In the translucent state, the transmittance is reduced to ~60% between 400 ≤ λ ≤ 900 nm. Because $\omega \approx 1$, the decrease in transmittance corresponds to a significant increase in reflectance from ~8% in the clear state to ~40% in the translucent state. The solar-weighted transmittance is 85% and 57% in the clear and translucent states, respectively.

The next step in designing the thermotropic material is to determine the effects of L and f_v on the solar weighted transmittance and reflectance (Figure 4-9 and Figure 4-10) and to optimize them for the desired optical performance. In the clear state (Figure 4-9a and Figure 4-10a), the solar-weighted transmittance decreases with increasing L and f_v.

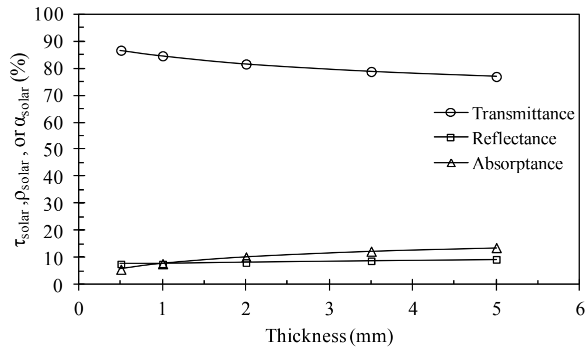

(a)

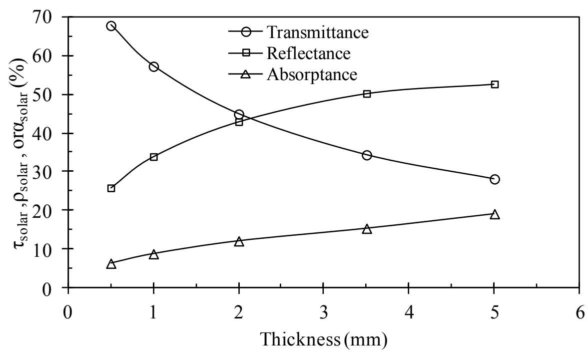

(b)

Figure 4-9 Effects of thickness in the (a) clear and (b) translucent states for low molecular weight PE in PMMA for fv = 5%.

For the range of L and f_v investigated, the transmittance is more sensitive to L. The solar weighted transmittance for f_v = 5% decreases from 87% at L = 0.5mm to 77% at L = 5mm. In comparison, the transmittance for L = 1mm decreases from 85% at f_v = 2.5% to 83% at f_v = 15%. In the translucent state (Figure 4-9b and Figure 4-10b) both L and f_v significantly affect the solar-weighted reflectance. An increase in L from 0.5 to 5 mm increases the reflectance from 26 to 53%. An increase in f_v from 2.5 to 15% increases the reflectance from 25 to 49%. Thickness also has a significant effect on solar weighted absorption. The absorption increases from 6% for L = 0.5 mm to 19% for L = 5 mm. Increasing f_v marginally increases absorption.

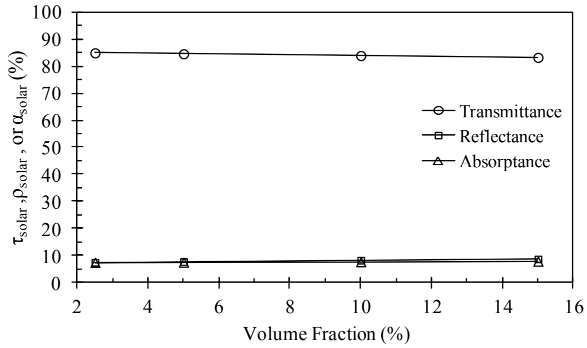

(a)

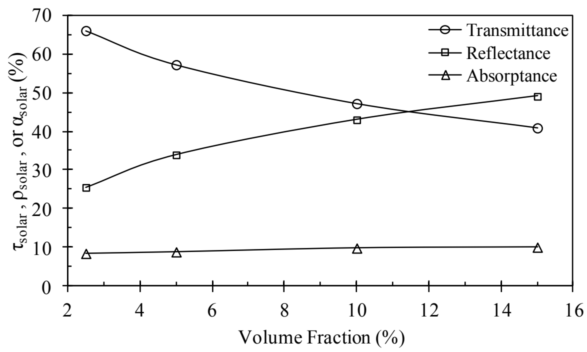

(b)

Figure 4-10 Effects of volume fraction in the (a) clear and (b) translucent states for L = 1 mm.

Thus, for the combination of low molecular weight PE in PMMA to provide maximum overheat protection while attaining a clear state solar-weighted transmittance of 85%, L should be 1 mm and f_v should be 10%. This combination would limit the stagnation temperature, of the collector in [15] to 122 °C. To limit the stagnation temperature to 115 °C, the solar-weighted reflectance in the translucent state must be 50%. To achieve this translucent state reflectance, L should be 1mm and f_v should be 15%. However, this combination has a clear state solar-weighted transmittance slightly less than the goal of 85%.

4.6 Conclusion

The present study uses a Monte Carlo model to guide the selection of phase change thermotropic materials for overheat protection of polymer solar absorbers. The steady state, solar-weighted optical properties (transmittance, reflectance, and absorptance) of potential thermotropic composite materials are evaluated in two states, referred to as the clear and translucent state. The states are differentiated by differences in transmittance due to differences the relative refractive index. The transient transition between the two states is not considered.

A parametric study of effects of the dimensionless particle size parameter, optical thickness, and scattering albedo on the normal-hemispherical transmittance, reflectance, and absorptance in the solar spectrum of thermotropic materials is provided. For a particle size parameter of 2, the optical thickness should be less than ~0.3 to achieve a spectral transmittance greater than 85%. The optical thickness should be greater than 10 (for a scattering albedo of 0.995) to increase the reflectance to ≥50% in the translucent state. For the reduction in transmittance to correspond to an increase in reflectance and not absorption, the scattering albedo must be greater than 0.995 in the translucent state. To achieve a scattering albedo of approximately one, it is recommended that the matrix polymer be an optical quality polymer such as polycarbonate or poly(methyl methacrylate).

From the requirements for optical thickness in the clear and translucent states, low molecular weight polyethylene in a matrix of poly(methyl methacrylate) is identified as a promising combination for a phase change thermotropic material. For these materials and a particle radius of 200 nm, the thickness should be 1.0 mm and the volume fraction should be 15% to limit the stagnation temperature to less than 115°C. This combination of variables significantly decreases the solar weighted transmittance from 83% in the clear state to 41% in the translucent state. As is desired, the solar weighted reflectance significantly increases from the clear to the translucent state (9 to 49%), and the solar weighted absorptance remains low in both states (9% in the clear state and 10% in the translucent state).

The results provide guidance to selection and design of thermotropic materials but additional research will be needed to evaluate the manufacturability and performance of the potential materials, including the transient heat transfer associated with a solar collector application.

4.7 Funding

This research is funded by the University of Minnesota Initiative for Renewable Energy and the Environment and by the National Renewable Energy Laboratory.

4.8 Nomenclature

a	radius of scattering domain (nm)
E	irradiance (W/m^2/nm)
f_v	volume fraction of scattering domains (%)
g	asymmetry factor
I	radiative intensity (W/m^2/sr)
T	temperature (°C)
i	imaginary number
k	absorptive coefficient

L	material thickness (mm)
m	relative index of refraction
N	complex index of refraction
n	refractive index
Q_{ext}	extinction efficiency factor
Q_s	scattering efficiency factor
R_θ	Random number used to determined scattered angle
$\hat{\mathbf{s}}$	unit vector describing direction of ray
$\hat{\mathbf{s}}_i$	unit vector describing direction of radiation before being scattered into $\hat{\mathbf{s}}$
x	particle size parameter
z	direction into the thermotropic material
$\overline{\alpha}$	absorptance (%)
θ	scattering angle (radians)
κ_{eff}	effective absorptive coefficient (mm^{-1})
λ	wavelength of incident radiation (nm)
$\overline{\rho}$	normal-hemispherical reflectance (%)
ρ	interface reflectivity (%)
σ_s	scattering coefficient (mm^{-1})
τ_L	optical thickness
τ	normal-hemispherical transmittance (%)
Φ	scattering phase function
ω	scattering albedo
Ω	solid angle (sr)

Subscripts

matrix	property of the matrix material
particle	property of the scattering domain material
solar	solar weighted
λ	wavelength dependent

4.9 Appendix

This appendix provides additional numerical data for particle size parameters of 0.5, 1.0, 1.5, 2.5, 3.0, 3.5, 5.0, 10.0, 12.5, and 15 for $0 \leq \tau_L \leq 30$ and $0.75 \leq \omega \leq 1.0$ (Figure 4-11 to Figure 4-20). The mean value and the range of the asymmetry factor for $0.9 \leq m \leq 1.1$ is also provided for each x. Data for particle size parameters of 2.0 and 7.0 are presented in the body of the paper.

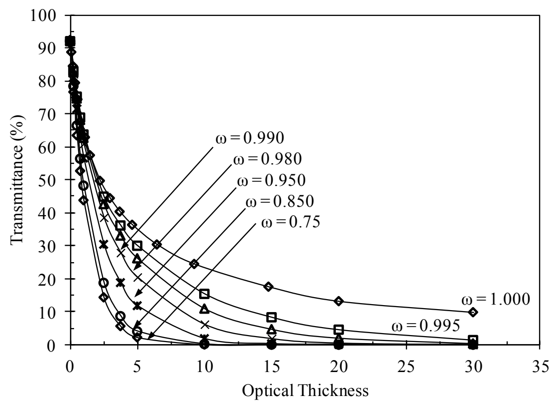

(a)

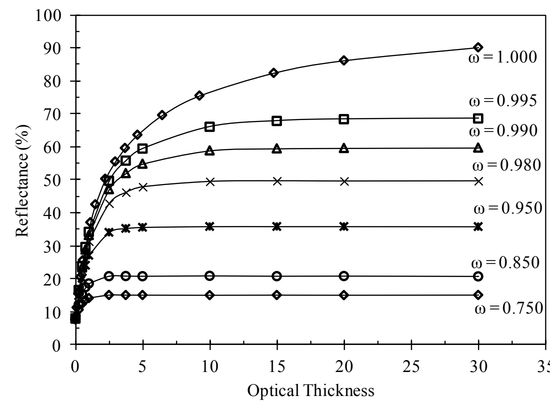

(b)

Figure 4-11 Normal-hemispherical (a) transmittance and (b) reflectance for x = 0.5 (g = 0.041 ± 0.001).

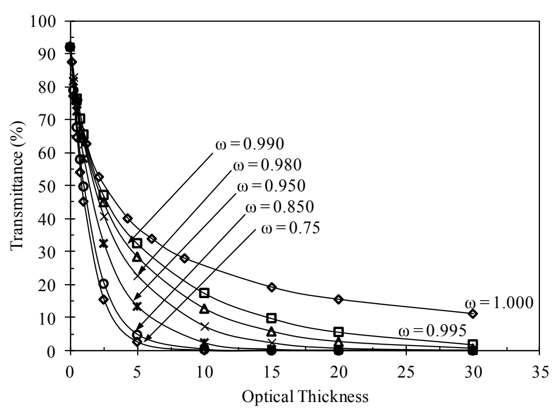

(a)

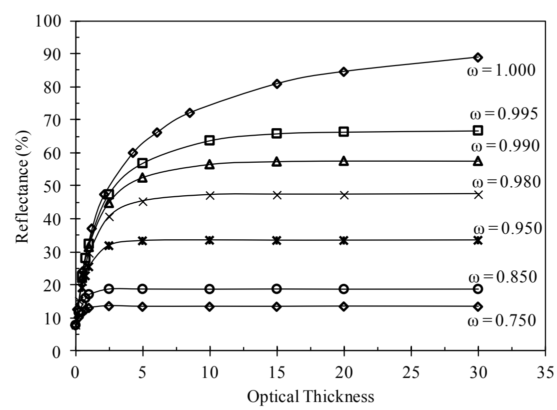

(b)

Figure 4-12 Normal-hemispherical (a) transmittance and (b) reflectance for x = 1.0 (g = 0.168 ± 0.003).

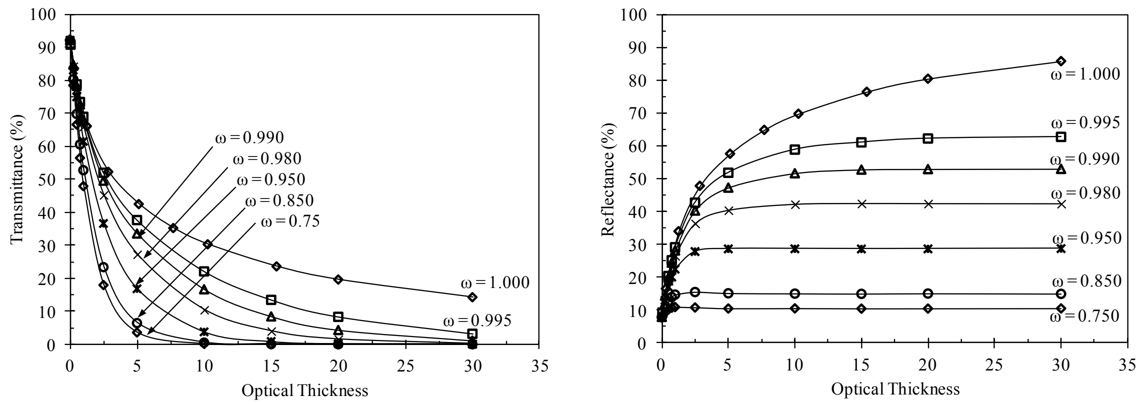

(a) (b)

Figure 4-13 Normal-hemispherical (a) transmittance and (b) reflectance for x = 1.5 (g = 0.385 ± 0.008).

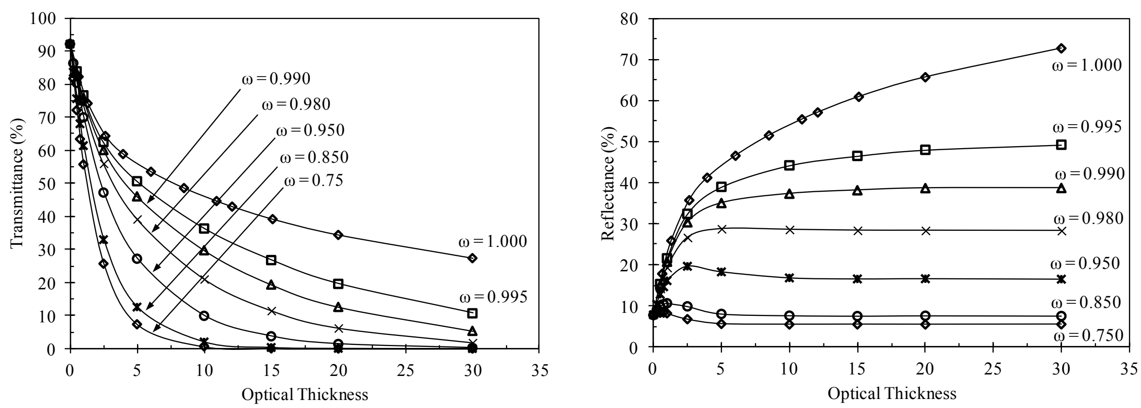

(a) (b)

Figure 4-14 Normal-hemispherical (a) transmittance and (b) reflectance for x = 2.5 (g = 0.739 ± 0.01).

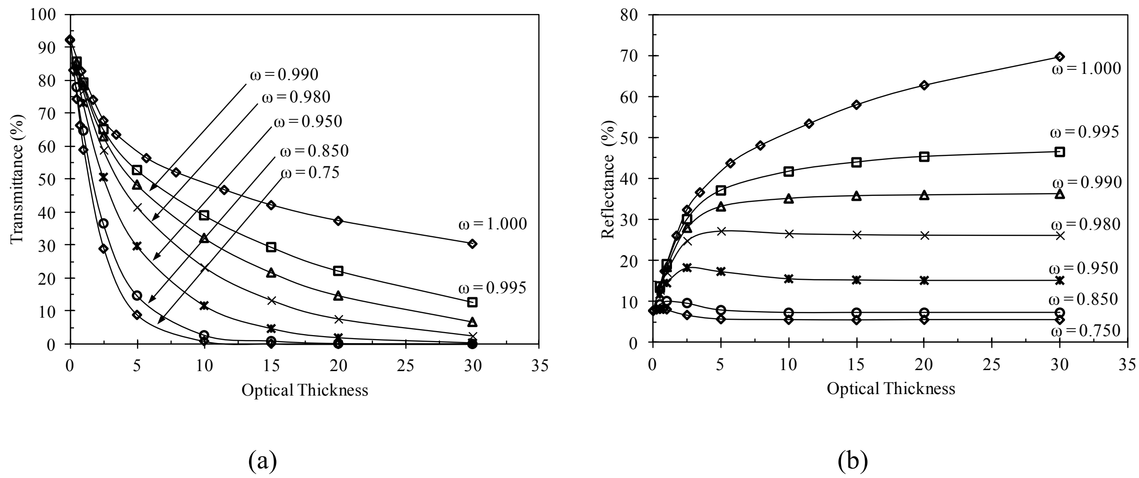

Figure 4-15 Normal-hemispherical (a) transmittance and (b) reflectance for x = 3.0 (g = 0.794 ± 0.005).

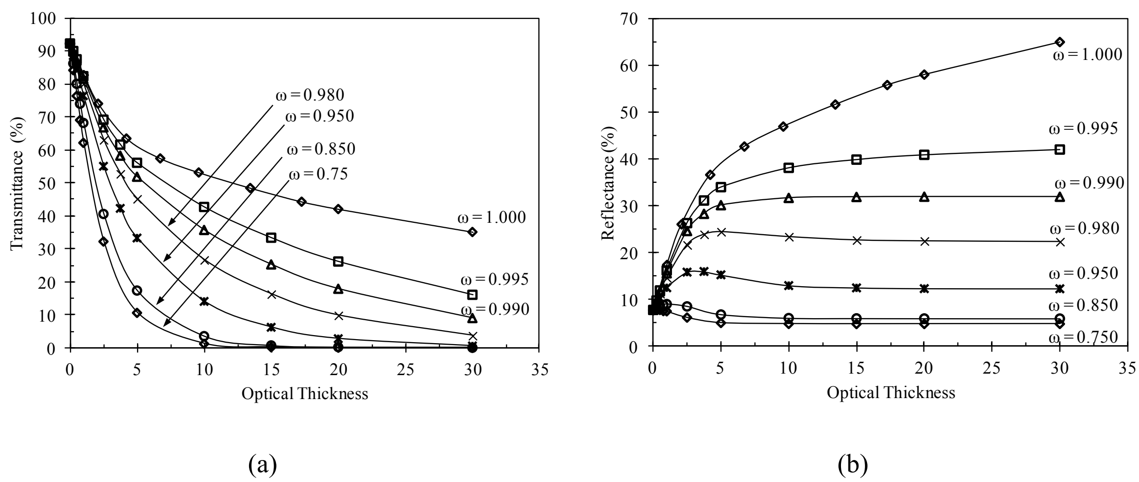

Figure 4-16 Normal-hemispherical (a) transmittance and (b) reflectance for x = 3.5 (g = 0.836 ± 0.005).

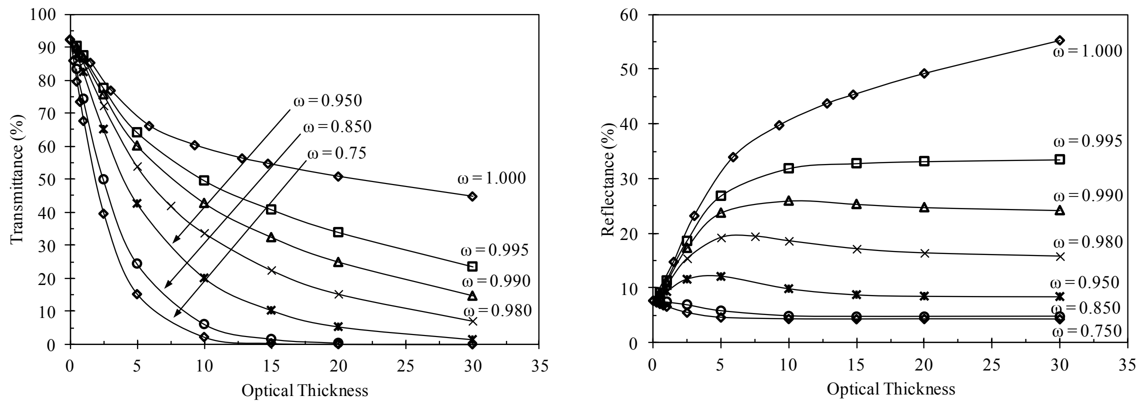

(a) (b)

Figure 4-17 Normal-hemispherical (a) transmittance and (b) reflectance for x = 5.0 (g = 0.907 ± 0.001).

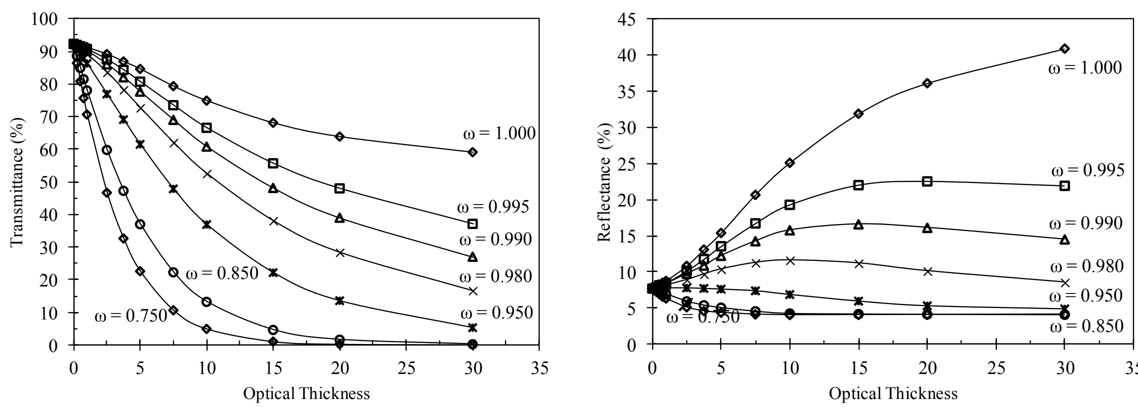

(a) (b)

Figure 4-18 Normal-hemispherical (a) transmittance and (b) reflectance for x = 10.0 (g = 0.967 ± 0.003).

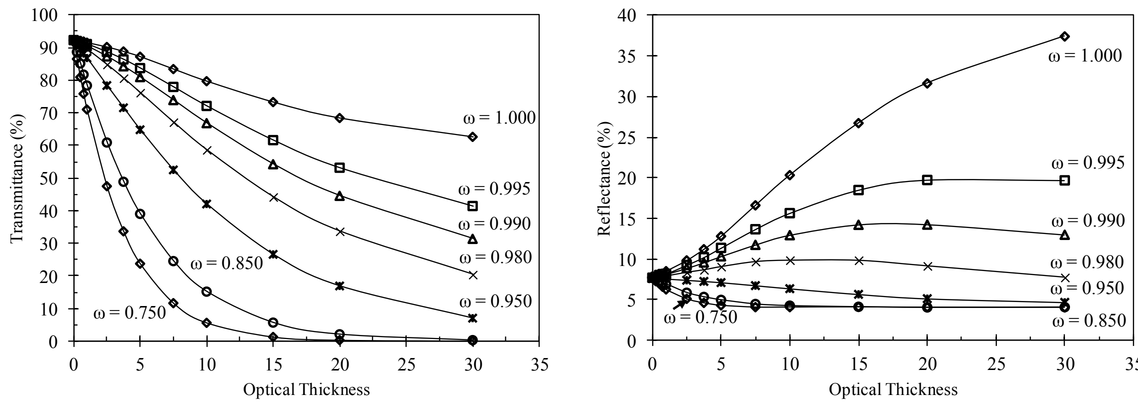

(a) (b)

Figure 4-19 Normal-hemispherical (a) transmittance and (b) reflectance for x = 12.5 (g = 0.976 ± 0.004).

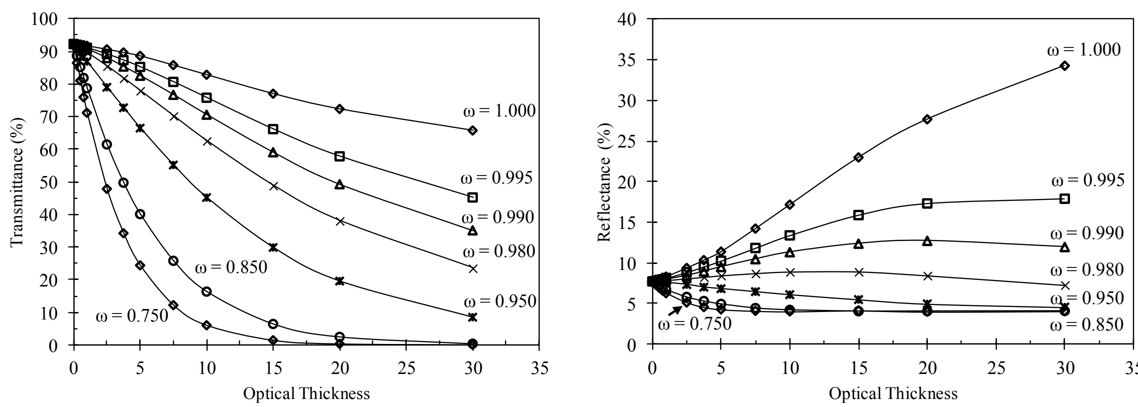

(a) (b)

Figure 4-20 Normal-hemispherical (a) transmittance and (b) reflectance for x = 15.0 (g = 0.981 ± 0.005).

4.10 References

[1] U.S. Energy Information Agency, 2009, "2009 Residential Energy Consumption Survey - Consumption and Expenditure Tables (by End use)," **2013**(07/31) http://www.eia.gov/consumption/residential/data/2009/index.cfm?view=consumption#end-use

[2] Buckles, W. E., and Klein, S. A., 1980, "Analysis of Solar Domestic Hot Water Heaters," Solar Energy, **25**(5) pp. 417-424.

[3] Hudon, K., Merrigan, T., Burch, J., and Maguire, J, 2012, "Low-Cost Solar Water Heating Research and Development Roadmap," National Renewable Energy Laboratory (NREL). Technical Report. NREL/TP-550054793.

[4] Merrigan, T., 2007, "Solar Heating & Lighting: Solar Water Heating R&D - DOE Solar Energy Technologies Program," DOE Solar Energy Technologies Program Peer Review meeting. April 17-19, 2007. Denver, CO USA.

[5] Tsilingiris, P. T., 1999, "Towards Making Solar Water Heating Technology feasible—the Polymer Solar Collector Approach," Energy Conversion and Management, **40**(12) pp. 1237-1250.

[6] Kohl, M., Meir, M.G., Papillon, P., 2012, "Polymeric Materials for Solar Thermal Applications,"Wiley-VCH Verlag & Co., Weinheim, German, pp. 73-106, Chap. 4.

[7] Rhodes, R. O., 2010, "Polymer Thin-Film Design Reduces Installed Cost of Solar Water Heater," *Proceedings of the 39th ASES national Solar Conference,* May 17-20, 2010. Phoenix, AZ USA.

[8] Kearney, M., Davidson, J., and Mantell, S., 2005, "Polymeric Absorbers for Flat-Plate Collectors: Can Venting Provide Adequate Overheat Protection?" Journal of Solar Energy Engineering, **127**(3) pp. 421-424.

[9] Resch, K., Hausner, R., and Wallner, G. M., 2009, "All Polymeric Flat-Plate Collector — Potential of Thermotropic Layers to Prevent Overheating," Proceedings of ISES World Conference 2007, pp. 561-565.

[10] Resch, K., and Wallner, G. M., 2009, "Thermotropic Layers for Flat-Plate collectors—A Review of various Concepts for Overheating Protection with Polymeric Materials," Solar Energy Materials and Solar Cells, **93**(1) pp. 119-128.

[11] UL746B, 1998, "Polymeric Materials - Long Term Property Evaluations," Underwriters Laboratories, Inc., Northbrook, IL.

[12] Raman, R., Mantell, S., Davidson, J., 2000, "A Review of Polymer Materials for Solar Water Heating Systems," Transactions-American Society of Mechanical Engineers Journal of Solar Energy Engineering, **122**(2) pp. 92-100.

[13] Kohl, M., Meir, M.G., Papillon, P., 2012, "Polymeric Materials for Solar Thermal Applications,"Wiley-VCH Verlag & Co., Weinheim, German, pp. 187-210, Chap. 10.

[14] Gladen, A. C., Davidson, J. H., and Mantell, S. C., 2013, "Selection of Thermotropic Materials for Overheat Protection of Polymer Absorbers," Solar Energy, (2013), http://dx.doi.org/10.1016/j.solener.2013.10.026.

[15] Wallner, G. M., Resch, K., and Hausner, R., 2008, "Property and Performance Requirements for Thermotropic Layers to Prevent Overheating in an all Polymeric Flat-Plate Collector," Solar Energy Materials and Solar Cells, **92**(6) pp. 614-620.

[16] Nitz, P., and Hartwig, H., 2005, "Solar Control with Thermotropic Layers," Solar Energy, **79**(6) pp. 573-582.

[17] Seeboth, A., Ruhmann, R., and Muehling, O., 2010, "Thermotropic and Thermochromic Polymer Based Materials for Adaptive Solar Control," Materials, **3**(12) pp. 5143-5168.

[18] Resch, K., Wallner, G. M., and Hausner, R., 2009, "Phase Separated Thermotropic Layers Based on UV Cured Acrylate Resins – Effect of Material Formulation on Overheating Protection Properties and Application in a Solar Collector," Solar Energy, **83**(9) pp. 1689-1697.

[19] Resch, K., and Wallner, G. M., 2009, "Morphology of Phase-Separated Thermotropic Layers Based on UV Cured Acrylate Resins," Polymers for Advanced Technologies, **20**(12) pp. 1163-1167.

[20] Weber, A., and Resch, K., 2012, "Thermotropic Glazings for Overheating Protection," Energy Procedia, **30** pp. 471-477.

[21] Schael, G. W., 1964, "Determination of Polyolefin Film Properties from Refractive Index Measurements," Journal of Applied Polymer Science, **8**(6) pp. 2717-2722.

[22] Krevelen, D.W.v., and Nijenhuis, K., 2009, "Properties of Polymers - Their Correlation with Chemical Structure; Their Numerical Estimation and Prediction from Additive Group Contributions (4th, Completely Revised Edition)," Elsevier.

[23] Buehler, D. F. S. R., 2004, "Reversible Thermotropic Composition, its Preparation and use," (EP0985709) .

[24] Dabisch, W., 1981, "Bodies with Reversibly Variable Temperature-Dependent Light Absorbence," US Patent (4268413) .

[25] Muehling, O., Seeboth, A., Haeusler, T., 2009, "Variable Solar Control using Thermotropic core/shell Particles," Solar Energy Materials and Solar Cells, **93**(9) pp. 1510-1517.

[26] Errico, M., Greco, R., Laurienzo, P., 2006, "Acrylate/EVA Reactive Blends and semi-IPN: Chemical, chemical–physical, and thermo-optical Characterization," Journal of Applied Polymer Science, **99**(6) pp. 2926-2935.

[27] Takahashi, S., Okada, H., Nobukawa, S., 2012, "Optical Properties of Polymer Blends Composed of Poly(Methyl Methacrylate) and ethylene–vinyl Acetate Copolymer," European Polymer Journal, **48**(5) pp. 974-980.

[28] Bernini, U., Malinconico, M., Martuscelli, E., 1995, "Ultra-Tough Synthetic Glasses made by Reactive Blending of PMMA and EVA Rubbers: Opto-Thermal Characterization," Journal of Materials Processing Technology, **55**(3–4) pp. 224-228.

[29] Weber, A., and Resch, K., 2014, "Thermotropic Glazings for Overheating Protection. I. Material Preselection, Formulation, and light-shielding Efficiency," Journal of Applied Polymer Science, **131**(4).

[30] Weber, A., Schmid, A., and Resch, K., 2014, "Thermotropic Glazings for Overheating Protection. II. Morphology and structure–property Relationships," Journal of Applied Polymer Science, **131**(4).

[31] Weber, A., and Resch, K., 2012, "Effect of Temperature-Cycling on the Morphology of Polymeric Thermotropic Glazings for Overheating Protection Applications," Journal of Polymer Research, **19**(6) pp. 1-8.

[32] Weber, A., Schlögl, S., and Resch, K., 2013, "Effect of Formulation and Processing Conditions on Light Shielding Efficiency of Thermotropic Systems with Fixed Domains Based on UV Curing Acrylate Resins," Journal of Applied Polymer Science, **130**(5) pp.3299-3310.

[33] Nitz, P., Ferber, J., Stangl, R., 1998, "Simulation of Multiply Scattering Media," Solar Energy Materials and Solar Cells, **54**(1-4) pp. 297-307.

[34] Kasarova, S. N., Sultanova, N. G., Ivanov, C. D., 2007, "Analysis of the Dispersion of Optical Plastic Materials," Optical Materials, **29**(11) pp. 1481-1490.

[35] Filmetrics, 2012, "Refractive Index of Polyethylene, PE," **2013**(01/25) http://www.filmetrics.com/refractive-index-database/Polyethylene/PE-Polyethene.

[36] Dell'Erba, R., Groeninckx, G., Maglio, G., 2001, "Immiscible Polymer Blends of Semicrystalline Biocompatible Components: Thermal Properties and Phase Morphology Analysis of PLLA/PCL Blends," Polymer, **42**(18) pp. 7831-7840.

[37] Gupta, A. K., Ratnam, B. K., and Srinivasan, K. R., 1992, "Impact Toughening of Polypropylene by Ethylene Vinyl Acetate Copolymer," Journal of Applied Polymer Science, **45**(7) pp. 1303-1312.

[38] Tien, C. L., and Drolen, B., 1987, "Thermal radiation in particulate media with dependent and independent scattering," IN: Annual review of numerical fluid mechanics

and heat transfer. Volume 1 (A88-18971 06-34). Washington, DC, Hemisphere Publishing Corp., 1987, p. 1-32.

[39] Gooch, J.W., 2011, "Encyclopedic Dictionary of Polymers, 2nd ed." Springer Science & Business Media, New York, NY USA, pp. 520.

[40] Viskanta, R., and Mengüç, M. P., 1987, "Radiation Heat Transfer in Combustion Systems," Progress in Energy and Combustion Science, **13**(2) pp. 97-160.

[41] Mishchenko, M.I., Travis, L.D., and Lacis, A.A., 2006, "Multiple Scattering of Light by Particles: Radiative Transfer and Coherent Backscattering," Cambridge University Press, New York, NY, pp. 478.

[42] Modest, M., 2003, "Radiative Heat Transfer, Second Edition,"Academic Press, USA, pp. 263-287, Chap. 9.

[43] Randrianalisoa, J., and Baillis, D., 2010, "Radiative Properties of Densely Packed Spheres in Semitransparent Media: A New Geometric Optics Approach," Journal of Quantitative Spectroscopy and Radiative Transfer, **111**(10) pp. 1372-1388.

[44] Dombrovskii, L. A., 2004, "The Propagation of Infrared Radiation in a Semitransparent Liquid Containing Gas Bubbles," High Temperature, **42**(1) pp. 146-153.

[45] Bohren, C.F., and Huffman, D.R., 1998, "Absorption and Scattering of Light by Small Particles," Wiley-Interscience, pp. 530.

[46] Randrianalisoa, J., Baillis, D., and Pilon, L., 2006, "Modeling Radiation Characteristics of Semitransparent Media Containing Bubbles Or Particles," J.Opt.Soc.Am.A, **23**(7) pp. 1645-1656.

[47] Baneshi, M., Maruyama, S., and Komiya, A., 2010, "Infrared Radiative Properties of Thin Polyethylene Coating Pigmented with Titanium Dioxide Particles," Journal of Heat Transfer, **132**(2).

[48] Modest, M., 2003, "Radiative Heat Transfer, Second Edition,"Academic Press, USA, pp. 644-679, Chap. 20.

[49] Farmer, J.T., and Howell, J.R., 1998, "Advances in Heat Transfer,"Elsevier, pp. 333-429.

[50] Modest, M., 2003, "Radiative Heat Transfer, Second Edition,"Academic Press, USA, pp. 31-60, Chap. 2.

[51] Busbridge, I., and Orchard, S., 1967, "Reflection and Transmission of Light by a Thick Atmosphere According to a Phase Function: 1 - χ COS θ," The Astrophysical Journal, **149** pp. 655.

[52] Sutton, W., and Özişik, M., 1979, "An Iterative Solution for Anisotropic Radiative Transfer in a Slab," Journal of Heat Transfer, **101** pp. 695.

[53] Lee, H., and Buckius, R., 1982, "Scaling Anisotropic Scattering in Radiation Heat Transfer for a Planar Medium," ASME Transactions Journal of Heat Transfer, **104** pp. 68-75.

[54] Maruyama, S., 1998, "Radiative Heat Transfer in Anisotropic Scattering Media with Specular Boundary Subjected to Collimated Irradiation," International Journal of Heat and Mass Transfer, **41**(18) pp. 2847-2856.

[55] Baumer, S.., “Handbook of Plastic Optics,” 2010, Wiley-VCH, Weinheim, Germany, pp. 123-160, Chp. 5.

[56] Lens, U. S. P., 1973, "The Handbook of Plastic Optics," US Precision Lens, Inc., Cincinnati, Ohio, pp. 11-23.

[57] Dombrovsky, L., Randrianalisoa, J., Baillis, D., 2005, "Use of Mie Theory to Analyze Experimental Data to Identify Infrared Properties of Fused Quartz Containing Bubbles," Appl.Opt., **44**(33) pp. 7021-7031.

[58] Rubin, M., 1985, "Optical Properties of Soda Lime Silica Glasses," Solar Energy Materials, **12**(4) pp. 275-288.

5 Numerical Evaluation of Encapsulated Phase Change Particles for a Thermotropic Material

To be submitted

5.1 Summary

Phase change thermotropic materials have been proposed as a low cost method of providing passive overheat protection for polymer solar thermal absorbers. One challenge to the development of these materials is controlling the size of the phase change particles dispersed within the matrix material. Here we explore encapsulation as a means to resolve this challenge with a focus on the selection of materials, including the encapsulating shell, to achieve desirable optical behavior. Hydroxystearic acid particles in a matrix of poly(methyl methacrylate) is down selected from candidate materials based on its optical properties and the melt temperature of the dispersed phase. The optical properties (normal-hemispherical transmittance, reflectance and absorptance) of this material as a function of the particle volume fraction and properties of the encapsulation shell are predicted using a Monte Carlo ray tracing model. A range of shell relative refractive indices, from 0.95 to 1, and thicknesses, up to 35 nm, can be employed to achieve greater than 80% transmittance in the clear state and greater than 50% reflectance in the translucent state.

5.2 Introduction

Over the past decade there has been an international effort to substantially reduce the cost of solar thermal collectors for domestic hot water and space heating through the development of polymeric absorbers and glazings [1-12]. The goal is to use commodity plastics, such as polypropylene, which are amenable to high-volume, low-cost manufacturing processes. The challenge is to overcome the limitation of relatively low service temperature (~100°C) of these materials because solar absorbers can exceed the service temperature of commodity polymers during the summer months or during dormant periods (e.g., when the homeowners are on vacation) [13-15]. Numerous approaches to provide overheat protection have been suggested [13, 16-29], including the passive approach considered in the present work of adding a phase-change thermotropic material to the top surface of the polymer absorber [13, 15, 26-28, 30-37]. Overheat protection is provided when the thermotropic layer changes from highly transparent (referred to as the clear state) to highly reflective (the translucent state) as the absorber approaches its service temperature. The solar-weighted transmittance in the clear state impacts the optical efficiency of the collector. The solar-weighted reflectance in the translucent state dictates the level of overheat protection provided and thus the choice of absorber material [14].

Phase change thermotropic materials consist of particles, collectively referred to as the scattering domain, of a phase change material embedded in a stable and optically matched matrix material. The phase change temperature should be slightly lower than the service temperature of the polymer absorber. In the clear state, the particles are solid and their refractive index should match the refractive index of the matrix material so that incident radiation is not scattered. A solar-weighted transmittance greater than 80% is desirable to maintain high optical efficiency during solar collection [13, 14]. In the translucent state, the particles melt which causes a change in refractive index. This change creates a mismatch in the refractive index between the particles and the matrix. Consequently, radiation is scattered and transmittance is reduced due to an increase in reflectance. The reflectance in the translucent state required to protect the absorber depends on ambient conditions, the collector design, and the polymer used for the absorber [14]. A solar-weighted reflectance greater than 50% is required to adequately protect a polypropylene absorber (service temperature of 115ºC). Other commodity polymers such as cross-linked polyethylene, which has a service temperature of 100ºC, require higher reflectance (≥65%) [14].

Based on a review of the scientific literature and to our knowledge, material development efforts have failed to yield phase change thermotropic materials that meet the dual requirements of high transmittance in the clear state and adequate reflectance in the translucent state. The best performance, in terms of decrease in transmittance with temperature, was achieved by Weber et al. with ethylene-co-glycidyl methacrylate (8%wt) in polyamide, fatty acids in epoxy acrylate, and fatty acids in polyester acrylate [30, 31]. In the clear state, the measured solar-weighted transmittances were 79, 72, and 79%, respectively. In the translucent state, the solar-weighted transmittances were 63, 60, and 65%, respectively [30]. These thermotropic materials failed to achieve the desired optical performance in part because of the inability to control the particle size distribution within the matrix. The developers report a particle radius distribution of 500 to 5,000 nm in materials which were fabricated via melt mixing. The mean particle radius is even larger and the particle size distribution more disperse, 500 to 50,000 nm, for thermotropic materials fabricated via mixing in a UV curable matrix [31].

The numerical analysis of Nitz et al. [38] of an unspecified thermotropic material (the constituent materials were not provided) suggests a particle radius of 150 nm for peak reflectance in the translucent state. Gladen et al. developed a set of dimensionless plots that can be used to select particle size for any material. In general, particle radius from 100 to 500 nm are desired. Smaller particles are undesirable because they do not effectively scatter incident solar radiation. Larger particles are undesirable because they preferentially forward scatter incident radiation resulting in lower reflectance. For example, for a 1 mm thick slab of poly(methyl methacrylate) (PMMA) with 10% by volume of low molecular weight 200 nm polyethylene particles yields a solar weighted reflectance in the translucent state of 43%. For 500, 1000, and 5000 nm, particles, the solar reflectance decreases to 41%, 38%, and 27%, respectively.

The challenge of fabricating thermotropic materials with submicron particles lies in the lack of direct control over the particle size during manufacture, which involves mixing the scattering domain with the matrix. The particle size is a function of numerous parameters. For example, in melt mixing, the particle size depends on the viscosity of the materials, the blending temperature, mixing speed, and the percent mass of scattering domain material. Particularly challenging is obtaining small particles for blends with a high volume fraction (>10%) of the disperse phase and for blends with a large difference in viscosity between the two materials, as is the case for thermotropic materials.

One approach suggested to control the particle size is encapsulation of the phase change material prior to mixing with the matrix material [26]. Research on encapsulation [39-41] demonstrates that paraffin waxes (or alkanes) and fatty acids, which are promising scattering domain materials for thermotropic materials [27, 30], can be encapsulated at the submicron scale [26, 42-52] with a narrow particle size distribution [43, 48, 52-54]. Encapsulation is possible with a wide range of shell materials including poly(methyl methacrylate) [48-50, 55, 56], polycarbonate [42, 57], urea-formaldehyde [41, 58], melamine-formaldehyde [41, 45, 59], polyurea [43, 60], polystyrene [44, 53], acrylonitrile-styrene [57], acrylonitrile-styrene-butadiene [57], poly(styrene-co-methyl methylacrylic) [47], and silica [46, 61, 62]. The wall thickness, which also affects the optical properties of the particle, can be controlled [43, 63, 64].

To-date, two studies of thermotropic materials with encapsulated particles have been conducted [26, 52]. In these studies, it was assumed that the best practice is to match the shell refractive index as closely as possible to the matrix. Muehling, et al. [26] encapsulated a mixture of n-octadecane/n-eicosane/n-docosane/n-tetracosane in a cross-linked polymer shell of vinyl monomers methyl methacrylate (MMA, 90 wt%) and ethylene glycol dimethacrylate (EGDMA, 10 wt%, cross-linking agent). By varying the percent weight of shell and core material, 200 nm (40%/60% ratio) to 800 nm (80%/20% ratio) radius particles were fabricated. The shell thickness was 35 – 40 nm. The encapsulated particles were dispersed in a 1.7 mm thick, acrylate-based resin matrix. For the two best performing samples, the solar weighted transmittance changed from 75% and 69% at 20°C to 54% and 41%, respectively, above 45°C [26]. Weber, et al.

encapsulated a paraffin wax (melting temperature of 55°C) in a shell consisting of a copolymer of MMA and EGDMA or a copolymer of MMA, EGDMA and isobornyl methacrylate (iBoMA) [52]. The particles had a mean radius of 177 nm for wax encapsulated in MMA-EGDMA and 244 nm for wax encapsulated in MMA-EGDMA-iBoMA. The shell thicknesses were 50 and 65 nm, respectively. The encapsulated particles were dispersed in a 0.9 mm thick, UV cured polyester acrylate matrix [52]. The thermotropic materials had a solar-weighted transmittance of 73 and 69%, respectively at 20°C and 49% (for both) at 70°C [52]. Previously Weber, et al. [32] reported an insignificant change in transmittance for the same phase change/matrix material combination with unencapsulated particles. The primary difference between the two studies is the particle size [52]. Although both studies of thermotropic materials with encapsulated particles [26, 52] show improved optical performance (in terms of change in optical properties with temperature), neither produced a thermotropic material which meets the requirements for providing overheat protection.

The objective of the present numerical study is to evaluate the effects of the shell refractive index, shell thickness, and volume fraction of particles on the optical performance of a thermotropic material with encapsulated particles.

5.3 Material Selection

The phase change/matrix material combination considered in this study was identified following the approach described in [15, 27] for selecting potential thermotropic materials with unencapsulated particles. Our study considers overheat protection of a polypropylene absorber, such that the transmittance in the clear state must be greater than 80% and the reflectance in the translucent state must be greater than 50% [14]. These optical performance requirements are the starting point for material selection.

Transmittance and reflectance data as a function of overall optical thickness τ_L, scattering albedo ω, and the particle size parameter x are provided in Gladen, et al. [15]. In identifying matrix/phase change combinations, absorption was neglected ($\omega = 1$) because at 589 nm, the wavelength for which the refractive index of many polymers is available, most polymers are weakly absorbing. The particle size parameter was selected to assure that the particle radius is less than 500 nm. For a wavelength 589 nm, a particle size parameter x of 2.5 was selected. The corresponding particle radius a is 234 nm. Given the desired optical performance and the particle size parameter, the optical thickness for the clear state and translucent state was determined from the data provided in [15] :

$\tau_L \le 0.8$ clear state.

$\tau_L \ge 8$ translucent state. (5.1)

Neglecting absorption, the optical thickness can be defined as a function of the efficiency factor Q_s, the particle volume fraction f_v, and the thickness of the thermotropic layer L:

$$\tau_L = \frac{0.75 Q_s f_v L}{a}. \tag{5.2}$$

These terms are described in greater detail in the Model Description section. The process of identifying thermotropic materials consists of determining the combinations of scattering efficiency factor Q_s, volume fraction f_v, and thickness L which satisfy the optical thickness criteria.

The scattering efficiency factor is a function of the relative refractive index between the matrix and the phase change material, and thus is the only parameter which is a function of temperature. It can be calculated using a Mie scattering code, such as the one provided by Bohren and Huffman [65], or determined from the data shown in Fig. 8 (Q_s as a function of m and x) of [27]. The scattering efficiency factor Q_s was evaluated for the potential combinations of matrix and phase change materials. The matrix materials of poly(methyl methacrylate) and polycarbonate were considered, because they are high clarity, low absorbing polymers required for the matrix material [15]. The scattering domain materials considered were drawn from the list provided Weber, et al. [30] because refractive index data in the solid and liquid phases at a wavelength of 589 nm are provided. From this list of phase change materials, the materials were down selected based on a melting temperature between 75 and 100 °C. Table 5-1 and Table 5-2 list the phase change materials from this down selection, along with the relative refractive indices for each combination in PMMA (Table 5-1) or PC (Table 5-2) and the scattering efficiency factor for a size parameter of 2.5.

Given the data provided in Table 5-1 and Table 5-2, the overall optical thickness was calculated for various combinations of volume fraction f_v and thickness L. An upper bound of 3mm was set for the thickness because of manufacturing considerations for co-extrusion of the absorber and the thermotropic material. An upper bound on volume fraction was set at 20% for practical considerations for manufacture. Moreover, larger volume fractions are above the limit for independent scattering [66]. The calculated optical thickness in each state is compared to the required optical thickness set by the

Table 5-1 Relative refractive index and scattering efficiency factor for a matrix of PMMA, n = 1.4919 (29°C); n = 1.4824 (90°C)

Phase Change Material	T_{melt} (°C)	$m_{c\text{-}m}$ (T=29 °C)	Q_s (T=29 °C)	$m_{c\text{-}m}$ ($T>T_{melt}$)	Q_s ($T>T_{melt}$)
Paraffin, high-molecular weight	86	1.0148	2.065E-03	0.9680	9.265E-03
Hydrogenated castor oil	87	1.0074	5.130E-04	0.9862	1.743E-03
Hydroxystearic acid	78	1.0054	2.727E-04	0.9734	6.431E-03
Fatty acid ester	81	1.0095	8.469E-04	0.9761	5.203E-03
Hydrogenated castor oil	86	1.0068	4.329E-04	0.9849	2.099E-03
E-co-BA (17%)-co-MAH (3.1%)	90	1.0007	4.564E-06	0.9842	2.099E-03
E-co-MA (16%)-co-MAH (3.1%)	87	1.0021	4.113E-05	0.9849	2.099E-03
E-co-MA (20%)-co-MAH (0.3%)	82	1.0007	4.564E-06	0.9835	2.487E-03
E-co-VA (28%)	77	0.9974	6.279E-05	0.9835	2.487E-03

Table 5-2 Relative refractive index and scattering efficiency factor for a matrix of PC, n = 1.5847 (29°C); n = 1.5773 (90°C)

Phase Change Material	T_{melt} (°C)	$m_{c\text{-}m}$ (T=29 °C)	Q_s (T=29 °C)	$m_{c\text{-}m}$ ($T>T_{melt}$)	Q_s ($T>T_{melt}$)
Paraffin, high-molecular weight	86	0.9554	1.783E-02	0.9098	7.012E-02
Hydrogenated castor oil	87	0.9484	2.373E-02	0.9269	4.675E-02
hydroxystearic acid	78	0.9466	2.537E-02	0.9149	6.275E-02
Fatty acid ester	81	0.9503	2.205E-02	0.9174	5.920E-02
Hydrogenated castor oil	86	0.9478	2.427E-02	0.9256	4.833E-02
E-co-BA (17%)-co-MAH (3.1%)	90	0.9421	2.972E-02	0.9250	4.913E-02
E-co-MA (16%)-co-MAH (3.1%)	87	0.9434	2.843E-02	0.9256	4.833E-02
E-co-MA (20%)-co-MAH (0.3%)	82	0.9421	2.972E-02	0.9244	4.993E-02
E-co-VA (28%)	77	0.9390	3.290E-02	0.9244	4.993E-02

optical performance criteria, and the materials are further down selected.

Using this selection process, a promising combination is hydroxystearic acid (HSA), a fatty acid derivative, in a matrix of PMMA ($m_{c\text{-}m,CS}$ = 1.0054 at T=29°C; $m_{c\text{-}m,TS}$ = 0.9734 T ≈ 80°C). At a volume fraction of particles of 18%, and a slab thickness of 3mm, the transmittance in the clear state is 80% (optical thickness of 0.49) and the reflectance in the translucent state is 51% (scattering albedo of 0.998, optical thickness of 11). These values of volume fraction and thickness are used as a baseline for the present study of encapsulated particles. The core radius is fixed at 234nm, and the thickness of the slab is fixed at 3 mm.

A Monte Carlo ray tracing model is used to predict the optical properties. In addition to the baseline of volume fraction of 18%, volume fractions of 16 and 20% are considered. Shell relative refractive indices from 0.95 to 1.05 and shell thicknesses up to 94 nm are investigated. To interpret the results, the relative refractive index of the shell $m_{s\text{-}m}$ is assumed to be constant with temperature because the shell material does not go through a phase change.

5.4 Model Description

An overview of the governing equations and the model are given with an emphasis on the modifications to a prior model of thermotropic materials without encapsulation [15, 27] to include encapsulated particles. The primary difference between modeling a thermotropic material with encapsulated particles and a thermotropic material with unencapsulated particles is the calculation of the scattering properties of a particle.

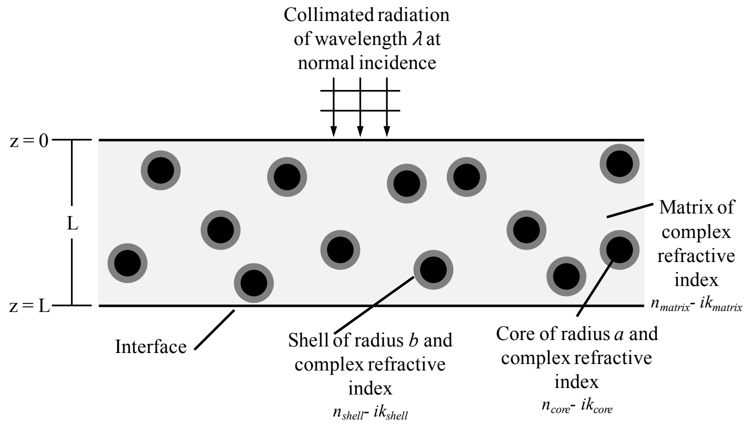

Figure 5-1 The modeling domain

The thermotropic material is modeled, as shown in Figure 5-1, as a slab of uniform thickness L irradiated with collimated radiation of wavelength λ = 589 nm at normal incidence. An incident wavelength of 589 nm is used because it is near the peak intensity of the solar spectrum and because the refractive index of many potential scattering domain materials as a function of temperature is known at this wavelength [30]. The slab comprises a matrix material with complex index of refraction N_{matrix}

$$N_{matrix} = n_{matrix} - ik_{matrix}, \tag{5.3}$$

and monodispersed, randomly distributed, spherical particles with core radius a and complex index of refraction N_{core}

$$N_{core} = n_{core} - ik_{core}. \tag{5.4}$$

The core is encapsulated with a shell of radius b and complex index of refraction N_{shell}

$$N_{shell} = n_{shell} - ik_{shell}. \tag{5.5}$$

The real portion of the relative refractive index is defined as,

$$m_{c-m} = \frac{n_{core}}{n_{matrix}} \tag{5.6}$$

for the core, and

$$m_{s-m} = \frac{n_{shell}}{n_{matrix}} \tag{5.7}$$

for the shell. The ratio of the refractive index of the shell to the core,

$$m_{s-c} = \frac{n_{shell}}{n_{core}} \tag{5.8}$$

is an important parameter in assessing performance. The particle volume fraction f_v is defined as the ratio of the volume occupied by the particles (core plus shell) to the total volume. The shell thickness t_{shell} is the radius of the shell minus the radius of the core.

The major assumptions of the model are:

- The thermotropic material is isothermal and at steady state. The model represents a thermotropic material at different temperatures by a change in the relative refractive index of the core.
- Emission by the thermotropic material is neglected. At a maximum temperature of ~423 K, the temperature of the thermotropic material is an order of magnitude lower than the effective black body temperature of the sun (5777 K). Therefore emission by the thermotropic material does not significantly contribute to the optical properties of the material 589 nm.
- Particles scatter radiation independently. This assumption is valid when the distance between particles is greater than half the wavelength of incident radiation [66]. At 589 nm and a particle size parameter of 2.5 to 5, the volume fraction must be ≤~20% to meet this criterion [66].
- Particles are the only source of radiation scattering which requires an optically clear matrix material.

- The shell has uniform thickness.

Volumetric scattering and absorption within the slab are governed by the equation of radiative transfer (RTE), which describes the change in radiative intensity, I, along the direction of propagation [67-69]. The RTE is given by

$$\frac{dI}{d\tau} = -I + \frac{\omega}{4\pi}\int_{4\pi} I(\hat{s}_i)\Phi(\hat{s}_i, \hat{s})d\Omega \tag{5.9}$$

where reemission is neglected. The overall optical thickness of the slab, which indicates how strongly the slab attenuates radiation, is

$$\tau_L = (\sigma_s + \kappa_{eff})L. \tag{5.10}$$

The scattering albedo of the slab, which indicates the extent of attenuation of radiation via scattering or absorption, is

$$\omega = \frac{\sigma_s}{(\sigma_s + \kappa_{eff})}. \tag{5.11}$$

A scattering albedo of one indicates no absorption; zero indicates no scattering. For disperse media with monodisperse particles, the scattering coefficient σ_s and effective absorption coefficient κ_{eff} reduce to the forms shown in eqs. (5.12) and (5.13) [70, 71], respectively.

$$\sigma_{s,\lambda} = \frac{0.75 f_v Q_s}{b} \tag{5.12}$$

$$\kappa_{eff,\lambda} = \frac{4\pi k_{matrix}}{\lambda} + \frac{0.75 f_v (Q_{ext} - Q_s)}{b} \tag{5.13}$$

The difference between modeling a thermotropic material with encapsulated particles and one with unencapsulated particles is the calculation the extinction Q_{ext} and scattering Q_s efficiency factors and the scattering phase function Φ. Qualitatively, scattering by a particle can be conceptualized by subdividing the particle into small regions which behave as oscillating dipole moments in the presence of an applied oscillating electromagnetic field [65]. The oscillating dipoles radiate radiation (wavelets) in all directions. The amplitude and phase of the induced dipole moment, and in turn the wavelets, depends on the particle refractive index and the local electromagnetic field. The scattered electromagnetic field outside the particle (which determines Q_{ext}, Q_s, and Φ) is the superposition of the wavelets. For encapsulated particles, the shell radiates wavelets of different amplitude and phase than those radiated by the core. These additional wavelets increase the possibility for mutual enhancement and cancellation with the other scattered wavelets. Therefore, both the thickness and the refractive index of the shell affect radiation scattered by a particle and ultimately the optical properties of the slab.

The extension of the Mie solution to Maxwell's equations for encapsulated spherical particles was first obtained by [72]. Using this extension, Bohren and Huffman developed the computer program BHCOAT [65], which is used in the present study, to calculate Q_{ext}, Q_s, and Φ for an encapsulated particle. To calculate Q_{ext}, Q_s, and Φ, the refractive index of the core n_{core}, shell n_{shell}, and matrix n_{matrix}, the absorptive index of the core k_{core} and shell k_{shell}, and the particle size parameter of the core

$$x_{core} = \frac{2\pi a}{\lambda} \tag{5.14}$$

and shell

$$x_{shell} = \frac{2\pi b}{\lambda} \tag{5.15}$$

are specified. The measured refractive index of PMMA is 1.4919 and 1.4824, at 29°C and 90°C, respectively. The absorptive index at 589 nm is 3.1×10^{-7} [73]. The refractive index for HSA is 1.50 at 29°C and 1.443 above its transition temperature [30]. The absorptive index for HSA is not reported in [30], thus it is assumed to be equivalent to the matrix, as is the shell absorptive index. The Mie solution to Maxwell's equations is valid for the ranges of k_{matrix} ($<10^{-4}$) and x_{shell} (<15) investigated in the present work [74, 75].

A pathlength Monte Carlo ray tracing algorithm uses the values of Q_{ext}, Q_s, and Φ for a particle and stochastically solves the RTE to calculate the normal-hemispherical transmittance, reflectance, and absorptance of the slab containing many particles. Explanation of Monte Carlo techniques can be found in standard monographs such as [76] and [77].

5.5 Results and Discussion

The optical properties of the selected thermotropic material with encapsulated particles are presented, in Figure 5-2 to Figure 5-4, in the form of contour plots of transmittance in the clear state ($m_{s\text{-}m}$ = 1.0054, representing operation below the phase change temperature of the core at 78 °C) and reflectance in translucent state ($m_{s\text{-}m}$ = 0.9734, representing operation at or above the phase change temperature of the core) with respect to the thickness t_{shell} and the relative refractive index $m_{s\text{-}m}$ of the shell for particle volume fractions of 18 (the baseline), 20, and 16%, respectively. For convenience, the shell relative-to-the-core refractive index $m_{s\text{-}c}$ is shown on the right ordinate. In interpreting these contour plots, note that for each volume fraction, the particle radius

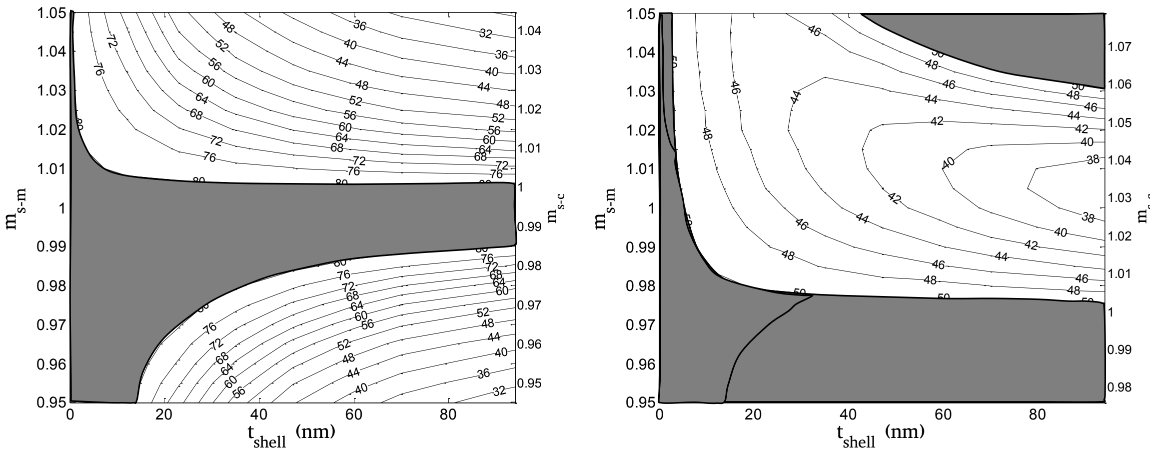

(a) (b)

Figure 5-2 Transmittance in the clear state, $m_{c\text{-}m,CS}$ = 1.0054 at T = 29°C, and (b) reflectance in the translucent state, $m_{c\text{-}m,TS}$ = 0.9734 at T > 78°C for HSA in PMMA at a volume fraction of 18% and thickness of 3 mm. The lightly shaded area indicates the region of acceptable transmittance (a) and reflectance (b). The darker shaded area in (b) is the solution space.

increases and the number of particles decreases as the shell thickness is increased. The transmittance and reflectance of an equivalent thermotropic material with unencapsulated particles is indicated along the left ordinate ($t_{shell} = 0$). Moreover, encapsulated particles behave as unencapsulated particles when the index of refraction of the shell equals that of the matrix, $m_{s\text{-}m} = 1$, or that of the core, $m_{s\text{-}c} = 1$ (an unlikely option since the melt temperature of the encapsulant should be above that of the phase change material).

As discussed previously, we define a solution space for the thermotropic material as the region of the plot in which transmittance is greater than 80% in the clear state and reflectance is greater than 50% reflectance in the translucent state [14]. For the baseline volume fraction of 18%, the regions of acceptable transmittance (Figure 5-2a) and reflectance (Figure 5-2b) are shaded in light gray. The confluence of these two regions, which represents the solution space for a slab thickness of 3 mm, is indicated by the darker overlaid shading in Figure 5-2b. The solution space encompasses shell relative

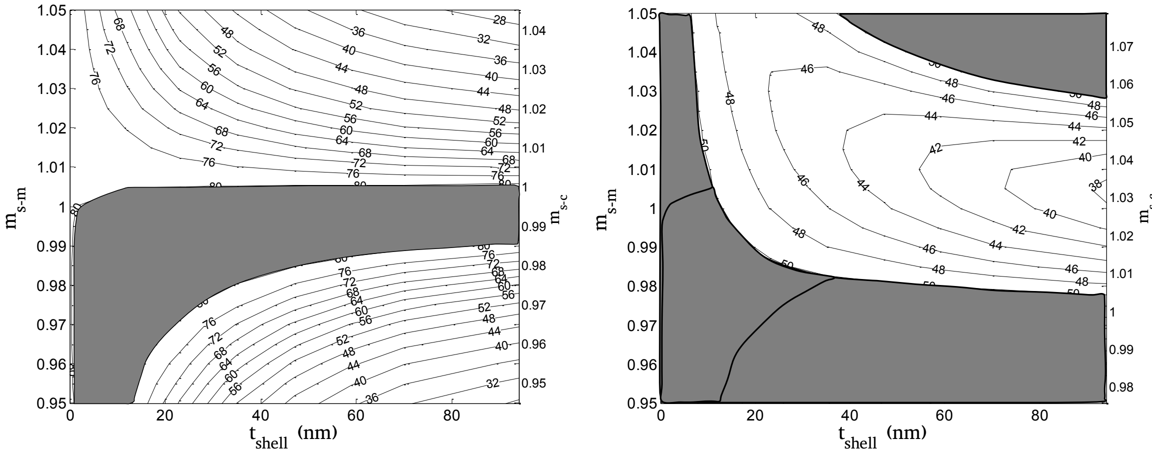

(a) (b)

Figure 5-3 Transmittance in the clear state, $m_{c\text{-}m,CS}$ = 1.0054 at T = 29°C, and (b) reflectance in the translucent state, $m_{c\text{-}m,TS}$ = 0.9734 at T > 78°C for HSA in PMMA at a volume fraction of 20% and thickness of 3 mm. The lightly shaded area indicates the region of acceptable transmittance (a) and reflectance (b). The darker shaded area in (b) is the solution space.

refractive indices from 0.95 to 1.015. However, for shell relative refractive indices greater than 0.99, the shell must be so thin (<10nm) that encapsulation is prohibitive. For shell relative refractive indices from 0.97 to 0.98, shell thickness up to 20 nm are acceptable. In addition to the benefit of improved control of particle size, encapsulation improves the optical performance due to the interaction between the scattered wavelets of the shell and core which, for some combinations, cancel each other and produce a lower scattering efficiency factor than that for unencapsulated particles. If the core relative refractive index is greater than one, the lower scattering efficiency factors occurs at shell relative refractive indices less than one and vice versa. This lower scattering efficiency factor is beneficial in the clear state because it results in higher transmittance. For example, at a shell relative refractive index of 0.975 and a shell thickness of 20 nm, the transmittance in the clear state (m = 1.0054) is 83% compared to 80% with unencapsulated particles. The reflectance in the translucent state (m = 0.9734) is 51%

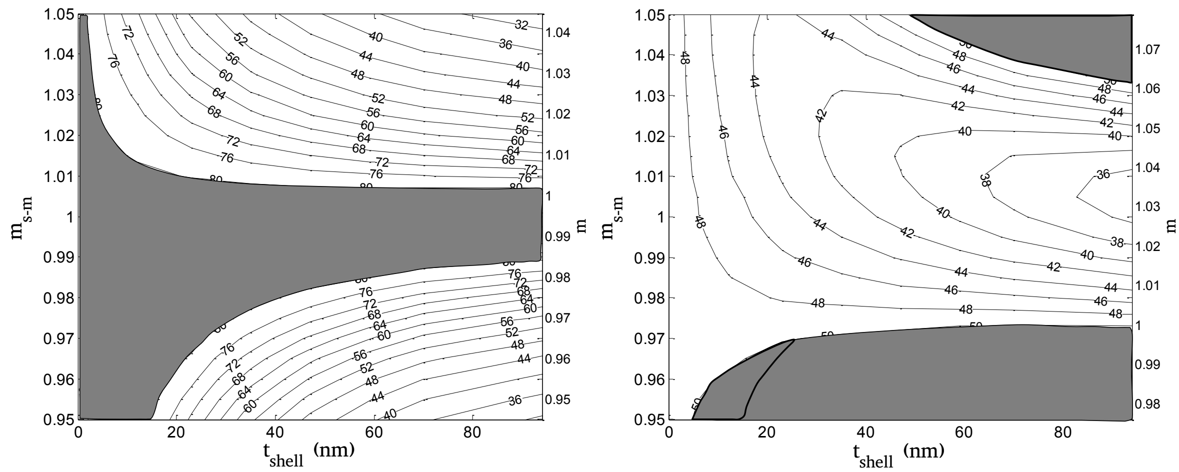

(a) (b)

Figure 5-4 Transmittance in the clear state, $m_{c\text{-}m,CS}$ = 1.0054 at T = 29°C, and (b) reflectance in the translucent state, $m_{c\text{-}m,TS}$ = 0.9734 at T > 78°C for HSA in PMMA at a volume fraction of 16% and thickness of 3 mm. The lightly shaded area indicates the region of acceptable transmittance (a) and reflectance (b). The darker shaded area in (b) is the solution space.

with or without encapsulation, assuming the size of the particles can be controlled in both cases.

Increasing the particle volume fraction increases the optical thickness of the slab. Thus, as shown in Figure 5-3, the region of acceptable transmittance decreases and the region of acceptable reflectance increases with an increase in volume fraction from the baseline of 18% to 20%. At 20% volume fraction, the range of acceptable shell relative refractive index is slightly less than for 18%, but thicker shells are acceptable. For example, for shell relative refractive indices from 0.9675 to 0.99, it is acceptable to use a 20 nm thick shell. At a shell relative refractive index of 0.97 and a thickness of 20 nm, the transmittance in the clear state is 81% and the reflectance in the translucent state is 53% compared to a transmittance of 79% and reflectance of 53% for unencapsulated particles Conceivably, the volume fraction could be increased beyond 20% to access more regions of the solution space. However, a volume fraction of 20% is at the upper bound for the assumption of independent scattering. Additionally, high volume fractions may have fabrication challenges such as agglomeration of the disperse phase during mixing with the matrix.

As shown by Figure 5-4, decreasing the volume fraction from the baseline reduces significantly the size of the solution space. The reduction in solution space compared to 18 and 20% volume fraction is attributed to a decrease in optical thickness that reduces the region of acceptable reflectance in the translucent state. However, even at 16% volume fraction, encapsulation, with the shell thickness and relative refractive index combinations in the solution space, is beneficial since unencapsulated particles provide a transmittance of 82% in the clear state, but only 49% reflectance in the translucent state.

The solution spaces in Figure 5-2 to Figure 5-4 point to selection of shell materials with relative index of refraction from 0.95 to 1 corresponding to refractive indices from 1.417 to 1.4919. Additionally, the shell must have a melting temperature greater than the processing temperature of PMMA (~150 °C). One potential shell material is fused silica (n = 1.458) [78], because it meets both criteria and because it has been used as an encapsulate for phase change materials [46, 61, 62].

5.6 Conclusion

The present study uses a Monte Carlo ray tracing algorithm to guide the design of encapsulated phase change materials for use in a thermotropic material. A method is outlined to down select potential thermotropic material combinations from relative refractive index data to obtain a target optical performance of greater than 80% transmittance in the clear state and greater than 50% reflectance in the translucent state. Through this process, hydroxystearic acid in poly(methyl methacrylate) is identified as a promising thermotropic material. The steady-state, optical properties for this combination with encapsulated particles are predicted at a wavelength of 589 nm as a function of the shell relative refractive index, shell thickness, and particle volume fraction. The core radius is fixed at 234 nm. To obtain the target optical performance with encapsulated particles, shell relative refractive indices from 0.95 to 1 and shell thickness up to 35 nm are acceptable.

Thus, the study demonstrates that thermotropic materials with encapsulated particles can achieve the optical requirements for use in a solar thermal collector. Additionally, the study reveals that, contrary to the prior assumption that only shell materials with a refractive index approximately equal to the matrix refractive index are acceptable, a wide range of shell refractive indices are acceptable.

5.7 Funding

This research is funded by the University of Minnesota Initiative for Renewable Energy and by the National Renewable Energy Laboratory (Supplement to Grant No. EFRI-1038308).

5.8 Nomenclature

Latin Symbols

a	Core radius	m
b	Shell radius	m
f_v	Volume fraction	(%)
i	Imaginary number	
I	Radiative intensity	$W/m^2/sr$
k	Absorptive index	-
L	Slab thickness	m
m	Relative Refractive Index	-
n	Real part of refractive index	-
N	Complex refractive index	-
Q_{ext}	Extinction efficiency factor	-
Q_s	Scattering efficiency factor	-
$\hat{\boldsymbol{s}}$	unit vector describing direction of ray	
$\hat{\boldsymbol{s}}_{\boldsymbol{i}}$	unit vector describing direction of radiation before being scattered into $\hat{\mathbf{s}}$	
t_{shell}	Shell thickness	m
x	Size parameter	-
Greek Symbols		
θ	scattering angle	radians
κ_{eff}	effective absorptive coefficient	mm^{-1}
λ	wavelength of incident radiation	nm
σ_s	scattering coefficient	mm^{-1}
τ_L	Overall optical thickness	-

Φ	scattering phase function	-
ω	scattering albedo	-
Ω	solid angle	sr
Subscripts		
core	Denotes property of the core	
c-m	Core-relative-to-the-matrix	
matrix	Denotes property of the matrix	
shell	Denotes property of the shell	
s-c	Shell-relative-to-the-core	
s-m	Shell-relative-to-the-matrix	

5.9 References

[1] IEA Task 39, 2014, "Polymeric Materials for Solar Thermal Applications, Solar Heating & Cooling Program, International Energy Agency (IEA). http://task39.iea-shc.org/," **2014**(02/24) .

[2] Hudon, K., Merrigan, T., Burch, J., 2012, "Low-Cost Solar Water Heating Research and Development Roadmap," National Renewable Energy Laboratory (NREL). Technical Report. NREL/TP-550054793.

[3] Kohl, M., Meir, M.G., Papillon, P., 2012, "Polymeric Materials for Solar Thermal Applications," Wiley-VCH Verlag & Co., Weinheim, German, pp. 393.

[4] Burch, J. D., 2006, "Polymer-based solar thermal systems: past, present and potential products," Proceedings of the 64th Annual Technical Conference & Exhibition, Society of Plastic Engineers, Charlotte, North Carolina, pp. 7-11.

[5] Martinopoulos, G., Missirlis, D., Tsilingiridis, G., 2010, "CFD Modeling of a Polymer Solar Collector," Renewable Energy, **35**(7) pp. 1499-1508.

[6] Tsilingiris, P., 2002, "Back Absorbing Parallel Plate Polymer Absorbers in Solar Collector Design," Energy Conversion and Management, **43**(1) pp. 135-150.

[7] Mintsa Do Ango, A., Medale, M., and Abid, C., 2013, "Optimization of the Design of a Polymer Flat Plate Solar Collector," Solar Energy, **87** pp. 64-75.

[8] Cristofari, C., Notton, G., Poggi, P., 2002, "Modelling and Performance of a Copolymer Solar Water Heating Collector," Solar Energy, **72**(2) pp. 99-112.

[9] Siqueira, D. A., Vieira, L. G. M., and Damasceno, J. J. R., 2011, "Analysis and Performance of a Low-Cost Solar Heater," Renewable Energy, **36**(9) pp. 2538-2546.

[10] Meir, M., and Rekstad, J., 2003, "Der Solarnor Kunststoffkollektor–The development of a polymer collector with glazing," Proceedings 1. Leobner Symposium Polymeric Solar Materials, November 6-7, pp. II-1-II-8.

[11] Resch, K., and Wallner, G.M., 2012, "Polymeric Materials for Solar Thermal Applications," Wiley-VCH Verlag & Co., Weinheim, German, pp. 129-134, Chap. 7.

[12] Rhodes, R. O., 2010, "Polymer Thin-Film Design Reduces Installed Cost of Solar Water Heater," Proceedings of the 39th ASES national Solar Conference; Phoenix, AZ, pp. 1588.

[13] Wallner, G. M., Resch, K., and Hausner, R., 2008, "Property and Performance Requirements for Thermotropic Layers to Prevent Overheating in an all Polymeric Flat-Plate Collector," Solar Energy Materials and Solar Cells, **92**(6) pp. 614-620.

[14] Gladen, A. C., Davidson, J. H., and Mantell, S. C., 2014, "The Effect of a Thermotropic Material on the Optical Efficiency and Stagnation Temperature of a Polymer Flat Plate Solar Collector," Journal of Solar Energy Engineering. Accepted for publication.

[15] Gladen, A. C., Mantell, S. C., and Davidson, J. H., 2014, "A Parametric Numerical Study of Optical Behavior of Thermotropic Materials for Solar Thermal Collectors," Journal of Heat Transfer, **136**(7), pp. 072703, doi: 10.1115/1.4027153.

[16] Baer, S. C., 1985, "Thermal Control System for Solar Collector," (4,528,976) .

[17] Harrison, S., and Cruickshank, C. A., 2012, "A Review of Strategies for the Control of High Temperature Stagnation in Solar Collectors and Systems," Energy Procedia, **30** pp. 793-804.

[18] Buckley, B. S., and Guldman, T. A., 1983, "Method and Apparatus for Overtemperature Control of Solar Water Heating System," US Patent (4,399,807) .

[19] Kusyy, O., and Vajen, K., 2011, "Theoretical Investigation on a Control-based Approach to Avoid Stagnation of Solar Heating Systems," Proceeding of ISES Solar World Congress, Kassel, Germany, Kassel, Germany, pp. 3323-3330.

[20] Kearney, M., Davidson, J., and Mantell, S., 2005, "Polymeric Absorbers for Flat-Plate Collectors: Can Venting Provide Adequate Overheat Protection?" Journal of Solar Energy Engineering, **127**(3) pp. 421-424.

[21] Mahdjuri, F., 1999, "Solar Collector with Temperature Limitation using Shape Memory Metal," Renewable Energy, **16**(1) pp. 611-617.

[22] Roberts, J., Brandemuehl, M., Burch, J., 2000, "Overheat Protection for Solar Water Heating Systems Using Natural Convection Loops," Proceedings of the Solar Conference, American Solar Energy Society; American Institute of Architects, pp. 273-278.

[23] Russell, L., and Guven, H., 1982, "Modeling and Analysis of an all-Plastic Flat-Plate Solar Collector," J.Sol.Energy Eng., **104**(4) pp. 333-339.

[24] Rich, A. C., 1995, "Solar Collector Venting System," US Patent (5,404,867) .

[25] Slaman, M., and Griessen, R., 2009, "Solar Collector Overheating Protection," Solar Energy, **83**(7) pp. 982-987.

[26] Muehling, O., Seeboth, A., Haeusler, T., 2009, "Variable Solar Control using Thermotropic core/shell Particles," Solar Energy Materials and Solar Cells, **93**(9) pp. 1510-1517.

[27] Gladen, A. C., Davidson, J. H., and Mantell, S. C., 2013, "Selection of Thermotropic Materials for Overheat Protection of Polymer Absorbers," Solar Energy, **104** pp. 42-51, doi: 10.1016/j.solener.2013.10.026.

[28] Resch, K., Hausner, R., and Wallner, G. M., 2009, "All Polymeric Flat-Plate Collector — Potential of Thermotropic Layers to Prevent Overheating," Proceedings of ISES World Congress

2007 (Vol. I – Vol. V), D. Y. Goswami and Y. Zhao, eds. Springer Berlin Heidelberg, pp. 561-565.

[29] Thür, A. V., Hintringer, C., Richtfeld, A., 2013, "Status Quo Der Entwicklungen Eines Überhitzungsgeschützten Kunststoffkollektors," Erneuerbare Energie, http://www.aee.at/aee/index.php?option=com_content&view=article&id=749&Itemid=113, 2014(6/12).

[30] Weber, A., and Resch, K., 2014, "Thermotropic Glazings for Overheating Protection. I. Material Preselection, Formulation, and light-shielding Efficiency," Journal of Applied Polymer Science, **131**(4) pp. doi: 10.1002/app.39950.

[31] Weber, A., Schmid, A., and Resch, K., 2014, "Thermotropic Glazings for Overheating Protection. II. Morphology and structure–property Relationships," Journal of Applied Polymer Science, **131**(4) pp. doi: 10.1002/app.39910.

[32] Weber, A., Schlögl, S., and Resch, K., 2013, "Effect of Formulation and Processing Conditions on Light Shielding Efficiency of Thermotropic Systems with Fixed Domains Based on UV Curing Acrylate Resins," Journal of Applied Polymer Science, **13**0(5) pp. 3299-3310.

[33] Weber, A., and Resch, K., 2012, "Thermotropic Glazings for Overheating Protection," Energy Procedia, **30** pp. 471-477.

[34] Resch, K., and Wallner, G. M., 2009, "Thermotropic Layers for Flat-Plate collectors—A Review of various Concepts for Overheating Protection with Polymeric Materials," Solar Energy Materials and Solar Cells, **93**(1) pp. 119-128.

[35] Gladen, A. C., Mantell, S. C., and Davidson, J. H., 2013, "A Parametric Numerical Study of Radiative Transfer in Thermotropic Materials," ASME 2013 Heat Transfer Summer Conference collocated with the ASME 2013 7th International Conference on Energy Sustainability and the ASME 2013 11th International Conference on Fuel Cell Science, Engineering and Technology,

American Society of Mechanical Engineers, Minneapolis, MN, pp. V001T01A002-V001T01A002.

[36] Seeboth, A., Ruhmann, R., and Muehling, O., 2010, "Thermotropic and Thermochromic Polymer Based Materials for Adaptive Solar Control," Materials, **3**(12) pp. 5143-5168.

[37] Nitz, P., and Hartwig, H., 2005, "Solar Control with Thermotropic Layers," Solar Energy, **79**(6) pp. 573-582.

[38] Nitz, P., Ferber, J., Stangl, R., 1998, "Simulation of Multiply Scattering Media," Solar Energy Materials and Solar Cells, **54**(1-4) pp. 297-307.

[39] Tyagi, V. V., Kaushik, S. C., Tyagi, S. K., 2011, "Development of Phase Change Materials Based Microencapsulated Technology for Buildings: A Review," Renewable and Sustainable Energy Reviews, **15**(2) pp. 1373-1391.

[40] Zalba, B., Marín, J. M., Cabeza, L. F., 2003, "Review on Thermal Energy Storage with Phase Change: Materials, Heat Transfer Analysis and Applications," Applied Thermal Engineering, **2**3(3) pp. 251-283.

[41] Zhao, C. Y., and Zhang, G. H., 2011, "Review on Microencapsulated Phase Change Materials (MEPCMs): Fabrication, Characterization and Applications," Renewable and Sustainable Energy Reviews, **15**(8) pp. 3813-3832.

[42] Zhang, T., Wang, Y., Shi, H., 2012, "Fabrication and Performances of New Kind Microencapsulated Phase Change Material Based on Stearic Acid Core and Polycarbonate Shell," Energy Conversion and Management, **64**(0) pp. 1-7.

[43] Cho, J., Kwon, A., and Cho, C., 2002, "Microencapsulation of Octadecane as a Phase-Change Material by Interfacial Polymerization in an Emulsion System," Colloid and Polymer Science, **280**(3) pp. 260-266.

[44] Fang, Y., Kuang, S., Gao, X., 2008, "Preparation and Characterization of Novel Nanoencapsulated Phase Change Materials," Energy Conversion and Management, **49**(12) pp. 3704-3707.

[45] Fang, G., Li, H., Yang, F., 2009, "Preparation and Characterization of Nano-Encapsulated n-Tetradecane as Phase Change Material for Thermal Energy Storage," Chemical Engineering Journal, **153**(1–3) pp. 217-221.

[46] Jin, Y., Lee, W., Musina, Z., 2010, "A One-Step Method for Producing Microencapsulated Phase Change Materials," Particuology, **8**(6) pp. 588-590.

[47] Sánchez-Silva, L., Rodríguez, J. F., Romero, A., 2010, "Microencapsulation of PCMs with a Styrene-Methyl Methacrylate Copolymer Shell by Suspension-Like Polymerisation," Chemical Engineering Journal, **157**(1) pp. 216-222.

[48] Sarı, A., Alkan, C., Karaipekli, A., 2009, "Microencapsulated n-Octacosane as Phase Change Material for Thermal Energy Storage," Solar Energy, **83**(10) pp. 1757-1763.

[49] Alkan, C., Sarı, A., and Karaipekli, A., 2011, "Preparation, Thermal Properties and Thermal Reliability of Microencapsulated n-Eicosane as Novel Phase Change Material for Thermal Energy Storage," Energy Conversion and Management, **52**(1) pp. 687-692.

[50] Sarı, A., Alkan, C., and Karaipekli, A., 2010, "Preparation, Characterization and Thermal Properties of PMMA/n-Heptadecane Microcapsules as Novel solid–liquid microPCM for Thermal Energy Storage," Applied Energy, **87**(5) pp. 1529-1534.

[51] Pan, L., Tao, Q., Zhang, S., 2012, "Preparation, Characterization and Thermal Properties of Micro-Encapsulated Phase Change Materials," Solar Energy Materials and Solar Cells, **98** pp. 66-70.

[52] Weber, A., and Resch, K., 2014, "Thermotropic Systems with Fixed Domains Exhibiting Enhanced Overheating Protection Performance," Journal of Applied Polymer Science, **131**(12) doi: 10.1002/app.40417.

[53] Mochane, M. J., and Luyt, A. S., 2012, "Preparation and Properties of Polystyrene Encapsulated Paraffin Wax as Possible Phase Change Material in a Polypropylene Matrix," Thermochimica Acta, **544**(0) pp. 63-70.

[54] Liang, C., Lingling, X., Hongbo, S., 2009, "Microencapsulation of Butyl Stearate as a Phase Change Material by Interfacial Polycondensation in a Polyurea System," Energy Conversion and Management, **50**(3) pp. 723-729.

[55] Wang, Y., Xia, T. D., Feng, H. X., 2011, "Stearic acid/polymethylmethacrylate Composite as Form-Stable Phase Change Materials for Latent Heat Thermal Energy Storage," Renewable Energy, **36**(6) pp. 1814-1820.

[56] Gschwander, S., Schossig, P., and Henning, H., 2005, "Micro-Encapsulated Paraffin in Phase-Change Slurries," Solar Energy Materials and Solar Cells, **89**(2–3) pp. 307-315.

[57] Yang, R., Zhang, Y., Wang, X., 2009, "Preparation of n-Tetradecane-Containing Microcapsules with Different Shell Materials by Phase Separation Method," Solar Energy Materials and Solar Cells, **93**(10) pp. 1817-1822.

[58] Tseng, Y., Fang, M., Tsai, P., 2005, "Preparation of Microencapsulated Phase-Change Materials (MCPCMs) by Means of Interfacial Polycondensation," Journal of Microencapsulation, **22**(1) pp. 37-46.

[59] Zhang, H., and Wang, X., 2009, "Fabrication and Performances of Microencapsulated Phase Change Materials Based on n-Octadecane Core and Resorcinol-Modified melamine–formaldehyde Shell," Colloids and Surfaces A: Physicochemical and Engineering Aspects, **332**(2–3) pp. 129-138.

[60] Zou, G. L., Tan, Z. C., Lan, X. Z., 2004, "Preparation and Characterization of Microencapsulated Hexadecane used for Thermal Energy Storage," Chinese Chemical Letters, **15**(6) pp. 729-732.

[61] Fang, G., Chen, Z., and Li, H., 2010, "Synthesis and Properties of Microencapsulated Paraffin Composites with SiO2 Shell as Thermal Energy Storage Materials," Chemical Engineering Journal, **163**(1–2) pp. 154-159.

[62] Li, H., Fang, G., and Liu, X., 2010, "Synthesis of Shape-Stabilized paraffin/silicon Dioxide Composites as Phase Change Material for Thermal Energy Storage," Journal of Materials Science, **45**(6) pp. 1672-1676.

[63] Jiang, Y., Wang, D., and Zhao, T., 2007, "Preparation, Characterization, and Prominent Thermal Stability of Phase-Change Microcapsules with Phenolic Resin Shell and n-Hexadecane Core," Journal of Applied Polymer Science, **104**(5) pp. 2799-2806.

[64] Berkland, C., Pollauf, E., Pack, D. W., 2004, "Uniform Double-Walled Polymer Microspheres of Controllable Shell Thickness," Journal of Controlled Release, **96**(1) pp. 101-111.

[65] Bohren, C.F., and Huffman, D.R., 1998, Absorption and Scattering of Light by Small Particles, Wiley-Interscience.

[66] Tien, C. L., and Drolen, B., 1987, "Thermal radiation in particulate media with dependent and independent scattering," In: Annual review of numerical fluid mechanics and heat transfer. Volume 1 (A88-18971 06-34). Washington, DC, Hemisphere Publishing Corp., 1987, **1** pp. 1-32.

[67] Viskanta, R., and Mengüç, M. P., 1987, "Radiation Heat Transfer in Combustion Systems," Progress in Energy and Combustion Science, **13**(2) pp. 97-160.

[68] Mishchenko, M.I., Travis, L.D., and Lacis, A.A., 2006, Multiple Scattering of Light by Particles: Radiative Transfer and Coherent Backscattering, Cambridge University Press, New York, NY.

[69] Modest, M., 2003, Radiative Heat Transfer, Second Edition, Academic Press, USA, pp. 263-287, Chap. 9.

[70] Randrianalisoa, J., and Baillis, D., 2010, "Radiative Properties of Densely Packed Spheres in Semitransparent Media: A New Geometric Optics Approach," Journal of Quantitative Spectroscopy and Radiative Transfer, **111**(10) pp. 1372-1388.

[71] Dombrovskii, L. A., 2004, "The Propagation of Infrared Radiation in a Semitransparent Liquid Containing Gas Bubbles," High Temperature, **42**(1) pp. 146-153.

[72] Aden, A. L., and Kerker, M., 1951, "Scattering of Electromagnetic Waves from Two Concentric Spheres," Journal of Applied Physics, **22**(10) pp. 1242-1246.

[73] Khashan, M., and Nassif, A., 2001, "Dispersion of the Optical Constants of Quartz and Polymethyl Methacrylate Glasses in a Wide Spectral Range: 0.2–3 mm," Optics Communications, **188**(1) pp. 129-139.

[74] Randrianalisoa, J., Baillis, D., and Pilon, L., 2006, "Modeling Radiation Characteristics of Semitransparent Media Containing Bubbles Or Particles," J.Opt.Soc.Am.A, **23**(7) pp. 1645-1656.

[75] Baneshi, M., Maruyama, S., and Komiya, A., 2010, "Infrared Radiative Properties of Thin Polyethylene Coating Pigmented with Titanium Dioxide Particles," Journal of Heat Transfer, **132**(2) pp. 023306.

[76] Modest, M., 2003, "Radiative Heat Transfer, Second Edition,"Academic Press, USA, pp. 644-679, Chap. 20.

[77] Farmer, J.T., and Howell, J.R., 1998, "Advances in Heat Transfer,"Elsevier, pp. 333-429.

[78] Gooch, J.W., 2011, Encyclopedic Dictionary of Polymers, 2nd ed., Springer Science & Business Media, New York, NY USA.

[79] Bass, M., DeCusatis, C., Enoch, J., 2009, "Handbook of Optics, Volume IV: Optical Properties of Materials, Nonlinear Optics, Quantum Optics (set)," McGraw Hill Professional.

[80] Polyanskiy, M., "Refractive Index Database," refractiveindex.info **2013**(07/19) .

6 Conclusion

6.1 Summary

This dissertation presents a numerical evaluation of thermotropic materials. These studies represent a significant advancement in the development of these materials. Previously, researchers had to rely on a time intensive, empirical approach. Now; however, there is a theoretical basis for the design and development of thermotropic materials.

The optical requirements for a thermotropic material to provide overheat protection were outlined by modeling a polymer, flat plate solar collector with a thermotropic material on the absorber. The optical requirement for a thermotropic material in the clear state was identified by relating the transmittance of a thermotropic material in the clear state to the optical efficiency of the collector. High solar-weighted transmittance (>~85%) is necessary to have an optical efficiency approximately equal to single glazed, flat plate collectors with non-selective absorbers rated by the SRCC. The optical requirement for a thermotropic material in the translucent state was identified by relating the stagnation temperature of the collector to the solar-weighted reflectance of the thermotropic material in its translucent state. The boundary conditions for this analysis were selected to represent a worst case scenario for overheating, i.e. induce higher stagnation temperatures. High solar-weighted reflectance in the translucent state is necessary for a thermotropic material to adequately provide overheat protection for a commodity polymer absorber. For a polypropylene absorber, the solar-weighted reflectance needs to be on the order of 50%. For absorbers constructed from other commodity polymers, which have lower service temperatures, the reflectance must be higher. These optical requirements give researchers a metric with which to assess the efficacy of thermotropic materials in providing overheat protection. The analysis also demonstrates that the optical requirements for a thermotropic material in a solar thermal collector are more stringent than previously articulated.

To determine how to achieve these stringent optical requirements the radiative transfer within a thermotropic material was modeled. The thermotropic material was model as a cold, isothermal slab with monodisperse, randomly distributed spherical particles. The thermotropic material was modeled at different temperatures by a change in the relative refractive index between the particles and the matrix. A Monte Carlo ray tracing program was used to predict the normal-hemispherical transmittance, reflectance, and absorptance of the slab. The model was validated by comparison to experimental data and analytical benchmark solutions. Both unencapsulated and encapsulated particles were investigated.

A parametric study of the effects of material properties (refractive index and absorptive index) and fabrication properties (particle radius, slab thickness, particle volume fraction) on the optical properties of thermotropic materials was conducted. The results are presented in dimensionless form as a function of overall optical thickness τ_L, scattering albedo ω, and particle size parameter x. This data can be used to either select a scattering domain/matrix combination based on desired performance criteria, or to predict the optical properties in the clear and translucent state of a specific combination of materials for various combinations of particle radius, volume fraction, and thickness.

The parametric study demonstrates that to have high transmittance in the clear state, the optical thickness must be low. To achieve high reflectance in the translucent state, a significant change in optical thickness must occur, the particles must be small ($x \leq 2.5$ for $\omega = 0.995$), and the scattering albedo must be greater than or equal to 0.990. For example, for a particle size parameter of two, the optical thickness must be ≤0.35 in the clear state to achieve a spectral transmittance greater than 85%. The optical thickness must be ≥10 (for a scattering albedo of 0.995) in the translucent state to achieve a spectral reflectance greater than 50%. To achieve a scattering albedo near unity necessitates using a low absorption polymer, such as poly(methyl acrylate), polycarbonate, or clarified polypropylene, as a matrix material.

A method for indentifying potential thermotropic materials using the dimensionless data is presented. This method provides a means to replace the trial and error methodology previously employed. Some potential thermotropic material combinations identified are poly(ethylene-co-vinyl acetate) in a matrix of poly(methyl methacrylate), n-hexatriacontane in a matrix of polycarbonate, hydroxystearic acid in poly(methyl methacrylate), and low molecular weight polyethylene in a matrix of poly(methyl methacrylate).

Low molecular weighted polyethylene in poly(methyl methacrylate) was further investigated through a case study to demonstrate how to optimize thermotropic materials with the parametric study data. For this combination and a particle radius of 200 nm ($x = 2.13$ at $\lambda = 589$ nm), the effects of thickness and volume fraction on the solar-weighted transmittance, reflectance, and absorptance were investigated. To achieve a solar-weighted transmittance in the clear state ≥85% and a solar-weighted reflectance in the translucent state ≥50%, the thickness should be 1 mm and the volume fraction should be 15%.

Lastly, the effects of using encapsulated particles in a thermotropic material were investigated. Encapsulated particles are of interest because encapsulation may provide a means to precisely control the particle size and thus to obtain the small particles necessary for ≥50% reflectance in the translucent state. The normal-hemispherical transmittance in the clear state and reflectance in the translucent state were predicted as a function of shell relative refractive index, shell thickness, and particle volume fraction at a wavelength of 589 nm for hydroxystearic acid in poly(methyl methacrylate).

The study demonstrates that a thermotropic material with encapsulated particles can achieve the required optical performance. Additionally, the study reveals that, contrary to the prior assumption that the shell relative refractive index be equal to one, a wide range of shell refractive indices are acceptable. For hydroxystearic acid in poly(methyl methacrylate), shell relative refractive indices from 0.95 to 1 and shell thickness up to 35 nm are acceptable.

6.2 Future Considerations

Future research into thermotropic materials is recommended primarily in material fabrication, but there are also intriguing avenues for further research modeling a thermotropic material in flat plate collector, modeling the non-normal radiative properties of thermotropic materials, and modeling the radiative transfer in a polydisperse thermotropic material.

With the theoretical basis for the development of thermotropic materials outlined, material development should be the primary concern of future research. The appendix contains the results of the preliminary material development. The information contained in the appendix, as well as the numerical results of the dissertation, can be used to guide future material development. One of the ways to expedite material development is to develop an in-house means of measuring the refractive index as a function of temperature. Having such a capability will aid in identifying potential thermotropic material combinations and in optimizing the combinations that have already been identified, particularly those identified through the Lorentz-Lorenz equation.

From an optical perspective, the most promising material combination for future research is paraffin wax (alkane) or low molecular weight polyethylene (PE) in a matrix of PMMA or clarified PP. Therefore, these combinations are recommended as the primary direction for future material development. A fabrication challenge associated with using paraffin wax or low molecular weight polyethylene as the scattering domain is the difference, with the matrix material, in viscosity in the melt phase and in coefficient of thermal expansion. The former makes blending a challenge and leads to the formation of large particles in the blend. The latter aids in vacuole formation. Encapsulation may help overcome both of these challenges. If unencapsulated particles are investigated, a compatibilizer, such as a poly(ethylene-co-vinyl acetate) (EVA), may be required. Using a compatibilizer will result in a narrower particle size distribution, smaller mean diameter, and may reduce the likelihood of vacuole formation than blending the two materials by themselves.

In the present study the effects of the steady-state, optical properties of a thermotropic material in the clear and translucent state on the collector optical efficiency and stagnation temperature are considered. Modeling the transient behavior of the thermotropic material in the collector would better quantify the acceptable switching behavior between the two states. To capture the transient behavior of the thermotropic material and its effects on the collector performance requires modeling the collector, the ambient conditions, and the load requirements. Additionally, the heat transfer within the thermotropic material coupled to the melting of the particles and to the optical properties of the thermotropic material must be modeled within the larger collector/system model.

The numerical results of the present work are limited to normal incidence. However, in a solar collector, the thermotropic material is often irradiated at non-normal incidence. A numerical evaluation of the non-normal optical properties of thermotropic materials is recommended. The ability to handle non-normal incidence angles has been incorporated into the current Monte Carlo model.

Lastly, the present work is restricted to thermotropic materials with monodisperse particles. This restriction was implemented because the objective of the study was to focus on the particle size, and because a polydispersion can be represented as a monodispersion through a weighted radius, such as the Sauter mean diameter. However, the thermotropic materials fabricated will be polydisperse. Therefore, knowing the effects of dispersion on the optical properties and knowing the dispersity at which the monodisperse approximation is no longer valid will help guide the fabrication process. The Monte Carlo model used in the present can be expanded to model polydisperse thermotropic materials by weighting the cumulative distribution function for the size parameter by the particle distribution function.

7 Bibiliography

Alkan C, Sarı A, Karaipekli A. Preparation, thermal properties and thermal reliability of microencapsulated n-eicosane as novel phase change material for thermal energy storage. Energy Conversion and Management 2011 1;52(1): p.687-92.

ASTM Standard D648. Test method for deflection temperature of plastics under flexural load. Annual Book of ASTM Standards 2007;08.01.

ASTM Standard G173. Standard Tables for Reference Solar Spectral Irradiances: Direct Normal and Hemispherical on 37^{o} Tilted Surface. Annual Book of ASTM Standards 2012;14.04.

Baer SC, inventor. Thermal control system for solar collector. US Patent 4,528,976. 1985 .

Baneshi M, Maruyama S, Komiya A. Infrared Radiative Properties of Thin Polyethylene Coating Pigmented With Titanium Dioxide Particles. Journal of Heat Transfer 2010;132(2):023306.

Berkland C, Pollauf E, Pack DW, Kim K. Uniform double-walled polymer microspheres of controllable shell thickness. J.Controlled Release 2004 4/16;96(1): p.101-11.

Bernini U, Malinconico M, Martuscelli E, Mormile P, Novellino A, Russo P, et al. Ultra-tough synthetic glasses made by reactive blending of PMMA and EVA rubbers: opto-thermal characterization. J.Mater.Process.Technol. 1995 12;55(3–4): p.224-8.

Bohren CF, Huffman DR. Absorption and Scattering of Light by Small Particles. : Wiley-Interscience; 1998.

Brunold S, Papillon P, Plaschkes M, Rekstad J, Wilhelms C. Collectors and Heat Stores. In: Kohl M, Meir MG, Papillon P, Wallner GM, Saile S, editors. Polymeric Materials for Solar Thermal ApplicationsWeinheim, German: Wiley-VCH Verlag & Co.; 2012a. p. 301-348.

Brunold S, Ruesch F, Kunic R, Rekstad J, Meir M, Wilhelms C. Durability Tests of Polymeric Components. In: Kohl M, Meir MG, Papillon P, Wallner GM, Saile S, editors. Polymeric Materials for Solar Thermal Applications, Weinheim, German: Wiley-VCH Verlag & Co.; 2012b. p. 319-349.

Buckles WE, Klein SA. Analysis of solar domestic hot water heaters. Solar Energy 1980; 25(5): p.417-24.

Buckley BS, Guldman TA, inventors. Method and apparatus for overtemperature control of solar water heating system. US Patent 4,399,807. 1983.

Buehler DFSR. Reversible thermotropic composition, its preparation and use. 2004 November (EP0985709).

Burch, Jay. Polymer-based solar thermal systems: past, present and potential products. Proceedings of the 64th Annual Technical Conference & Exhibition; May 6 - 11; Charlotte, North Carolina: Society of Plastic Engineers; 2006.

Burch J, Merrigan T, Jorgensen G, Christensen C, Hewett R. Low-Cost Residential Solar Thermal Systems. 2006.

Busbridge I, Orchard S. Reflection and Transmission of Light by a Thick Atmosphere According to a Phase Function: 1 - chi COS theta. Astrophys.J. 1967;149: p.655-64.

Cariou J, Dugas J, Martin L, Michel P. Refractive-index variations with temperature of PMMA and polycarbonate. Appl.Opt. 1986;25(3): p.334-6.

Cho J, Kwon A, Cho C. Microencapsulation of octadecane as a phase-change material by interfacial polymerization in an emulsion system. Colloid Polym.Sci. 2002;280(3): p.260-6.

Cristofari C, Notton G, Poggi P, Louche A. Modelling and performance of a copolymer solar water heating collector. Solar Energy 2002;72(2): p.99-112.

Dabisch W. Bodies with reversibly variable temperature-dependent light absorbence. 1981 US Patent 4268413.

Dell'Erba R, Groeninckx G, Maglio G, Malinconico M, Migliozzi A. Immiscible polymer blends of semicrystalline biocompatible components: thermal properties and phase morphology analysis of PLLA/PCL blends. Polymer 2001 8;42(18): p.7831-40.

Denholm P. The Technical Potential of Solar Water Heating to Reduce Fossil Fuel Use and Greenhouse Gas Emissions in the United States. National Renewable Energy Laboratory (NREL). Technical Report. NREL/TP-640-41157 2007.

Dombrovskii LA. The Propagation of Infrared Radiation in a Semitransparent Liquid Containing Gas Bubbles. High Temperature 2004;42(1): p.146-53.

Dombrovsky L, Randrianalisoa J, Baillis D, Pilon L. Use of Mie theory to analyze experimental data to identify infrared properties of fused quartz containing bubbles. Appl.Opt. 2005 Nov;44(33): p.7021-31.

Duffie J, Beckman W. Solar Engineering of Thermal Processes. Solar Engineering of Thermal Processes
Third Edition. Second ed. Hoboken, NJ: Wiley-Interscience; 2006a. p. 139-173.

Duffie J, Beckman W. Solar Engineering of Thermal Processes. Solar Engineering of Thermal Processes
Third Edition. Second ed. Hoboken, NJ: Wiley-Interscience; 2006b. p. 204-237.

Duffie J, Beckman W. Solar Engineering of Thermal Processes
Third Edition. Second ed. Hoboken, NJ: Wiley-Interscience; 2006c.

Errico M, Greco R, Laurienzo P, Malinconico M, Viscardo D. Acrylate/EVA reactive blends and semi-IPN: Chemical, chemical–physical, and thermo-optical characterization. J Appl Polym Sci 2006;99(6): p.2926-35.

European Commission. Energy Markets in the European Union in 2011. Available at: http://ec.europa.eu/energy/observatory/annual_reports/annual_reports_en.html. Accessed 08/08, 2013.

Fang G, Chen Z, Li H. Synthesis and properties of microencapsulated paraffin composites with SiO2 shell as thermal energy storage materials. Chem.Eng.J. 2010 9/15;163(1–2): p.154-9.

Fang G, Li H, Yang F, Liu X, Wu S. Preparation and characterization of nano-encapsulated n-tetradecane as phase change material for thermal energy storage. Chem.Eng.J. 2009 11/1;153(1–3): p.217-21.

Fang Y, Kuang S, Gao X, Zhang Z. Preparation and characterization of novel nanoencapsulated phase change materials. Energy Conversion and Management 2008 12;49(12): p.3704-7.

Farmer JT, Howell JR. Comparison of Monte Carlo Strategies for Radiative Transfer in Participating Media. Advances in Heat Transfer: Elsevier; 1998. p. 333-429.

Filmetrics. Refractive Index of Polyethylene, PE. 2012; Available at: http://www.filmetrics.com/refractive-index-database/Polyethylene/PE-Polyethene. Accessed 01/25, 2013.

Fischer S, Druck H, Bachmann S, Streicher E, Ullmann J, Traub B. Conventional Collectors, Heat Stores, and Coatings. In: Kohl M, Meir MG, Papillon P, Wallner GM, Saile S, editors. Polymeric Materials for Solar Thermal Applications Weinheim, German: Wiley-VCH Verlag & Co.; 2012. p. 73-106.

Georg A, Graf W, Schweiger D, Wittwer V, Nitz P, Wilson HR. Switchable glazing with a large dynamic range in total solar energy transmittance (TSET). Solar Energy 1998 3;62(3): p.215-28.

Gladen AC, Davidson JH, Mantell SC. The Effect of a Thermotropic Material on the Optical Efficiency and Stagnation Temperature of a Polymer Flat Plate Solar Collector. Journal of Solar Energy Engineering Under Review. 2014.

Gladen AC, Davidson JH, Mantell SC. Selection of thermotropic materials for overheat protection of polymer absorbers. Solar Energy 2013; doi:10.1016/j.solener.2013.10.026.

Gladen AC, Mantell SC, Davidson JH. A Parametric Numerical Study of Optical Behavior of Thermotropic Materials for Solar Thermal Collectors. Journal of Heat Transfer 2014;doi: 10.1115/1.4027153.

Gladen AC, Mantell SC, Davidson JH A Parametric Numerical Study of Radiative Transfer in Thermotropic Materials. ASME 2013 Heat Transfer Summer Conference collocated with the ASME 2013 7th International Conference on Energy Sustainability and the ASME 2013 11th International Conference on Fuel Cell Science, Engineering and Technology; July 14-19; Minneapolis, MN: American Society of Mechanical Engineers; 2013.

Goedhart D. Communication Gel Permeation Chromatography International Seminar. Monaco, Oct 1969:12-5.

Gooch JW editor. Encyclopedic Dictionary of Polymers, 2nd ed. New York, NY USA: Springer Science & Business Media; 2011.

Gschwander S, Schossig P, Henning H-. Micro-encapsulated paraffin in phase-change slurries. Solar Energy Mater.Solar Cells 2005 11/15;89(2–3): p.307-15.

Gupta AK, Ratnam BK, Srinivasan KR. Impact toughening of polypropylene by ethylene vinyl acetate copolymer. J Appl Polym Sci 1992;45(7): p.1303-12.

Harrison HC, inventor. Protective cooling system for solar heat collector. US Patent 4,153,040. 1979 .

Harrison S, Cruickshank CA. A review of strategies for the control of high temperature stagnation in solar collectors and systems. Energy Procedia 2012;30: p.793-804.

Hollands K, Unny T, Raithby G, Konicek L. Free convective heat transfer across inclined air layers. Journal of Heat Transfer 1976;98(2): p.189-93.

Hudon K, Merrigan T, Burch J, Maguire J. Low-Cost Solar Water Heating Research and Development Roadmap. National Renewable Energy Laboratory (NREL). Technical Report. NREL/TP-550054793 2012.

IEA Task 39. Polymeric Materials for Solar Thermal Applications, Solar Heating & Cooling Program, International Energy Agency (IEA). http://task39.iea-shc.org/. 2014; Accessed 02/24, 2014.

Jiang Y, Wang D, Zhao T. Preparation, characterization, and prominent thermal stability of phase-change microcapsules with phenolic resin shell and n-hexadecane core. J Appl Polym Sci 2007;104(5): p.2799-806.

Jin Y, Lee W, Musina Z, Ding Y. A one-step method for producing microencapsulated phase change materials. Particuology 2010 12;8(6): p.588-90.

Kasarova SN, Sultanova, NG, Nikolov ID. Temperature dependence of refractive characteristics of optical plastics. Journal of Physics: Conference Series: IOP Publishing; 2010.

Kasarova SN, Sultanova NG, Ivanov CD, Nikolov ID. Analysis of the dispersion of optical plastic materials. Optical Materials 2007 7;29(11): p.1481-90.

Kearney M, Davidson J, Mantell S. Polymeric Absorbers for Flat-Plate Collectors: Can Venting Provide Adequate Overheat Protection? J.Sol.Energy Eng. 2005 08/00;127(3): p.421-4.

Khashan M, Nassif A. Dispersion of the optical constants of quartz and polymethyl methacrylate glasses in a wide spectral range: 0.2–3 μm. Opt.Commun. 2001;188(1): p.129-39.

Kohl M, Meir MG, Papillon P, Wallner GM, Saile S. Polymeric Materials for Solar Thermal Applications. Weinheim, German: Wiley-VCH Verlag & Co.; 2012.

Krevelen DWv, Nijenhuis K. Properties of Polymers - Their Correlation with Chemical Structure; Their Numerical Estimation and Prediction from Additive Group Contributions (4th, Completely Revised Edition): Elsevier; 2009.

Kusyy O, Vajen K. Theoretical Investigation on a Control-based Approach to Avoid Stagnation of Solar Heating Systems. Proceeding of ISES Solar World Congress, Kassel, Germany; August 28 - September 2; Kassel, Germany; 2011.

Laing K, inventor. Intermittent through-flow collector. US Patent 4,519,380. 1985.

Lee H, Buckius R. Scaling anisotropic scattering in radiation heat transfer for a planar medium. ASME Transactions Journal of Heat Transfer 1982;104: p.68-75.

Lenel UR, Mudd PR. A review of materials for solar heating systems for domestic hot water. Solar Energy 1984;32(1): p.109-20.

Li H, Fang G, Liu X. Synthesis of shape-stabilized paraffin/silicon dioxide composites as phase change material for thermal energy storage. J.Mater.Sci. 2010;45(6): p.1672-6.

Liang C, Lingling X, Hongbo S, Zhibin Z. Microencapsulation of butyl stearate as a phase change material by interfacial polycondensation in a polyurea system. Energy Conversion and Management 2009 3;50(3): p.723-9.

Mahdjuri F. Solar collector with temperature limitation using shape memory metal. Renewable Energy 1999;16(1): p.611-7.

Mantell SC, Davidson JH. Polymer Durability for Solar Thermal Applications. In: Kohl M, Meir MG, Papillon P, Wallner GM, Saile S, editors. Polymeric Materials for Solar Thermal Applications. Weinheim, German: Wiley-VCH Verlag & Co.; 2012. p. 187-210.

Martinopoulos G, Missirlis D, Tsilingiridis G, Yakinthos K, Kyriakis N. CFD modeling of a polymer solar collector. Renewable Energy 2010;35(7): p.1499-508.

Maruyama S. Radiative heat transfer in anisotropic scattering media with specular boundary subjected to collimated irradiation. Int.J.Heat Mass Transfer 1998;41(18): p.2847-56.

McAdams WH. Heat transmission. : McGraw-Hill New York; 1954.

Meir M, Rekstad J. Der Solarnor Kunststoffkollektor–The development of a polymer collector with glazing. Proceedings 1. Leobner Symposium Polymeric Solar Materials, November 6-7; November 6-7; ; 2003.

Merrigan T.Solar Heating & Lighting: Solar Water Heating R&D - DOE Solar Energy Technologies Program. ; April 17-19; Denver, CO; 2007.

Mintsa Do Ango A, Medale M, Abid C. Optimization of the design of a polymer flat plate solar collector. Solar Energy 2013;87: p.64-75.

Mishchenko MI, Travis LD, Lacis AA. Multiple Scattering of Light by Particles: Radiative Transfer and Coherent Backscattering. New York, NY: Cambridge University Press; 2006.

Mochane MJ, Luyt AS. Preparation and properties of polystyrene encapsulated paraffin wax as possible phase change material in a polypropylene matrix. Thermochimica Acta 2012 9/20;544(0):63-70.

Modest M. Radiative Heat Transfer, second editionUSA: Academic Press; 2003a. p. 263-287.

Modest M. Radiative Heat Transfer, second editionUSA: Academic Press; 2003b. p. 644-679.

Muehling O, Seeboth A, Haeusler T, Ruhmann R, Potechius E, Vetter R. Variable solar control using thermotropic core/shell particles. Solar Energy Mater.Solar Cells 2009 9;93(9): p.1510-7.

Nitz P, Ferber J, Stangl R, Rose Wilson H, Wittwer V. Simulation of multiply scattering media. Solar Energy Mater.Solar Cells 1998 7/13;54(1-4): p.297-307.

Nitz P, Hartwig H. Solar control with thermotropic layers. Solar Energy 2005 12;79(6): p.573-82.

Palmatier EP, inventor. Solar heating system. US Patent 4,384,568. 1983.

Pan L, Tao Q, Zhang S, Wang S, Zhang J, Wang S, et al. Preparation, characterization and thermal properties of micro-encapsulated phase change materials. Solar Energy Mater.Solar Cells 2012;98: p.66-70.

Papillon P, Wilhelms C. Thermal Solar Energy for Polymer Experts. In: Kohl M, Meir MG, Papillon P, Wallner GM, Saile S, editors. Polymeric Materials for Solar Thermal Applications. Weinheim, German: Wiley-VCH Verlag & Co.; 2012. p. 29-70.

Polyanskiy M. Refractive Index Database. Available at: refractiveindex.info. Accessed 07/19, 2013.

Raicu A, Wilson HR, Nitz P, Platzer W, Wittwer V, Jahns E. Facade systems with variable solar control using thermotropic polymer blends. Solar Energy 2002 1;72(1): p.31-42.

Raman R, Mantell S, Davidson J, Wu C, Jorgensen G. A review of polymer materials for solar water heating systems. Transactions-ASME Journal of Solar Energy Engineering 2000;122(2): p.92-100.

Randrianalisoa J, Baillis D. Radiative properties of densely packed spheres in semitransparent media: A new geometric optics approach. Journal of Quantitative Spectroscopy and Radiative Transfer 2010 7;111(10): p.1372-88.

Randrianalisoa J, Baillis D, Pilon L. Modeling radiation characteristics of semitransparent media containing bubbles or particles. J.Opt.Soc.Am.A 2006 Jul;23(7): p.1645-56.

Reiter C, Trinkl C, Zorner W. Conventional Collectors, Heat Stores, and Coatings. In: Kohl M, Meir MG, Papillon P, Wallner GM, Saile S, editors. Polymeric Materials for Solar Thermal Applications. Weinheim, German: Wiley-VCH Verlag & Co.; 2012. p. 107-117.

Resch K, Wallner GM. Plastics Market. In: Kohl M, Meir MG, Papillon P, Wallner GM, Saile S, editors. Polymeric Materials for Solar Thermal Applications. Weinheim, German: Wiley-VCH Verlag & Co.; 2012. p. 129-134.

Goswami DY, Zhao Y, editors. All Polymeric Flat-Plate Collector — Potential of Thermotropic Layers to Prevent Overheating. Proceedings of ISES World Congress 2007 (Vol. I – Vol. V): Springer Berlin Heidelberg; 2009.

Resch K, Wallner GM. Morphology of phase-separated thermotropic layers based on UV cured acrylate resins. Polym.Adv.Technol. 2009a;20(12): p.1163-7.

Resch K, Wallner GM. Thermotropic layers for flat-plate collectors—A review of various concepts for overheating protection with polymeric materials. Solar Energy Mater.Solar Cells 2009b 1;93(1): p.119-28.

Resch K, Wallner GM, Hausner R. Phase separated thermotropic layers based on UV cured acrylate resins – Effect of material formulation on overheating protection properties and application in a solar collector. Solar Energy 2009 9;83(9): p.1689-97.

Rhodes RO. Polymer Thin-Film Design Reduces Installed Cost of Solar Water Heater. Proceedings of the 39th ASES national Solar Conference; May17-22; Phoenix, AZ; 2010.

Rich AC, inventor. Solar collector venting system. US Patent 5,404,867. 1995 .

Roberts J, Brandemuehl M, Burch J, Gawlik K. Overheat Protection for Solar Water Heating Systems Using Natural Convection Loops. Proceedings of the Solar Conference: American Solar Energy Society; American Institute of Architects; 2000.

Rubin M. Optical properties of soda lime silica glasses. Solar Energy Materials 1985;12(4): p.275-88.

Ruhmann R, Seeboth A, Muehling O, Loetzsch D. Thermotropic Materials for Adaptive Solar Control. Advances in Science and Technology 2013;77: p.124-31.

Russell L, Guven H. Modeling and analysis of an all-plastic flat-plate solar collector. J.Sol.Energy Eng. 1982;104(4): p.333-9.

Sánchez-Silva L, Rodríguez JF, Romero A, Borreguero AM, Carmona M, Sánchez P. Microencapsulation of PCMs with a styrene-methyl methacrylate copolymer shell by suspension-like polymerisation. Chem.Eng.J. 2010 2/15;157(1): p.216-22.

Sarı A, Alkan C, Karaipekli A. Preparation, characterization and thermal properties of PMMA/n-heptadecane microcapsules as novel solid–liquid microPCM for thermal energy storage. Appl.Energy 2010 5;87(5): p.1529-34.

Sarı A, Alkan C, Karaipekli A, Uzun O. Microencapsulated n-octacosane as phase change material for thermal energy storage. Solar Energy 2009 10;83(10): p.1757-63.

Schael GW. Determination of polyolefin film properties from refractive index measurements. J Appl Polym Sci 1964;8(6): p.2717-22.

Scharfman H, inventor. Vented solar collector. US Patent 4,043,317. 1977.

Scott PB, inventor. Solar heater with automatic venting. US Patent 4,046,134. 1977.

Seeboth A, Ruhmann R, Muehling O. Thermotropic and Thermochromic Polymer Based Materials for Adaptive Solar Control. Materials 2010;3(12): p.5143-68.

Siqueira DA, Vieira LGM, Damasceno JJR. Analysis and performance of a low-cost solar heater. Renewable Energy 2011 9;36(9): p.2538-46.

Slaman M, Griessen R. Solar collector overheating protection. Solar Energy 2009;83(7): p.982-7.

Solar Ratings & Certification Corporation (SRCC). 2014; Available at: http://www.solar-rating.org/index.html. Accessed 06/17, 2014.

Sutton W, Özişik M. An iterative solution for anisotropic radiative transfer in a slab. Journal of Heat Transfer 1979;101:695.

Takahashi S, Okada H, Nobukawa S, Yamaguchi M. Optical properties of polymer blends composed of poly(methyl methacrylate) and ethylene–vinyl acetate copolymer. European Polymer Journal 2012 5;48(5): p.974-80.

Thür AV, Hintringer C, Richtfeld A, Streicher W, Kaiser A, Hausner R, et al. Status Quo der Entwicklungen eines überhitzungsgeschützten Kunststoffkollektors. Erneuerbare Energie 2013;http://www.aee.at/aee/index.php?option=com_content&view=article&id=749&Itemid=113:6/12/2014.

Tien CL, Drolen BL. Thermal radiation in particulate media with dependent and independent scattering. IN: Annual review of numerical fluid mechanics and heat transfer. Volume 1 (A88-18971 06-34). Washington, DC, Hemisphere Publishing Corp., 1987, p. 1-32.; 1987.

Tseng Y, Fang M, Tsai P, Yang Y. Preparation of microencapsulated phase-change materials (MCPCMs) by means of interfacial polycondensation. J.Microencapsul. 2005;22(1): p.37-46.

Tsilingiris P. Back absorbing parallel plate polymer absorbers in solar collector design. Energy conversion and management 2002;43(1): p.135-50.

Tsilingiris PT. Towards making solar water heating technology feasible—the polymer solar collector approach. Energy Conversion and Management 1999 8;40(12): p.1237-50.

Tyagi VV, Kaushik SC, Tyagi SK, Akiyama T. Development of phase change materials based microencapsulated technology for buildings: A review. Renewable and Sustainable Energy Reviews 2011 2;15(2): p.1373-91.

U.S. Energy Information Agency. 2011 Annual energy Review 2011. 2011; Available at: http://www.eia.gov/totalenergy/data/annual/index.cfm#consumption. Accessed 08/08, 2013.

U.S. Energy Information Agency. 2009 Residential Energy Consumption Survey - Consumption and Expenditure Tables (by End Use). 2009; Available at: http://www.eia.gov/consumption/residential/data/2009/index.cfm?view=consumption#end-use. Accessed 01/30, 2013.

UL746B. Polymeric Materials - Long Term Property Evaluations. Underwriters Laboratories, Inc., Northbrook, IL. 1998.

Viskanta R, Mengüç MP. Radiation heat transfer in combustion systems. Progress in Energy and Combustion Science 1987;13(2): p.97-160.

Wallner GM, Resch K, Hausner R. Property and performance requirements for thermotropic layers to prevent overheating in an all polymeric flat-plate collector. Solar Energy Mater.Solar Cells 2008 6;92(6): p.614-20.

Walsh D, Zoller P. Standard Pressure Volume Temperature Data for Polymers. Technomic Publishing Company, Inc. Lancaster, PA USA 1995.

Wang Y, Xia TD, Feng HX, Zhang H. Stearic acid/polymethylmethacrylate composite as form-stable phase change materials for latent heat thermal energy storage. Renewable Energy 2011;36(6): p.1814-20.

Weber A, Resch K. Thermotropic glazings for overheating protection. I. Material preselection, formulation, and light-shielding efficiency. J Appl Polym Sci 2014;131(4):doi: 10.1002/app.39950.

Weber A, Resch K. Effect of temperature-cycling on the morphology of polymeric thermotropic glazings for overheating protection applications. Journal of Polymer Research 2012a;19(6): p.1-8.

Weber A, Resch K. Thermotropic glazings for overheating protection. Energy Procedia 2012b;30: p.471-7.

Weber A, Schlögl S, Resch K. Effect of formulation and processing conditions on light shielding efficiency of thermotropic systems with fixed domains based on UV curing acrylate resins. J Appl Polym Sci 2013;130(5): p.3299-310.

Weber A, Schmid A, Resch K. Thermotropic glazings for overheating protection. II. morphology and structure–property relationships. J Appl Polym Sci 2014;131(4):doi: 10.1002/app.39910.

Weber A, Resch K. Thermotropic systems with fixed domains exhibiting enhanced overheating protection performance. J Appl Polym Sci 2014;131(12).

Weiss W, Biermayr P. Potential of Solar Thermal in Europe. 2006; Available at: http://www.estif.org/. Accessed 08/08, 2013.

Wilson H, Eck W. Transmission variation using scattering/transparent switching layers. Proc. SPIE 1992 2004-12-10T09:16:04;1728(1): p.261-11.

Wylie R, inventor. Passive three-phase heat tube for the protection of apparatus from exceeding maximum or minimum safe working temperatures. US Patent 5,135,575. 1993.

Yang R, Zhang Y, Wang X, Zhang Y, Zhang Q. Preparation of n-tetradecane-containing microcapsules with different shell materials by phase separation method. Solar Energy Mater.Solar Cells 2009 10;93(10): p.1817-22.

Zalba B, Marín JM, Cabeza LF, Mehling H. Review on thermal energy storage with phase change: materials, heat transfer analysis and applications. Appl.Therm.Eng. 2003 2;23(3): p.251-83.

Zhang H, Wang X. Fabrication and performances of microencapsulated phase change materials based on n-octadecane core and resorcinol-modified melamine–formaldehyde shell. Colloids Surf.Physicochem.Eng.Aspects 2009 1/15;332(2–3): p.129-38.

Zhang T, Wang Y, Shi H, Yang W. Fabrication and performances of new kind microencapsulated phase change material based on stearic acid core and polycarbonate shell. Energy Conversion and Management 2012 12;64(0): p.1-7.

Zhao CY, Zhang GH. Review on microencapsulated phase change materials (MEPCMs): Fabrication, characterization and applications. Renewable and Sustainable Energy Reviews 2011 10;15(8): p.3813-32.

Zou GL, Tan ZC, Lan XZ, Sun LX, Zhang T. Preparation and characterization of microencapsulated hexadecane used for thermal energy storage. Chinese Chemical Letters 2004;15(6): p.729-32.

A Appendix

A.1 Introduction

This appendix details the preliminary material development which has been focused on various types of poly(ethylene-co-vinyl acetate) (EVA) in a matrix of polypropylene (PP) or poly(methyl methacrylate) (PMMA) and low molecular weight polyethylene in polycarbonate. These material combinations were investigated because the model predicts they should have a decrease in transmittance with temperature. Additionally, EVA in PMMA has been reported to have a change in optical properties with temperature [1-3], and the refractive index and melt temperature of EVA can be adjusted by changing the percent weight of vinyl acetate in the copolymer or by changing the tacticity.

The preliminary material development has produced two thermotropic materials which have a decrease in transmittance with temperature: EVA (33%wt VA) in PMMA and EVA (14%wt) in PP. Currently, however, these materials do not meet the optical requirements for overheat protection in a polymer collector. The preliminary development of low molecular weight PE in PC has revealed some challenges to successfully producing a thermotropic material. The transmittance increases with temperature. Recommendations are given to improve the optical performance. Based on the model predictions, this combination (or low molecular weight PE in PMMA or PP) should be given prior in future material development because it is the most likely combination to obtain ≥85% transmittance in the clear state and ≥50% reflectance in the translucent state. Low molecular weight PE has a much larger change in refractive index with temperature than EVA.

Table A-1 lists all the materials associated with the project, the material source, and the application. The structure of this appendix is in three main parts. First, the method and the results for determining the complex refractive index of the various materials are presented. Second, the methods for blending and hot pressing the identified material combinations into samples are presented. Third, the experimental analysis of the

Table A-1 Materials associated with the thermotropic material project

Material	Abbreviation	Source	Application
Isotactic Polypropylene	iPP	Donated - Agility NX Clear PP Agility NX5502-12	Matrix Material with EVA/ absorptive index /refractive index
Poly(methyl methacrylate) – commercial sheet	cPMMA	Plexiglass – Scrap from ME shop	absorptive index measurement
Polycarbonate – commercial sheet	cPC	Makrolon – Scrap from ME Shop	absorptive index measurement
Poly(methyl methacrylate) – low viscosity	lvPMMA	Donated by RTP Company: Flow rate of 27g/10min @ 300°C and 1.2kg; T_g =76°C	Matrix Material with EVA
Polycarbonate – low viscosity	lvPC	Donated by RTP Company: (RTP 300HF) – Flow rate of 22g/10min @ 300°C and 1.2kg	Matrix Material with PE
Poly(methyl methacrylate) – M17	M17PMMA	From Hillmyer group – Elf. Atochem Plexiglass (M17)	Refractive index measurement
Polycarbonate	mPC	From Hillmyer group	Refractive index measurement
Poly(ethylene-co-vinyl acetate) (14% VA) – Commercial	cEVA14	Scientific Polymer Products, inc. (CAT#243)	Scattering domain in iPP/absorptive index/refractive index
Poly(ethylene-co-vinyl acetate) (33% VA) – Commercial	cEVA33	Scientific Polymer Products, inc. (CAT#245)	Scattering domain in lvPMMA/ absorptive index/refractive index
Poly(ethylene-co-vinyl acetate) (14% VA) – ROMP	rEVA14	Polymerized by Youngmin	Potential scattering domain material/ refractive index
Poly(ethylene-co-vinyl acetate) (33% VA) – ROMP	rEVA33	Polymerized by Youngmin	Potential scattering domain material/ refractive index
Random tacticity poly(ethylene-co-vinyl acetate)	rmEVA	Polymerized by Youngmin	Potential scattering domain material/ refractive index
atactic poly(ethylene-co-vinyl acetate)	aEVA	Polymerized by Youngmin	Potential scattering domain material/ refractive index
Isotactic poly(ethylene-co-vinyl acetate)	iEVA	Polymerized by Youngmin	Potential scattering domain material/ refractive index
Low molecular weight (~3k) polyethylene	PE	Sigma Aldrich (CAS: 9002-88-4)	Scattering domain in lvPC
Hextriacontane	Hexa.	Sigma Aldrich (CAS: 630-06-8)	Potential scattering domain material
ICO wax polyethylene 520	ICO PE	Donated by RTP company	Potential scattering domain material – possibly branched PE
Poly(ethylene-co-methacrylic acid)	EMA	Sigma Aldrich (CAS: 25053-53-6)	Potential scattering domain material

samples is presented. This analysis includes scanning electron microscopy of the blends and measurement of the temperature dependent optical properties.

Special thanks needs to be given to Dr. Matthew Atkinson of 3M who measured the refractive index of the polymers as a function of temperature, to Dr. Youngmin Lee who polymerized some of the EVA and help prepare the samples for the refractive index measurements, and to Christopher Thurber who helped make the blends in the twin screw extruder, and preformed the microtoming and SEM imaging of the blends. Chris also has been a tremendous resource on polymer blending.

A.2 Refractive Index Measurements

This section details how the refractive index of PMMA, PC, and various types of EVA were measured as a function of temperature. The room temperature absorptive index was also measured.

A.2.1 Measurement Methods

Table A-2 lists the samples that had their refractive indices measured, along with the corresponding melt (T_{melt}) or glass transition (T_g) temperature, type of sample (free standing film or film on silicon), and sample thickness. Some materials (rmEVa, aEVA, iEVA) were prepared as thin films on silicon because there was not sufficient material available to make a free standing film. Other materials (cEVA14, iPP) were prepared as free standing films because they do not readily dissolve and thus are difficult to make into a film on silicon. Some materials (rEVA14, cEVA33, M17PMMA, and mPC) were prepared as free standing films and thin films on silicon to determine if there was a difference in the measurements between the two types of samples.

The refractive index of the samples was measured using a Metricon Model 2010 Prism Coupler configured with the heated prism clamp and thermal controller. The coupling head held the sample in contact with the prism at 30-40 psi. Measurement were taken in the transverse-electric (TE) orientation at wavelengths of 532, 405, and 633 nm. Measurements were taken from 25 to 150 °C in 5°C increments. If 150 °C could not be reached, the maximum measurement temperature was the temperature at which the

Table A-2 Samples for refractive index measurement

Material	Type of Sample	T_g (°C)	T_{melt} (°C)	Thickness
cEVA14	F	--	90	0.33 mm
cEVA33	F/S	--	60	0.31 mm /20 μm
rEVA14	F/S	--	100	0.11 mm /20 μm
rEVA33	F	--	50	0.38 mm
rmEVA	S	--	--	20 μm
aEVA	S	--	50	20 μm
iEVA	S	--	80	20 μm
M17PMMA	F/S	100	--	0.4 mm /20 μm
mPC	F/S	150	--	0.42 mm /20 μm
iPP	F	--	160	0.38 mm
F – Free standing Film; S – Film on Silicon Wafer				

software ceased automatic calculations of the refractive index. The cessation usually corresponded to the sample flowing away from the prism. The data was used to determine the Cauchy coefficients as a function of temperature.

The absorptive index of cPMMA, cPC, cEVA14, and cEVA33 were measured using the transmittance method [4, 5]. For cPMMA and cPC, the transmittance of commercially prepared sheets was measured. For cPMMA, the sheets were 3.1, 3.3 5.85, 9.34, and 9.6 mm thick. For PC, the sheets were 1.5, 3.1, and 9.2 mm thick. For cEVA14, ~0.975 mm samples were prepared via hot pressing. For cEVA33, ~0.96 mm samples were prepared via hot pressing. The spectral absorptive index was calculated from the measured transmittance data and the spectral refractive index calculated by the Cauchy equation. For wavelengths greater than 1000nm, the approximate limit Cauchy equation, the refractive index was fixed at the 1000 nm value.

A.2.2 Refractive Index Results

The temperature dependent refractive index measurements are validated by comparison to published data for PMMA [6, 7] and PC [6]. Figure A-1a,b compares the refractive index for temperatures from 30 to 140 °C at a wavelength of 578nm to the data

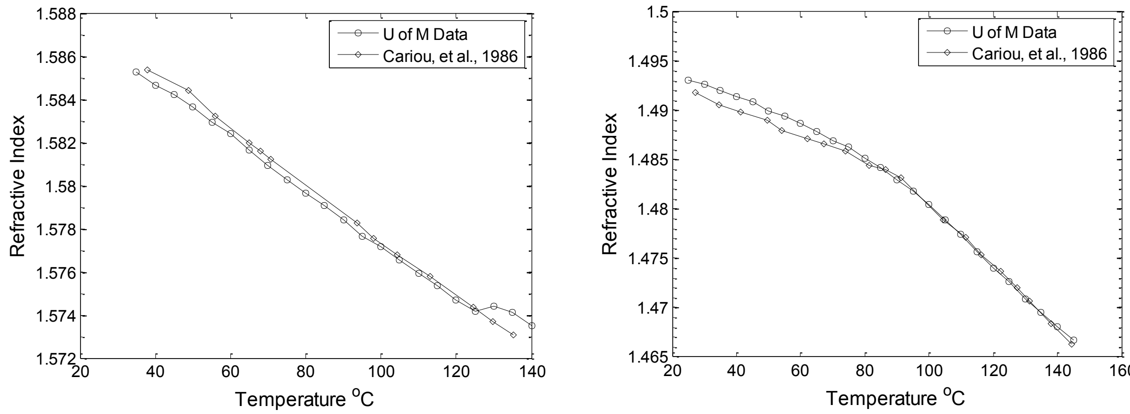

(a) (b)

Figure A-1 Comparison of (a) PC and (b) free standing film M17PMMA refractive index measurements to [6]

Table A-3 Comparison of free standing film M17PMMA measurements to [7]

	430 nm (g-line)		486 nm (F-line)		546 nm (e-line)		588 nm (d-line)		656 nm (C-line)	
T (°C)	UofM	[7]	UofM	[7]	UofM	[7]	UofM	[7]	UofM	[7]
25	1.5065	1.5018	1.5007	1.4970	1.4954	1.4931	1.4924	1.4910	1.4884	1.4885
30	1.5061	1.5011	1.5003	1.4963	1.4950	1.4924	1.4920	1.4904	1.4879	1.4879
35	1.5054	1.5004	1.4996	1.4956	1.4944	1.4919	1.4914	1.4897	1.4875	1.4873
40	1.5049	1.4999	1.4991	1.4951	1.4938	1.4911	1.4908	1.4891	11.4867	1.4865
45	1.5045	1.4992	.4986	1.4943	1.4933	1.4905	1.4902	1.4884	1.4860	1.4859
50	1.5036	1.4985	1.4976	1.4937	1.4923	1.4899	1.4893	1.4878	1.4853	1.4853

reported by [6]. The measured values compare well to the published data. For PMMA, the measured data is within 0.0015 of the published data. For PC, the measured data is within 0.001 of the published data, and below 120 °C, the two data sets are even closer. Table A-3 compares the refractive index of PMMA for temperatures from 25 to 50 °C at five wavelengths in the visible spectrum to the data reported by [7]. There is a greater discrepancy between the measured data and the data from [7] than the measured data and the data from [6]. For wavelengths of 430 and 486 nm, there is approximately a 0.004 to 0.005 difference. For wavelengths greater than 486 nm, the difference is less than 0.0025.

Figure A-2 to Figure A-11 report the refractive index data of the polymers measured by 3M. Data is not available for the rEVA14 and mPC films on silicon because the surfaces of these samples were too rough for optical coupling to the prism. Additionally, confocal microscopy showed that the rEVA14 film was not continuous. For the two polymers, cEVA33 and M17PMMA, with refractive index data from a free standing sample and a thin film on silicon, the data from the two sample preparations are slightly different. The most notable aspects of the refractive index data of Figure A-2 to Figure A-11 are: iEVA is the only type of EVA which has a sharp change in refractive index at a temperature appropriate for providing overheat protection (~90°C), and cEVA14 and rEVA14 have the largest change in refractive index.

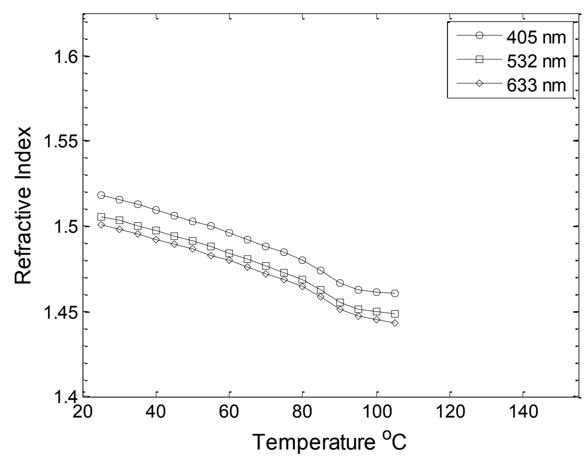

Figure A-2 cEVA refractive index as a function of temperature

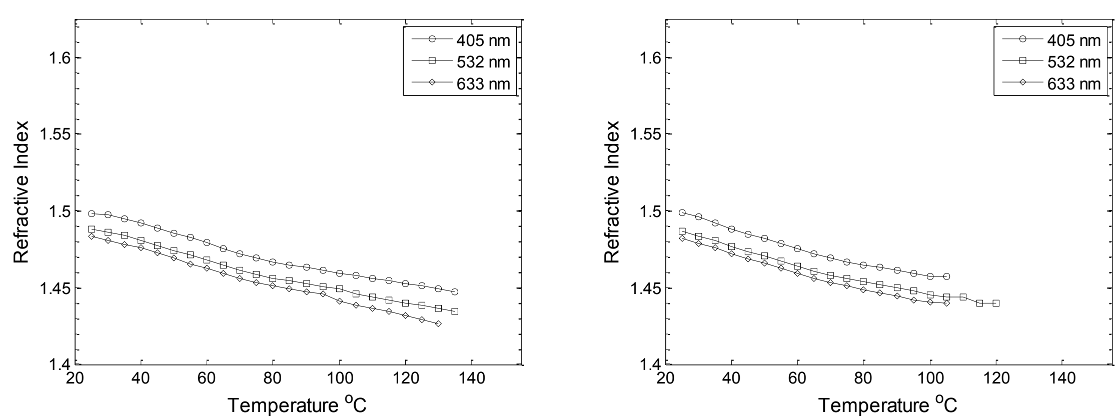

Figure A-3 cEVA (a) free standing film and (b) film on silicon refractive index as a function of temperature

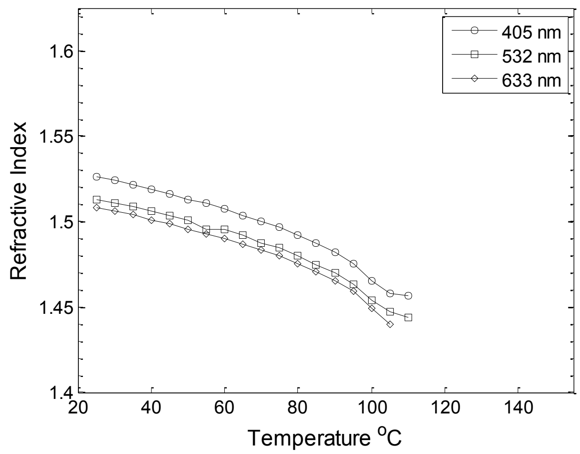

Figure A-4 rEVA14 refractive index as a function of temperature

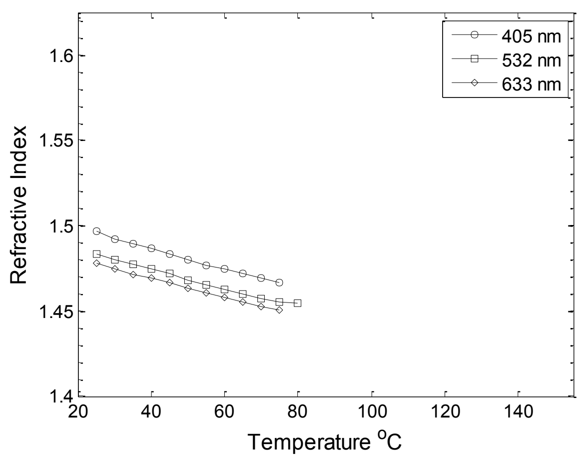

Figure A-5 rEVA33 refractive index as a function of temperature

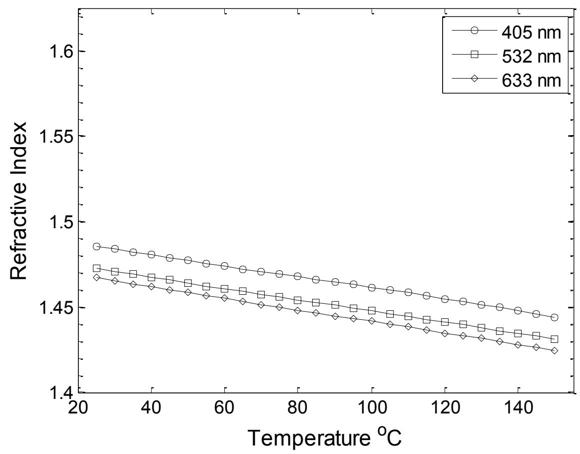

Figure A-6 rmEVA refractive index as a function of temperature

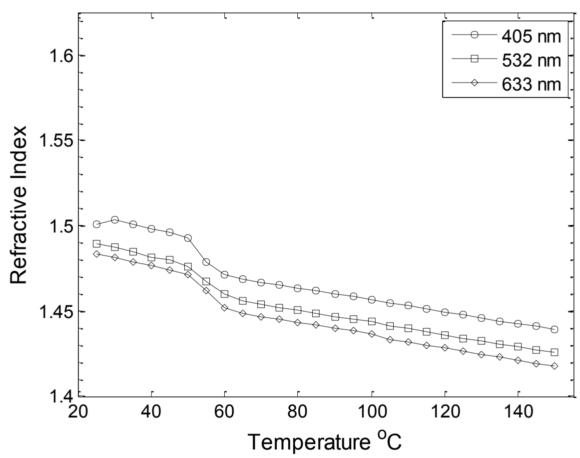

Figure A-7 aEVA refractive index as a function of temperature

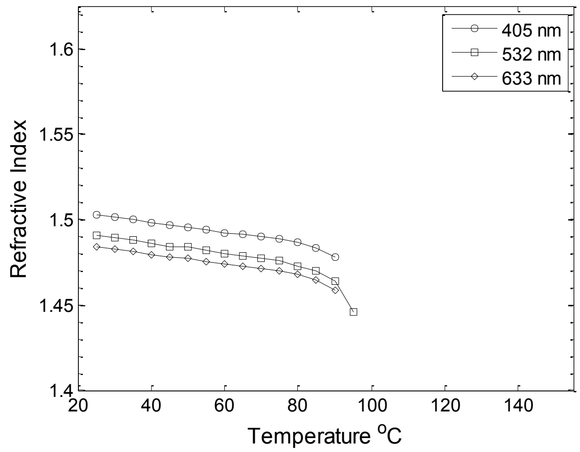

Figure A-8 iEVA refractive index as a function of temperature

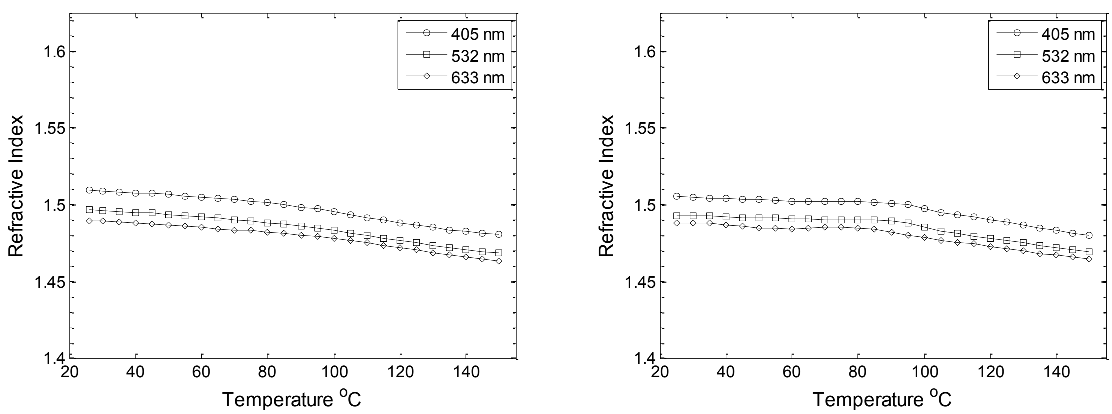

Figure A-9 M17PMMA (a) free standing film and (b) film on silicon refractive index as a function of temperature

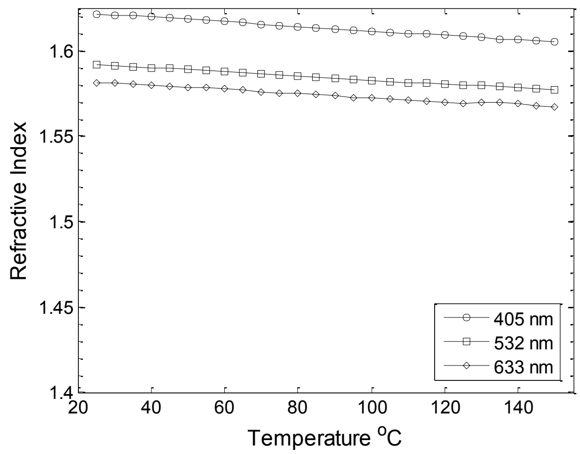

Figure A-10 mPC refractive index as a function of temperature

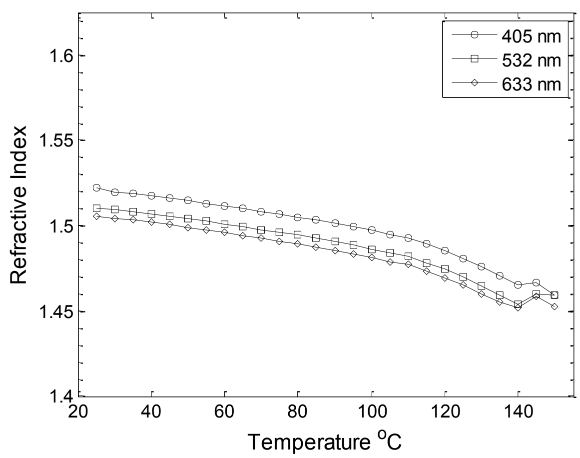

Figure A-11 iPP refractive index as a function of temperature

Figure A-12 to Figure A-14 shows the relative refractive index for each potential scattering domain in PMMA, iPP, and PC respectively at a wavelength of 533 nm. For the same matrix material, the various scattering domain materials have similar relative refractive index at temperatures ≥90 °C (~0.975 in PMMA, 0.9725 in PP, 0.915 in PC). Thus, the selection of combinations for fabrication was primarily determined by how closely the relative refractive index is to unity at 30 °C. Additionally, the selection was limited to commercially available materials because relatively a large quantity of material (minimum 100 to 150g) is necessary for blending in the TSE. Commercial EVA14 in iPP

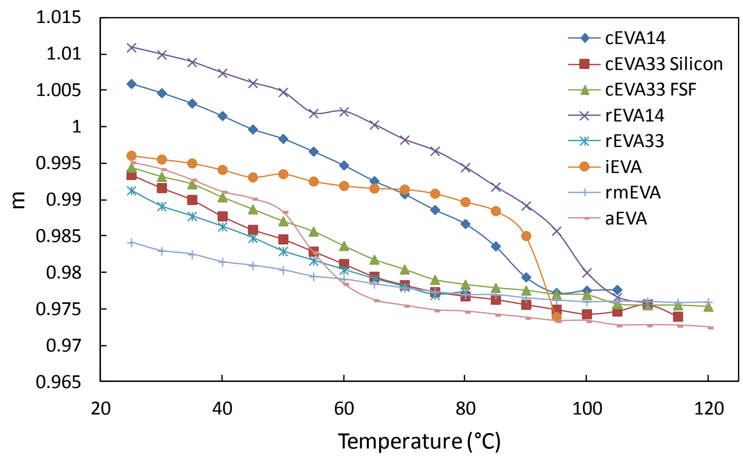

Figure A-12 Relative refractive index for a matrix of PMMA (533 nm)

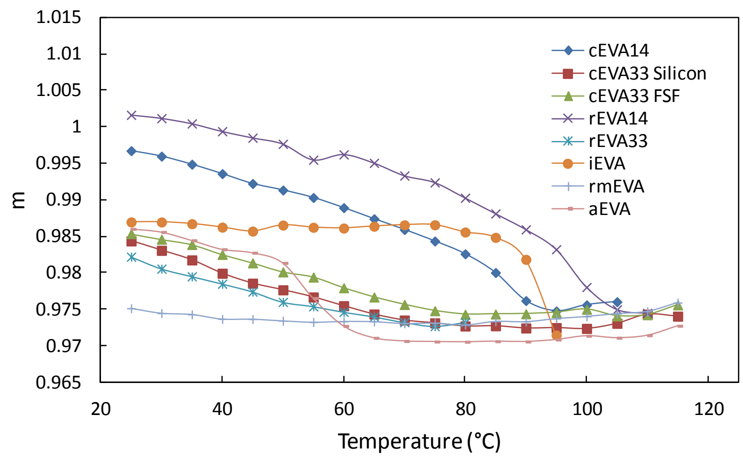

Figure A-13 Relative refractive index for a matrix of iPP (533 nm)

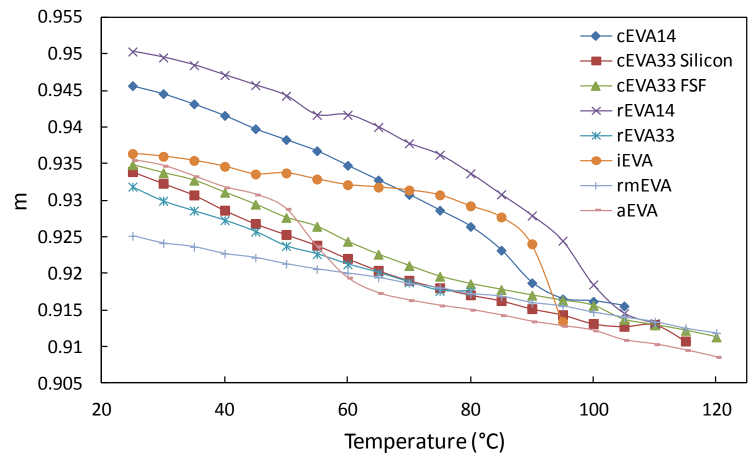

Figure A-14 Relative refractive index for a matrix of PC (533 nm)

and cEVA33 in PMMA were selected. For the non-commercial materials, iEVA in PMMA looks promising. Below 80 °C, the relative refractive index of this combination is within 0.001 of unity which should have high transmittance (Figure A-12). At ~90 °C, there is a sharp decrease in the relative refractive index. However, at the last data point, the relative refractive index is only 0.974. Thus like the other thermotropic combinations with EVA, a relatively thick slab (~3mm) and a high volume fraction (>15%) are necessary to obtain >50% reflectance in the translucent state.

Figure A-15 and Figure A-16 show the absorptive index of cPMMA, cPC, cEVA14, and cEVA33. As expected, the absorptive index of cPMMA and cPC are low ($<1x10^{-6}$) for $350 \leq \lambda \leq 1000$nm. The absorptive index of both types of EVA are $<1x10^{-5}$ for $350 \leq \lambda \leq 1000$nm.

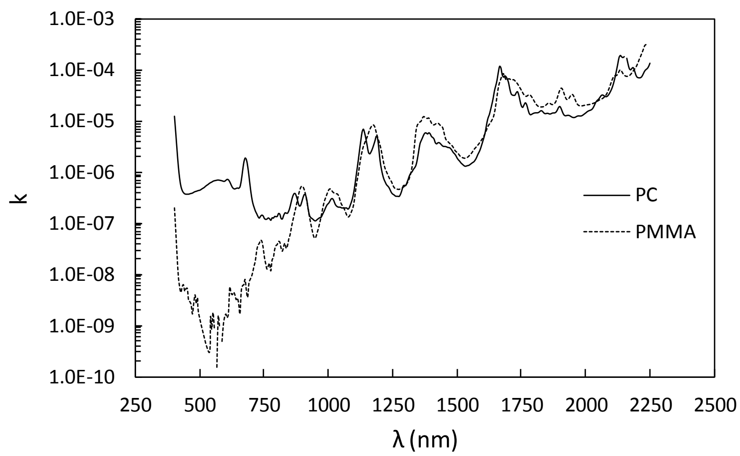

Figure A-15 Absorptive index for cPC and cPMMA

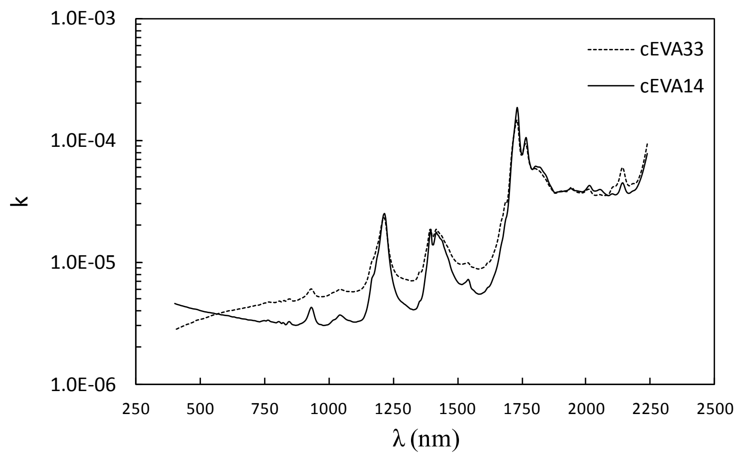

Figure A-16 Absorptive index for cEVA14 and cEVA33

A.3 Thermotropic Material Fabrication

Prior to mixing and hot pressing, the polymers were dried in a vacuum oven overnight. The scattering domain and matrix material were blended via melt mixing with a PRISM Twin Screw Extruder (TSE) 16 TC. Commercial EVA14 and cEVA33 were blended with their respective matrix materials at a mass fraction of 10%. Based on the Lorenz-Lorentz prediction of refractive index for low molecular weight PE (~3k) (predicted to be 1.54), it was mixed with lvPC at volume fractions of 2 and 7%. However, after the testing with PE in lvPC was completed, Weber, et al. [8] published a measured refractive index of paraffin wax, which is similar to low molecular weight PE, of ~1.50 at room temperature. The refractive index of the low molecular weight PE should be measured, and the matrix material adjusted (to PMMA or iPP) if necessary.

The blending temperatures and mixing speed for cEVA14 in iPP and cEVA14 in lvPMMA are shown in Figure A-17. The temperatures, starting at the temperature read out in the lower right hand corner of Figure A-17 and moving clock-wise, for low molecular weight PE in lvPC are 215, 220, 230, 230, 225, error (TC was not working at time of mixing), 235, 236, and 230 °C. The mixing speed was 34 RPM. Pure matrix material (iPP, lvPMMA, and lvPC) was also processed through the TSE.

Blending cEVA14 in iPP resulted in a blend that came out as clear as the pure iPP. The cEVA33 in lvPMMA came out slightly whiter than the lvPMMA. The PE in lvPC blend extruded out of the mixer a white color. Blending PE in lvPC was more challenging than blending EVA with iPP or lvPMMA, because of the difference in viscosity. The TSE had difficulty extruding the PE/PC blend. It extruded the blend slowly, and it appeared to extrude a core material with liquid layer surrounding it. However, SEM analysis revealed that the two materials did mix, but that the particle size is much larger for PE in lvPC than EVA in iPP or lvPMMA.

The blends were hot pressed into free standing films. The resulting films are pictured in Figure A-18, and the processing conditions are summarized in Table A-4. The blends with EVA were pressed into films 0.95 thick. Poly(ethylene-co-vinyl acetate) (14%wt VA) in iPP was also pressed into a 3 mm thick film. The PE in lvPC blend was pressed into a film 0.25 mm thick. Commercial EVA14 in iPP was robust to the pressing

(a) (b)

Figure A-17 TSE processing temperatures for (a) cEVA14 in iPP (b) cEVA33 in lvPMMA

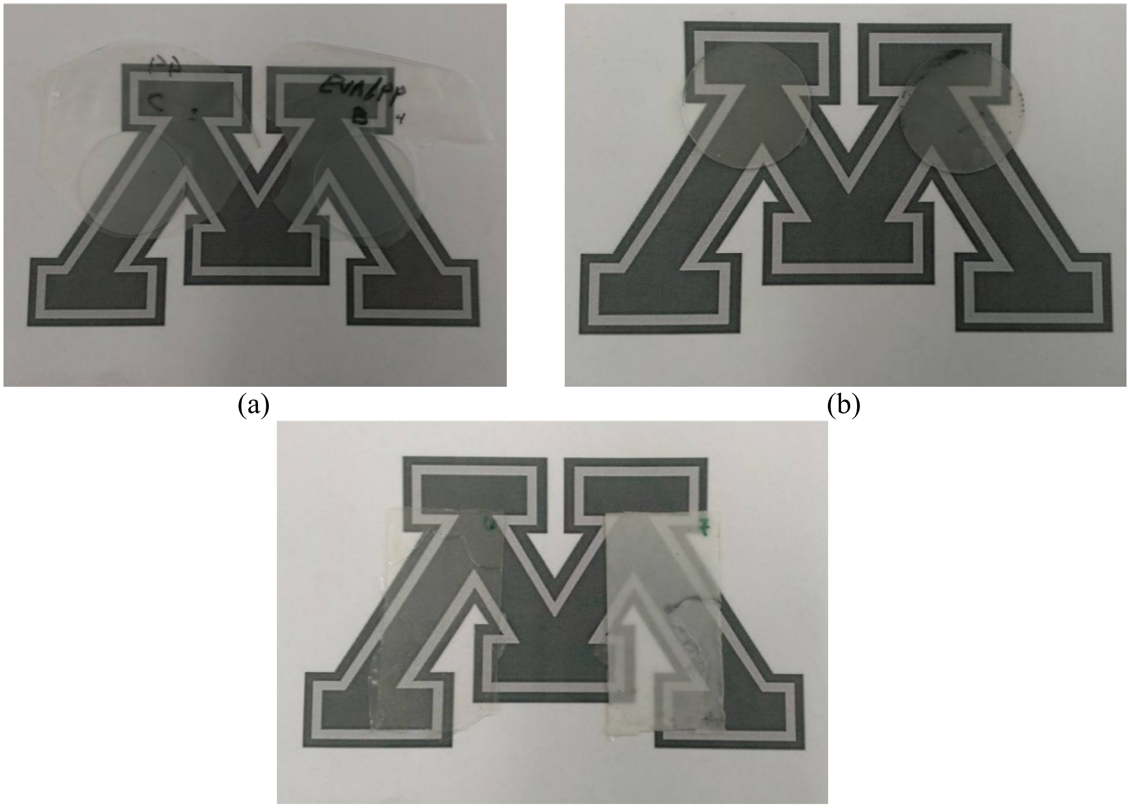

(a) (b) (c)

Figure A-18 Pictures of samples. Control (100% matrix material) is left sample in each picture. (a) cEVA14 in iPP; (b) cEVA33 in lvPMMA; (c) PE in lvPC

Table A-4 Hot press processing parameters

Material	T (°C)	Preheat (min.)	Press Force (lbs)	Press Time (min)	Quench
cEVA14/iPP	180	6	3000	3	Water cooled on old press
cEVA33/lvPMMA	210 (probably could be less. ~180)	7	3000	3	Let cool on forms on the table for 7 min. then removed from forms and continued to let cool sitting on table
PE/lvPC	250 (probably could be less)	5	3000	3	Water cooled on old press

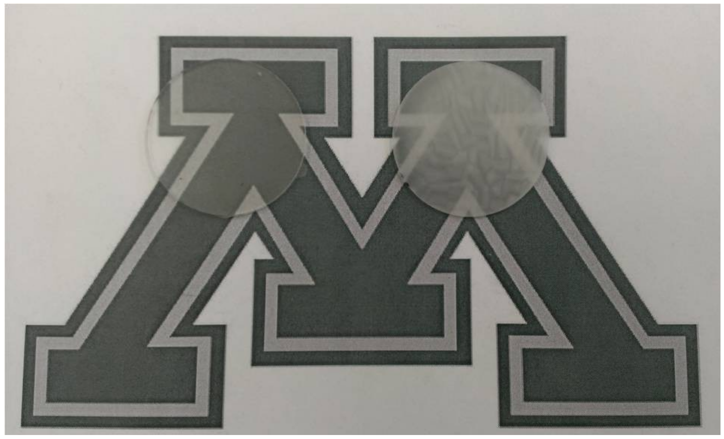

Figure A-19 Sample defect for cEVA33 in lvPMMA: the white areas in right sample. Left sample is the control

process. Numerous combinations of pressing temperature, preheat time, and cooling method resulted in satisfactory samples. Commercial EVA33 in lvPMMA was highly sensitive to the pressing processing. The main sample defect was large white areas in the film as shown by Figure A-19. A slow cooling rate was found to be the best method to minimize the appearance of these white areas. Changing other parameters such as the pressing temperature and preheat time had little to no effect on these white areas. Low molecular mass PE in lvPC was successfully pressed into a free standing film, but the resulting film was a white color (Figure A-17c).

A.4 Experimental Analysis

A.4.1 SEM Analysis

Scanning electron microscopy images of the blends were taken after processing in the TSE to determine the particle size distribution. To prepare the samples for SEM, the samples were first whittled to a point using a razor. Then the point was cryo-microtomed at -160 °C using a glass knife cutting at 2μm increments. Next the disperse phase was washed out via an 11 hour soak in a solvent. Toluene at 60 °C was used as the solvent for cEVA14 in iPP. N-heptane was used for cEVA33 in lvPMMA. Low molecular mass PE in lvPC was not washed out because the interface between the particle and the matrix needed to be examined for the presence of vacuoles. Lastly, the samples were mounted on SEM sample platforms using carbon tape and coated with a 50 angstrom platinum coating. A JSM-6500F JEOL Field Emission Scanning Electron Microscope set at 5 kV was used to take the images. Images at two to four locations were taken.

Figure A-20 to Figure A-22 show the SEM images of the blends. From the images, one can see that the disperse phase is spherical. Qualitatively, cEVA14 in iPP (Figure A-20) has the smallest particle size. Low molecular weight PE in lvPC (Figure A-22) has, qualitatively, the largest particle size; on the order of a couple microns. Of note is the rough surface of the cEVA14 in iPP (Figure A-20). It is hypothesized that the bumps on the surface are the recondensation of cEVA14. After the disperse phase was washed out, the sample was allowed to cool in the toluene. Thus, it is possible that some of the cEVA14 dropped out of suspension and recondensed on the surface of the sample. Because of the rough surface, it is possible that the particle size estimated from the images is underestimated.

The particle diameters were measured using ImageJ software. The 5000X magnification images were used to determine the particle size. For cEVA14 in iPP, 500 particles were measured. For cEVA33 in lvPMMA, 279 particles were measured. Figure A-23 and Figure A-24 show the particle distribution histograms for cEVA14 in iPP and cEVA33 in lvPMMA, respectively. The bin size was determined by taking the difference between the maximum and minimum particle diameters and dividing it by the square root of the number of particles measured. The Sauter mean diameter of the blends was 212 nm for cEVA14 in iPP and 681 nm for cEVA33 in lvPMMA. In addition to having a smaller mean particle diameter, cEVA14 in iPP has a much narrower particle distribution than cEVA in lvPMMA. The smaller distribution is probably because the viscosities in the melt phase are more similar for cEVA14 and iPP than cEVA33 and lvPMMA.

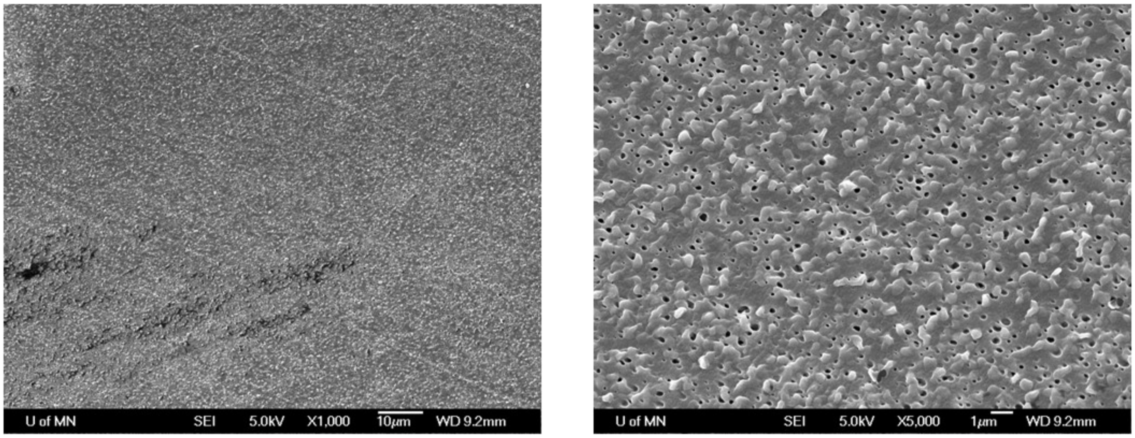

(a) (b)

Figure A-20 cEVA14 in iPP at (a) 1000x and (b) 5000x

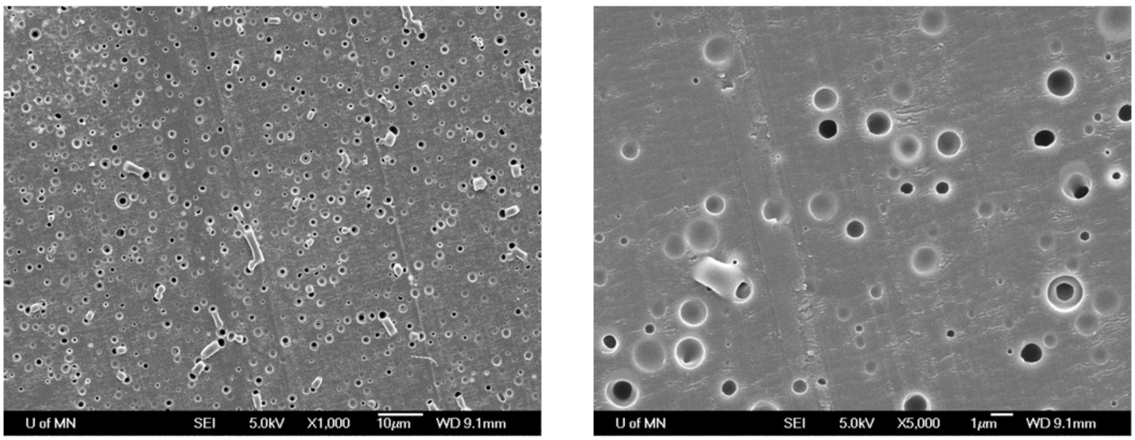

(a) (b)

Figure A-21 cEVA33 in lvPMMA at (a) 1000x and (b) 5000x

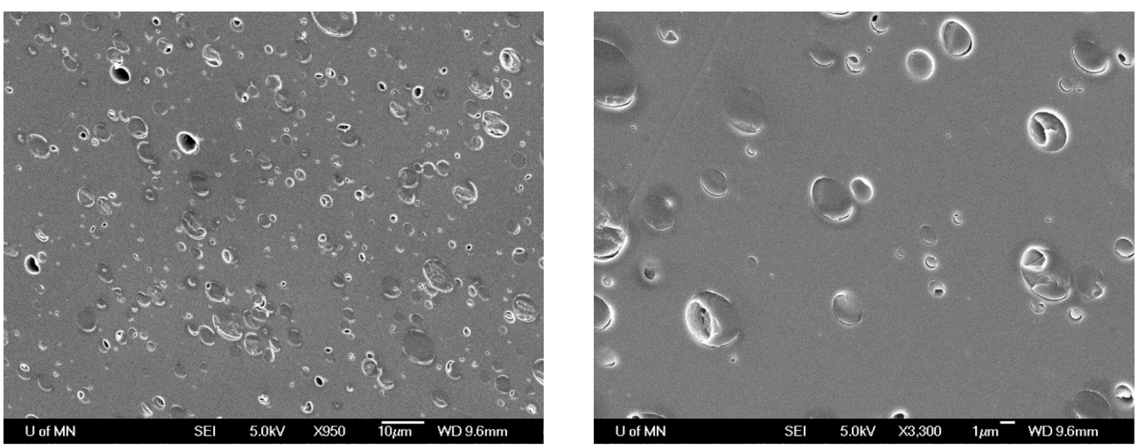

(a) (b)

Figure A-22 low molecular weight PE in lvPC at (a) 950x and (b) 3300x

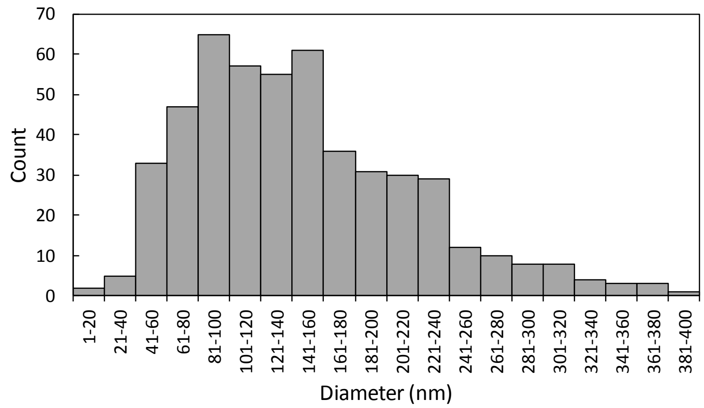

Figure A-23 Particle size distribution for cEVA14 in iPP

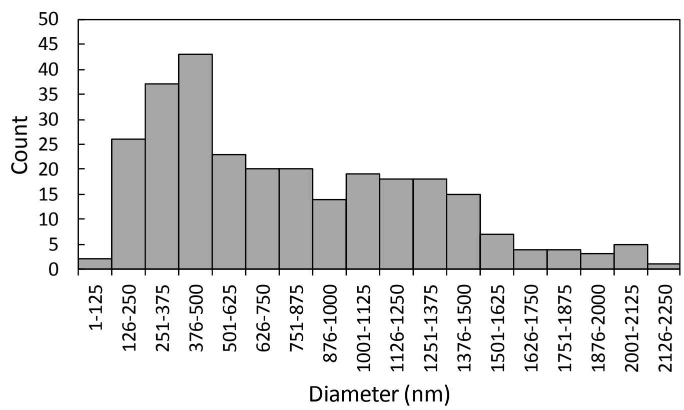

Figure A-24 Particle size distribution for cEVA33 in PMMA

A.4.2 Spectroscopy Analysis

The spectral, normal-hemispherical transmittance and reflectance of the blends were measured from 250 to 2400 nm at 24 °C and above the melting temperature of the scattering domain material using a Perkin-Elmer Lambda 1050 spectrophotometer equipped with a 150 mm integrating sphere. For elevated temperature measurements, the samples were heated with a hot plate, shown schematically in Figure A-25. The hot plate consists of a one inch thick copper plate heated by four resistance heaters. The copper plate has a measurement window which allows the radiation from the spectrophotometer to irradiate the sample. For reflectance measurements, the beam from the spectrophotometer must be reduced via the common beam mask (CBM) to the approximate size of the measurement window (a CBM of ~18%) and aligned to be centered on the window. The temperature of the hot plate is controlled by an Omega CN4416 temperature controller. The temperature distribution of the copper plate was measured at various locations and determined to be within one degree Celsius.

The relationship between the hot stage temperature and the sample temperature is shown in Figure A-26. Figure A-26 was made by embedding thermocouples in ~1mm thick piece of iPP, and measuring the temperature of the polymer as a function of the set temperature. The peaks for each steady state region correspond to the sample temperature over the copper, i.e. the maximum temperature of the sample. The low points of each steady state region correspond to the sample temperature over the measurement window, i.e. it is the temperature of the portion of the sample being measured. The set temperatures for cEVA14 in iPP and cEVA33 in lvPMMA were 110 °C and 100 °C,

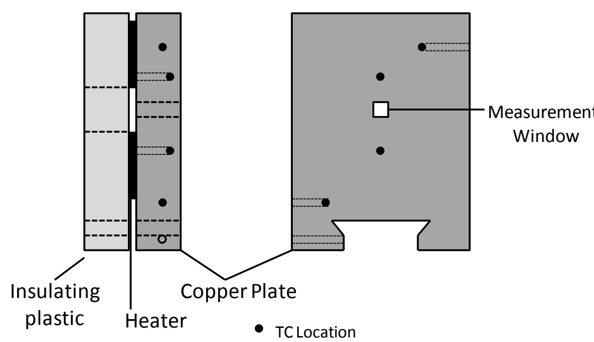

Figure A-25 Side and front schematic views of the hot stage

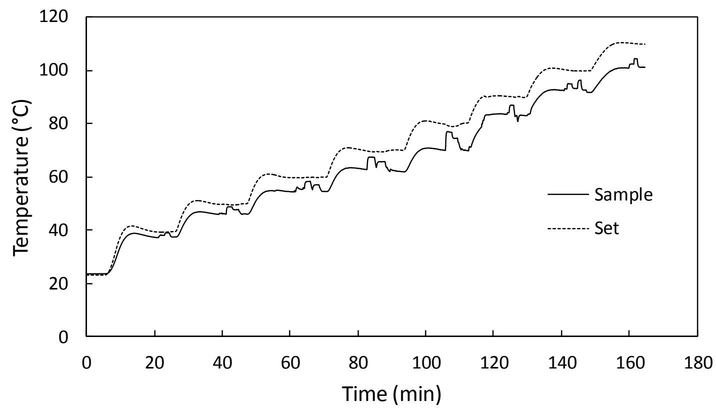

Figure A-26 Relationship between the hot stage set temperature and the sample temperature

respectively. These set temperatures correspond to sample temperatures of approximately 100 and 92 °C, respectively. The set temperature for low molecular weight PE in lvPC was 120 °C.

The transmittance and reflectance of the blends are shown in Figure A-27 to Figure A-29. Both cEVA14 in iPP and cEVA33 in lvPMMA demonstrate a decrease in transmittance and an increase in reflectance with temperature. The solar-weighted transmittance of cEVA14 in iPP decreases from 83.5% at 24 °C to 69% at 100 °C. The solar weighted reflectance increases from 9.5 to 27%. The transmittance in the clear state is acceptable. The reflectance in the translucent state is too low to provide overheat protection for commodity polymer absorbers. The addition of cEVA14 to iPP did not reduce the transmittance in the clear state relative to the control sample of 100% iPP which had a solar-weighted transmittance of 82.5%. Thus, it may be possible to increase the volume fraction of cEVA14 in iPP to increase the reflectance in the translucent state while maintaining high transmittance in the clear state. For the 3 mm thick sample of cEVA14 in iPP, the solar-weighted transmittance is 70% at 24 °C and 48% at 100 °C. The solar weighted reflectance increased from 13.5 to 38%. The solar weighted transmittance of the control sample of iPP is 69% at 24 °C and 71.5% at 100 °C. The solar weighted reflectance remained constant at 13.5%.

Figure A-28 shows the transmittance and reflectance for cEVA33 in lvPMMA. The solar-weighted transmittance of cEVA33 in lvPMMA decreases from 78 to 64%.

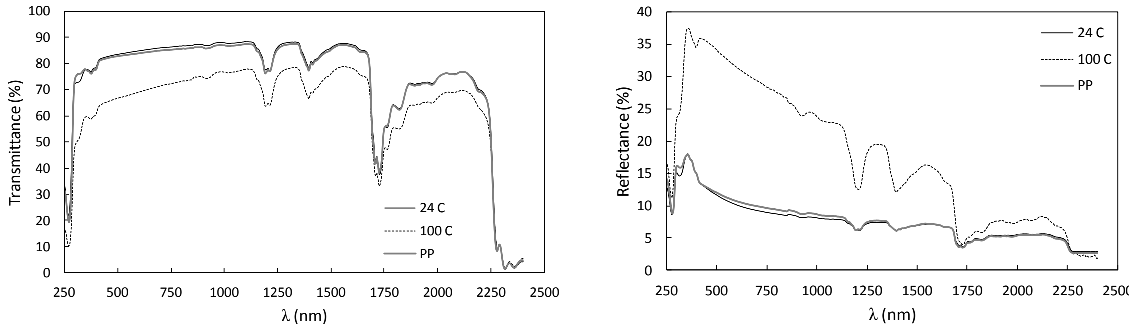

(a) (b)

Figure A-27 (a) Transmittance and (b) reflectance for cEVA14 in iPP and control iPP

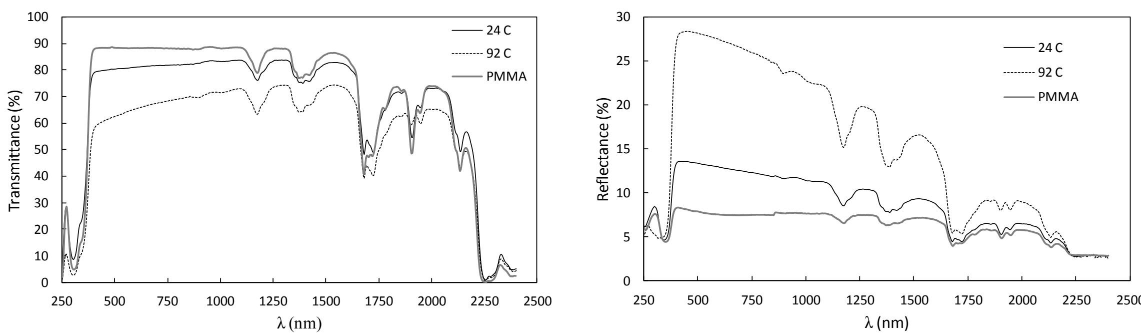

(a) (b)

Figure A-28 (a) Transmittance and (b) reflectance for cEVA33 in lvPMMA and control lvPMMA

The solar-weighted reflectance of cEVA33 in lvPMMA increases from 11 to 23%. For cEVA33 in lvPMMA, the transmittance in the clear state is lower than desired. Further refinement in the fabrication process may improve the transmittance in state because the sample still had remnants of the white area defect. The control lvPMMA sample has a solar-weighted transmittance of 83% which also could be improved; a 3 mm thick sample of commercial lvPMMA has a measured solar-weighted transmittance of 85%. The reflectance is in the translucent state is too low to provide overheat protection for a commodity polymer absorber.

Figure A-29 shows the measured transmittance for PE in lvPC. As expected from the white color of the sample, the transmittance at room temperature is relatively low. At elevated temperature, the transmittance of the blend increases. The solar-weighted transmittance of the blend increases from 61.5% at 24 °C to 69% at a set temperature of

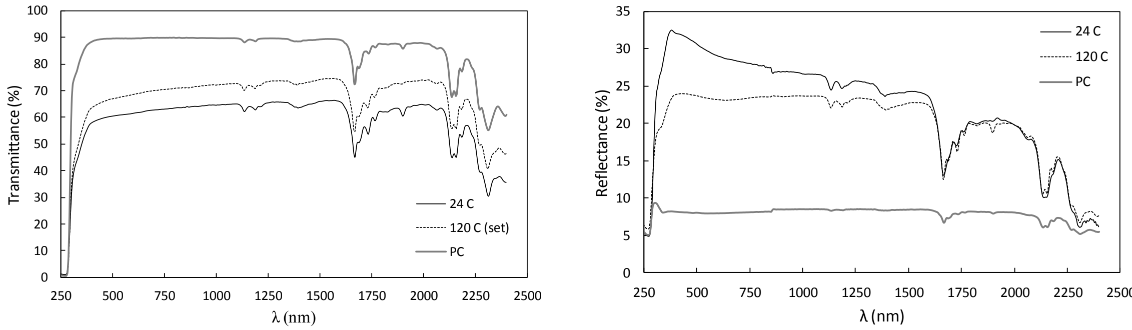

(a) (b)

Figure A-29 (a) Transmittance and (b) reflectance for low molecular weight PE in lvPC and control lvPC

120 °C. The control sample of lvPC has a solar-weighted transmittance of 8%. The solar-weighted reflectance decreases from 38% to 28%. The mostly likely cause of the increase transmittance is the presence of vacuoles around the disperse phase in the clear state. The vacuoles may be created during cooling of the blend. Since the blends are mixed above their melt temperatures, when they cool, they contract at different rates. If the low molecular mass PE contracts more than the lvPC, which is likely, it may pull away from the lvPC interface; thus, creating 'encapsulated' particles in the clear state which have a 'shell' with a refractive index equal to one. In the translucent state, the PE expands to fill the void. Transmittance would increase if the vacuole/particle in the clear state scatters radiation more strongly than the just the particle in the translucent state. Weber, et al. [9] also reported an increase in transmittance with temperature for a paraffin wax (which is similar to low molecular weight PE) in an acrylate based matrix. The cause was radiation scattering by vacuoles in the clear state. When the percentage of particles with vacuoles was minimize, transmittance decreased with temperature [9].

To investigate the possibility of vacuoles, the PE in lvPC blend was analyzed via SEM without washing out the disperse phase. Figure A-22 shows that most particles have a vacuole surrounding it. However, there is there is a possibility that these vacuoles were created during microtoming process. Thus the SEM analysis is inconclusive. However, vacuoles are the most probably cause of the increase in transmittance with temperature. Two solutions to reduce the number of vacuoles are to use compatibilizers or to encapsulate the PE. A potential compatibilizer is poly(ethylene-co-vinyl acetate).

Experimentation is required to determine the percent weight of vinyl acetate that is most efficacious. In addition to potentially reducing the number of vacuoles, compatibilizers also reduce the mean particle size and the size distribution [10]. As detailed in chapter 5, encapsulation is an intriguing avenue for future research. However, before encapsulated particles of low molecular weighted PE in a thermotropic material can be modeled, an accurate measurement of the refractive index of low molecular weight PE must be taken. A challenge to using encapsulation is finding an encapsulant which will retain structural integrity through the melt mixing process.

A.5 References

[1] Errico, M., Greco, R., Laurienzo, P., 2006, "Acrylate/EVA Reactive Blends and semi-IPN: Chemical, chemical–physical, and thermo-optical Characterization," Journal of Applied Polymer Science, **99**(6) pp. 2926-2935.

[2] Bernini, U., Malinconico, M., Martuscelli, E., 1995, "Ultra-Tough Synthetic Glasses made by Reactive Blending of PMMA and EVA Rubbers: Opto-Thermal Characterization," Journal of Materials Processing Technology, **55**(3–4) pp. 224-228.

[3] Takahashi, S., Okada, H., Nobukawa, S., 2012, "Optical Properties of Polymer Blends Composed of Poly(Methyl Methacrylate) and ethylene–vinyl Acetate Copolymer," European Polymer Journal, **48**(5) pp. 974-980.

[4] Dombrovsky, L., Randrianalisoa, J., Baillis, D., 2005, "Use of Mie Theory to Analyze Experimental Data to Identify Infrared Properties of Fused Quartz Containing Bubbles," Appl.Opt., **44**(33) pp. 7021-7031.

[5] Rubin, M., 1985, "Optical Properties of Soda Lime Silica Glasses," Solar Energy Materials, **12**(4) pp. 275-288.

[6] Cariou, J., Dugas, J., Martin, L., 1986, "Refractive-Index Variations with Temperature of PMMA and Polycarbonate," Applied Optics, **25**(3) pp. 334-336.

[7] Kasarova, S. N., Sultanova, N. G., and Nikolov, I. D., 2010, "Temperature dependence of refractive characteristics of optical plastics," Journal of Physics: Conference Series, Anonymous IOP Publishing, **253,** pp. 012028.

[8] Weber, A., and Resch, K., 2014, "Thermotropic Glazings for Overheating Protection. I. Material Preselection, Formulation, and light-shielding Efficiency," Journal of Applied Polymer Science, **131**(4) pp. doi: 10.1002/app.39950.

[9] Weber, A., Schlögl, S., and Resch, K., 2013, "Effect of Formulation and Processing Conditions on Light Shielding Efficiency of Thermotropic Systems with Fixed Domains Based on UV Curing Acrylate Resins," Journal of Applied Polymer Science, **130**(5) pp. 3299-3310.

[10] Sundararaj, U., and Macosko, C., 1995, "Drop Breakup and Coalescence in Polymer Blends: The Effects of Concentration and Compatibilization," Macromolecules, **28**(8) pp. 2647-2657.